Università degli Studi di Pavia

Dipartimento di Scienze della Terra e dell'Ambiente

SCUOLA DI ALTA FORMAZIONE DOTTORALE

MACRO-AREA SCIENZE E TECNOLOGIE

DOTTORATO DI RICERCA IN SCIENZE DELLA TERRA E DELL'AMBIENTE

Marina Clausi

Alkali activated materials as alternative binders for the built heritage: study of their interaction with ornamental stones in mortars, composites and cements

Anno Accademico 2015-2016
Ciclo XXIX

Coordinatore
Prof. Annamaria Picco

Tutore
Prof. Serena Chiara Tarantino

Co-tutore
Prof. Maria Pia Riccardi

TABLE OF CONTENTS

PREFACE

The alkaline activation is a chemical process through which precursors sufficiently rich in reactive silica and alumina, mainly available as amorphous or vitreous phases, interact with a strongly alkaline medium to give rise, under mild processing conditions, to materials with good binding and cementing properties. Nowadays, these materials are largely known as Alkali Activated Materials (AAMs), although over time, different terms have been coined, including the widespread trade name geopolymers.

AAMs have emerged as alternative to traditional construction materials, such as mortars or Ordinary Portland Cement (OPC), with the aim to become primary components in the development of environmentally sustainable building products, above all considering the growing interest of the scientific community for the themes of sustainability and CO_2 footprint reduction. Many studies have been carried out employing calcined clays and industrial wastes, like ground blast furnace slags and fly ashes, or wastes deriving by various human activities, until now under-utilized or simply dismissed. It has been assessed that, depending on the raw material selection and processing conditions, AAMs can exhibit a wide variety of properties, such as high level of resistance to a range of different acids and salt solutions, fire resistance, low shrinkage and low thermal conductivity. Furthermore, they may be suitable to be used in extreme environmental conditions. All these properties may be of high relevance when dealing with conservation of the built heritage, where their potential applicability has been little explored so far.

With this premise, the present PhD Thesis was designed with the aim of exploring the potentiality and suitability of AAMs for the synthesis of binders and mortars to be used for conserving and restoring ancient and contemporary art and architecture as well as natural and artificial stone objects. Furthermore, this research aims at addressing the issue of reuse by evaluating the employment of industrial waste as precursor materials. The versatility of AAMs has led to evaluate their synergic use and interaction with stones used for ornamental purposes, in order to increase/improve the compatibility with the materials to be repaired, fundamental issue when dealing with conservation.

Materials for conservation should guarantee functional and aesthetic compatibilities with the substrate and the whole construction. The knowledge of basic properties of the new material allows to formulate suitable products depending on the different destinations of use. For this

reason, it has been chosen to employ mainly metakaolin, both because widely studied in literature, and because a pure starting material better helps to understand the final reaction products.

The Thesis is organized in three chapters. A **state-of-the-art** section introduces the AAMs by presenting a brief literature review in which reaction mechanisms, structural features and environmental and engineering benefits, carried out from alkaline activation of aluminosilicates, are defined.

Chapter 1 is based on a paper submitted in April 2016 and accepted for publication with the journal *Applied Clay Science* (Volume 132-133, November 2016, pp. 589-599) and entitled: "Metakaolin as a precursor of materials for applications in Cultural Heritage: geopolymer-based mortars with ornamental stone aggregates" by Marina Clausi, Serena C. Tarantino, Laura Lorenza Magnani, M. Pia Riccardi, Cristina Tedeschi and Michele Zema. Mortars, prepared by adding aggregates of Italian ornamental stones to alkali-activated metakaolin, have been studied in order to evaluate the possible use of geopolymers as restoration materials in conservation of historic manufactures. A detailed study of different geopolymer binders, characterized by different water/solid weight ratios between 0.33 and 0.66, has been carried out prior to synthetize mortars to evaluate their workability. Good mechanical properties, with compressive and flexural strength values as high as 72 MPa and 6 MPa, respectively, and decreasing with increasing water/solid ratio, have been obtained. Mortars analyzed by several techniques, including mechanical strength tests according to UNI EN 196-1, have displayed a homogeneous and compact matrix, bonded (silicoaluminate aggregates) or interlocked (carbonate) with aggregates. Their compressive strengths fall in the masonry mortars class M20 range. Their pore size distribution guarantees good breathability and adaptability to the substrate and the final features mimic the original stones, with good aesthetic compatibility.

Chapter 2 is based on a paper submitted in June 2016 and accepted for publication with the journal *International Journal of Conservation Science* (Volume 7, Special Issue 2, 2016, pp. 871-884) and entitled "Interaction of metakaolin-based geopolymers with natural and artificial stones and implications on their use in Cultural Heritage" by Marina Clausi, Laura Lorenza Magnani, Roberta Occhipinti, M. Pia Riccardi, Michele Zema and Serena C. Tarantino. SEM-EDS analyses have been used to assess the effects at interfaces of natural and artificial stones with metakaolin-based AAMs. Three ornamental stones, widely used in the historic Italian

architecture, have been selected: Pietra Serena (sandstone), Pietra di Angera (dolostone) and Pietra di Noto (limestone). Widespread construction materials like concrete and brick have been also included in the study. Furthermore, the interactions between geopolymers and historic elements, like a decorative stone and a mortar, have been also studied in order to evaluate a possible application of these materials in conservation of built heritage. The results have revealed that adhesion is good with all analyzed materials. Large differences at the boundary have been observed and related to the composition of the materials: silicoaluminate phases partially dissolve and increase the Si and Al availability at the interface that resulted strongly interlinked, whereas carbonatic phases and rocks supply Ca that changes the local composition of the binder.

Chapter 3 is based on a paper in preparation, provisionally entitled "Valorisation of Pietra Serena sewage sludge in matrices of fly ash and metakaolin" and developed in collaboration with Ana Maria Fernández Jimènez, Angel Palomo, Serena C. Tarantino and Michele Zema, during my stay at the Institute of Science and Construction Building Eduardo Torroja of Madrid, Spain (from February to May 2016). The opportunity of using sewage sludge resulting from the cultivation of Pietra Serena as starting material in the alkali activation process has been evaluated. AAMs have been prepared by mixing sewage sludge with class-F fly ash and metakaolin in different proportions. Activation has been done using NaOH solutions 8M and 12M, respectively. Furthermore, Pietra Serena sludge have also been used for the synthesis after thermal treatment at 800ºC. Characterization was performed by X-ray power diffraction (XPRD), Fourier transform infrared (FTIR) spectroscopy, scanning electron microscope (SEM), colorimetry and mechanical tests. Results have revealed the double usability of the Pietra Serena sewage sludge. The sludge can be incorporated as filler in fly ash matrix by alkaline activation, or used in binary or ternary matrices with metakaolin and fly ash after a decarbonation pretreatment that leads to the formation of CaO and contributes to increase the mechanical strength.

The general **conclusions** of the thesis are reported at the end of the manuscript.

STATE OF THE ART

Alkali Activated Materials (AAMs) are defined as amorphous materials obtained by the combination of an aluminosilicate source, supplied mainly in powder form, with an alkaline activator, usually in concentrated aqueous solution. The aluminosilicate sources can be rich or poor in calcium silicate, such as metallurgical slag or fly ashes, respectively. The alkali sources can include essentially any soluble substance which can supply alkali metal cations, raise the pH of the reaction mixture and accelerate the dissolution of the solid precursor. The final products, generated after a suitable curing process, give rise to mechanically strong and chemically durables materials. In the last twenty years, a wide variety of alkaline activated binders, mainly conceived for the construction industry, have been developed with the aim of a technological, environmental and economic earning (Van Deventer et al., 2012).

"AAMs" is the broadest and generally accepted terminology for these materials (Provis and Bernal, 2014; Provis and Van Deventer, 2014b). However, the technology of alkali-activation predates this designation, with a first patent awarded to Kühl in 1908 (Kühl, 1908), the research conducted by Purdon in the 1930s-1950s (Purdon, 1940) and the extensive program of research, development and commercial-scale production grown from the work of Glukhovsky from the 1950s onwards (Glukhovsky, 1959). Davidovits, in the 1970s, developing and patenting materials obtained from the alkali-activation of metakaolin, contributed to give wide resonance to alkali activation. He introduced the name "geopolymers", nowadays largely known and used also for marketing purposes, highlighting the similarities between these synthetic materials and the three-dimensional silico-aluminate structures of natural tectosilicate minerals, like feldspathoids and zeolites (Davidovits, 1988; Davidovits, 1991). Anyway there are a surplus of names referring to alkali activated aluminosilicate materials as mineral polymers (Wastiels et al., 1994), inorganic polymers (Barbosa et al., 2000), soil-cements (Krivenko, 1997; Krivenko and Kovalchuk, 2007), hydroceramic (Siemer, 2002), low temperature aluminosilicate glass (Rahier et al., 1997), zeocements (Krivenko et al., 2007) and zeocemamics (Fernández-Jiménez et al., 2008). These, despite indicate the same type of materials, could mislead researchers, who are not familiar with the field.

In this Thesis, the terms AAMs and geopolymers will be used to indicate these compounds. In (Provis and van Deventer, 2014a) is reported an illustration (Figure I) that clearly shows the distinction between these materials. The image is a simplified representation of the chemistry of concrete-forming systems, based mainly on systems CaO-Al_2O_3-SiO_2-M_2O-Fe_2O_3-

SO_3-H_2O (where M is the alkali cation), that indicates the classification and position of the AAMs with respect to OPC and sulfoaluminate cementing systems. Geopolymers are shown as a subset of AAMs, with the highest Al and lowest Ca concentrations, to enable the formation of a network structure rather than the chains characteristic of calcium silicate hydrates. Low-calcium fly ashes and calcined clays are the most prevalent precursors used in geopolymer synthesis.

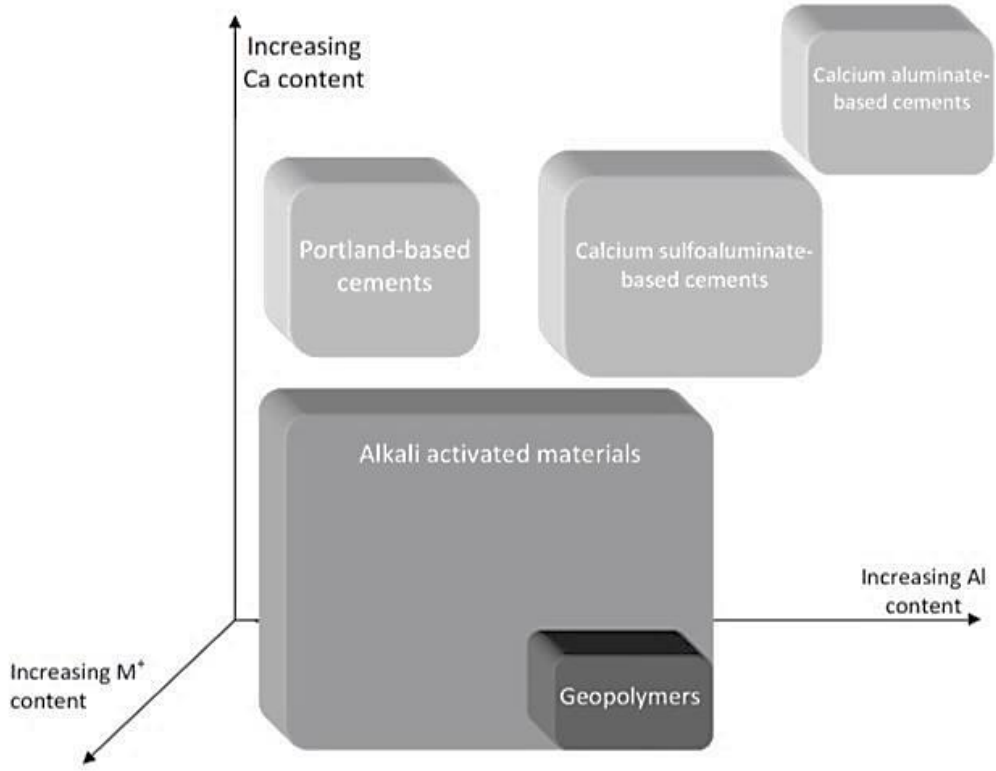

Figure I. Classification of AAMs, with comparisons to OPC and calcium sulfoaluminate binder chemistry. Shading indicates approximate alkali content; darker shading corresponds to higher concentrations of alkali (indicated as M^+ on the axis) (Provis and van Deventer, 2014a).

The main reasons why alkali-activation is gaining increasing recognition and interest are related to innovations that these materials are reaching, principally due to the points listed below.

From an environmental point of view, AAMs could be potential alternative to Portland cement (OPC). The manufacturing process of OPC has always been one of major source of emissions of carbon dioxide from industrial activities. This CO_2 is mainly generated by two processes: the combustion of a large amount of fossil fuels and the decomposition of $CaCO_3$ into CaO and CO_2 as main reaction chemistry. CO_2 emissions and energy consumption needed for the production of AAMs can be considerably lower than traditional OPC due to the absence in their synthesis of the calcination step necessary for clinker formation. In the production cycle of the

AAMs, the main source of CO_2 is attributed to the synthesis of alkaline hydroxide or silicate activating solutions (Turner and Collins, 2013). Many studies have been realized with a view towards reducing the CO_2 footprint (Duxson et al., 2007; Flatt et al., 2012; Pacheco-Torgal et al., 2008a), denoting that the potential reduction of CO_2 depend on the particular mix formulation and source of feedstock (Habert et al., 2011).

AAMs achieve good mechanical performances already after one day of curing, developing strengths comparables to OPC after 28 days of hardening (Hawa et al., 2013). Furthermore, they achieve similar or greater durability than that offered by traditional cements. It was in fact assessed their resistance to attack by sulphates (Bakharev, 2005a; Fernandez-Jimenez et al., 2007; Palomo et al., 1999a); resistance to acid attacks by chloride, like sea water, acids alkali (Bakharev, 2005b; Zhang et al., 2012); resistance to freeze-thaw (Husbands et al., 1994), leading to maintain until the 70% of their mechanical strength after 150 cycles (Škvára et al., 2005). Studies have shown also that these materials maintain good properties at high temperatures, enduring a very little structural damages up to 700-800°C (Barbosa and MacKenzie, 2003; Fernández-Jiménez et al., 2008; Fernández-Jiménez et al., 2010; Kong et al., 2007). AAMs can be used as immobilizers of certain toxic and/or hazardous waste, underlining their potentiality not only in construction but in many other fields (Deja, 2002; Shi and Fernandez-Jimenez, 2006). Certainly not all materials possess all of these properties, but modifying recipes and formulations is possible to achieve the required features.

Wastes developed by industrial processing, such as fly ash produced by burning coal in power plants or blast furnace slag, can be used as starting materials, thus avoiding the accumulation of wastes. Furthermore, a growing interest for the themes of sustainability and reuse of waste materials has been observed. In fact wastes derived by various human activities, until now under-utilized or simply dismissed, start to be valorised by the alkaline activation, producing economic and environmental benefits (Bernal et al., 2016; Payá et al., 2014).

I. Synthesis procedure and reaction process

Simply stated, the alkaline activation procedure can be described as the mechanical mixing of the alkaline solution and a finely milled aluminosilicate precursor. The workability of the mixture depends both on the desired chemical composition of the final product and on the solid/liquid ratio (Duxson et al., 2006a; Duxson et al., 2005a; Palomo and Glasser, 1992). The maturation phase, commonly called curing, can be carried out at temperature between 20°C and

about 100°C in controlled R.H. conditions, for different lengths of time. At the end of the curing, specimens are generally stored at room temperature until their use (Duxson et al., 2006b; Fernández-Jiménez and Palomo, 2005; Zuhua et al., 2009).

The reaction process can be conceptually described using the model proposed for the formation of some zeolites. Initially, the aluminum and silicon dissolved in the medium react to form a three-dimensional poly-hydroxy-silicoaluminate complex (Fernández-Jiménez et al., 2006; Weng et al., 2005). The Al and the Si, found in this product, are tetrahedrally coordinated, while the alkalis, that balance the electric charge generated by the substitution of Al^{3+} for Si^{4+}, are located in the voids of this framework. The resulting product is an alkaline aluminosilicate hydrate ($Na_2O{\cdot}Al_2O_3{\cdot}2SiO_2{\cdot}nH_2O$ type gel (N-A-S-H gel)), with a three-dimensional structure that, on an atomic to nanometric scale, resembles zeolitic structures (Provis et al., 2005; Shi et al., 2011). It is worth to highlight that the alkali-activation of aluminosilicates differs from the chemical process involved in traditional cement hydration, where the main reaction product is a calcium silicate gel ($CaO{\cdot}SiO_2{\cdot}nH_2O$ gel type (C-S-H)) (Shi et al., 2011).

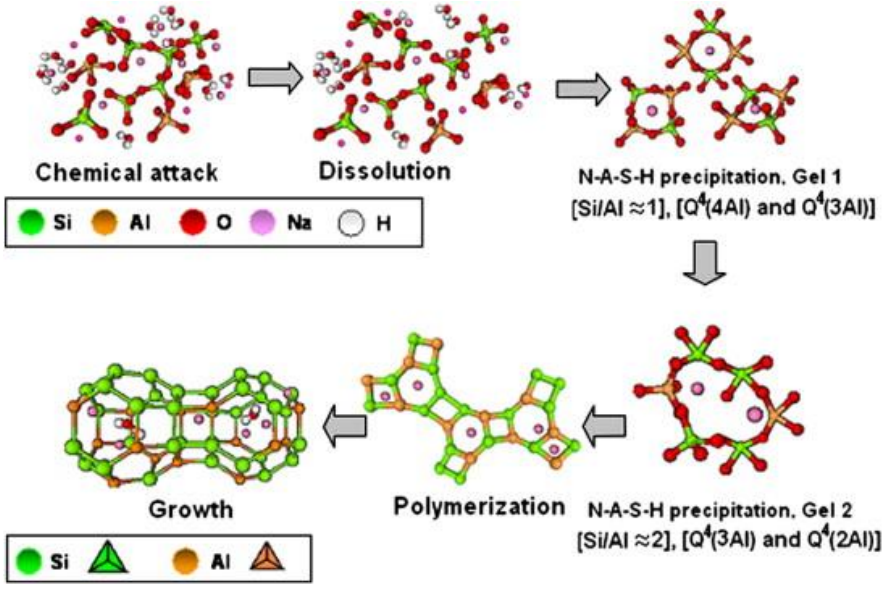

Figure II. Descriptive model for alkali activation of aluminosilicates (Shi et al., 2011).

A model that explains the mechanisms governing the formation of the three-dimensional structure of aluminosilicate alkaline gel, was first proposed by Glukhovsky (1959). The model describes a number of destruction–condensation transformations that take place in the starting solid. The initial units, with an unstable structure, give rise to a series of coagulated structures,

that at the end condense to generate the hydrated products. In the last years, the model projected by Glukhovsky has been improved by the work of different researchers (Duxson et al., 2006a; Shi et al., 2011) that proposed schematic models of N-A-S-H gel reaction process. The Figure II (Shi et al., 2011) outlines the processes occurring in the transformation of a solid aluminosilicate source into a synthetic alkali aluminosilicate. At first, disaggregation process entails the break of the M-O (M indicates the alkaline cation), Si-O-Si, Al-O-Al and Al-O-Si bonds in the starting material. This process is promoted by the strongly basic environment associated to water consumption and the formation of complex unstable products. The dissolution rate increases linearly with pH of the solution, and it is favoured by reducing the dimension of the alkaline cation used in the activation solution . At high pH, the fast dissolution rate, gives rise to the formation of a supersaturated aluminosilicate solution, which, by condensation, leads first to the formation of oligomers and then of large networks gel. This process releases the water that was consumed during dissolution, forming a bi-phasic system which is composed by the aluminosilicate binder and the water. The first intermediate reaction product (denominated Gel 1) contains high aluminium amounts due to the higher concentration of Al^{3+} ions in the alkaline medium during the early period of the process. Such higher concentration, in turn, can be attributed to the faster dissolution of aluminium than silicon, because Al-O bonds are weaker and hence more easily severed than Si-O bonds (Fernández-Jiménez et al., 2006; Provis et al., 2005). As the reaction progresses, more Si-O groups of the initial solid source are dissolved, favoring the evolution of the initial Gel 1 into a new Si-rich gel (Gel 2). After gelation, the gel structure continues to rearrange and reorganize, increasing oligomers connectivity and developing a three-dimensional aluminosilicate network. These processes of structural reorganization generate the microstructure and pore distribution of the material, which are fundamental in determining many physical properties (Duxson et al., 2005b).

The abovementioned three-dimensional order exists on the atomic scale only. The general chemical formula of resulting amorphous material can be summarised as $M_n[-(SiO_2)_z-AlO_2]_n \bullet wH_2O$, where M is the alkali cation, n is the degree of polymerization and z usually varies from 1 to 3.

II. Starting materials

Two main compounds, an alkaline activator and an aluminosilicate precursor are the starting materials required in the synthesis of AAMs, as described in previous paragraphs.

Among the natural raw materials, largely widespread are clay minerals, such as kaolinite, illite and smectite, which need to be activated to improve their reactivity under alkaline conditions. The clay activation generally consists in the thermal treatments in a temperature range between about 500°C and 800°C (Buchwald et al., 2009; Elimbi et al., 2011; Gasparini et al., 2013), but a mechanochemical prolonged milling was also and successfully used (Makó et al., 2001; Rescic et al., 2011; Temuujin et al., 2009). The result is the loss of structural hydroxyl ions of the clay minerals and the consequently breakdown or partial breakdown of their layered structure, which is responsible of the material reactivity under alkaline conditions. Among the calcined clays, metakaolin represents the most studied precursor, due to its high reactivity and the good properties in terms of resistance and durability of the final products (Duxson et al., 2006a; Palomo et al., 1999a; Rashad, 2013; Siddique and Klaus, 2009). The base structure of metakaolin is that of a highly disrupted phyllosilicate structure containing silicon and aluminum only. Although most commercial metakaolin contains levels of impurities, the effect of these impurities is limited both by their low dissolution and the inability of the products of their dissolution to affect the formation mechanism. In general, the knowledge gained by investigation of metakaolin-based alkali activated materials may be applied to all metakaolin supplies in the world (Duxson et al., 2006a).

Among the industrial by-products, largely used are the blast furnace slags (BFS) from iron-making processes and the fly ashes from coal combustion power plant. In literature, many studies on their characterization and on the performances of pastes, mortars and concrete can be found (Duxson and Provis, 2008; Fernández-Jiménez and Palomo, 2005; Palomo et al., 1999b; Puertas et al., 2000). In particular fly ashes are an industrial waste that not derived from a well-defined starting material. They are the incombustible mineral associated with the coal, predominantly made up of silicon, aluminum and iron oxides, as well as different amounts of calcium (class C and F ashes). Fly ashes pass through the boiler furnace and are collected in the chimneys by electrostatic precipitators. The particles in fly ash are generally spherical, but inhomogeneous, such as is inhomogeneous the particle size distribution, and comprise glassy as well as crystalline (often mullite and quartz) phases (Duxson et al., 2006a). Pioneering investigations on the main characteristics of fly ashes were performed by (Fernández-Jiménez and Palomo, 2005; Fernández-Jiménez et al., 2006; Palomo et al., 1999b). Slags and/or fly ashes can be further combined with secondary raw materials to maximise the conversion of wastes into novel resources (Horpibulsuk et al., 2015; Ruiz-Santaquiteria et al., 2013).

Alkali activation can be applied to any material with a sufficiently high content of reactive Al_2O_3 and SiO_2 species. Studies concerning the identification of other potential raw precursors in the synthesis of AAMs, have been recently collected in two recent reviews (Bernal et al., 2016; Payá et al., 2014). Based on their chemical compositions, content of amorphous phases and degree of reactivity, the potential valorisation of wastes through alkali activation can be addressed through two general alternative pathways: using the waste as main precursor for the production of an alkali activated binder; using the as a secondary precursor or blending agent or even as an aggregate. In recent years, there has been a significant growth in the use of different urban, industrial and mining wastes (Lancellotti et al., 2010; Pacheco-Torgal et al., 2009; Provis, 2009), sewage sludges and reservoir sludges (Chen et al., 2009; Ferone et al., 2013; Yang et al., 2013), waste glasses (Avila-López et al., 2015; Puertas and Torres-Carrasco, 2014), rice husk (Mejía et al., 2013; Sturm et al., 2016) and other mining and mineral wastes (Ahmari and Zhang, 2012; Ferone et al., 2015; Li et al., 2014; Pacheco-Torgal et al., 2008c) as precursors for the production of alkali-activated materials.

Alkali activators are compounds that, either in liquid or solid state, are capable of generating a basicity high enough to successfully hydrolyze the starting aluminosilicate. The alkaline solutions are usually alkaline metal or alkaline-earth hydroxides (MOH, $M(OH)_2$), weak acid salts (M_2CO_3, M_2S, MF), strong acid salts (Na_2SO_4, $CaSO_4 \cdot 2H_2O$), aluminates ($M_2O \bullet nAl_2$) and $N_2O(n)SiO_2$-type siliceous salts, where M is the alkaline ion such as Na or K. Sodium and potassium hydroxides (NaOH, KOH) are commonly used (*e.g.* Pachego-Torgal et al., (2008b) and reference therein), however the related hydrated silicates solutions, also called waterglass, are largely employed especially because alkaline activator behaves more swiftly when the soluble silica is present, as reported by (Palomo et al., 1999b). That statement is also shared by (Criado et al., 2005; Fernández-Jiménez et al., 1999), according to whom waterglass favours the polymerization process leading to a reaction product with mechanical strength and good durability. Recently alternative alkaline activators, derived by waste materials, have been also tested (Torres-Carrasco et al., 2015).

In this Thesis will be used an high quality kaolin, class F fly ashes, sewage sludges derived by the cultivation of an ornamental stone and NaOH and $Na_2O \bullet nSiO_2$ (waterglass) respectively as starting materials and activator solutions.

III. Chemistry and structure of hardened alkali activated materials

Aluminosilicate sources and activation solutions are responsible of the good mechanical, physical and chemical properties of AAMs. Based on the nature of starting components, AAMs show extremely diverse chemistry and structure, so much to be grouped under two main categories: low-calcium and rich-calcium AAMs. Calcium appears to be the main determinant in terms of silicates structure. The Figure III proposed by (Provis and Bernal, 2014) shows how the primary reaction products are either an alkali aluminosilicate (N-A-S-H) type gel or a calcium aluminosilicate hydrate (C-A-S-H) type gel[1].

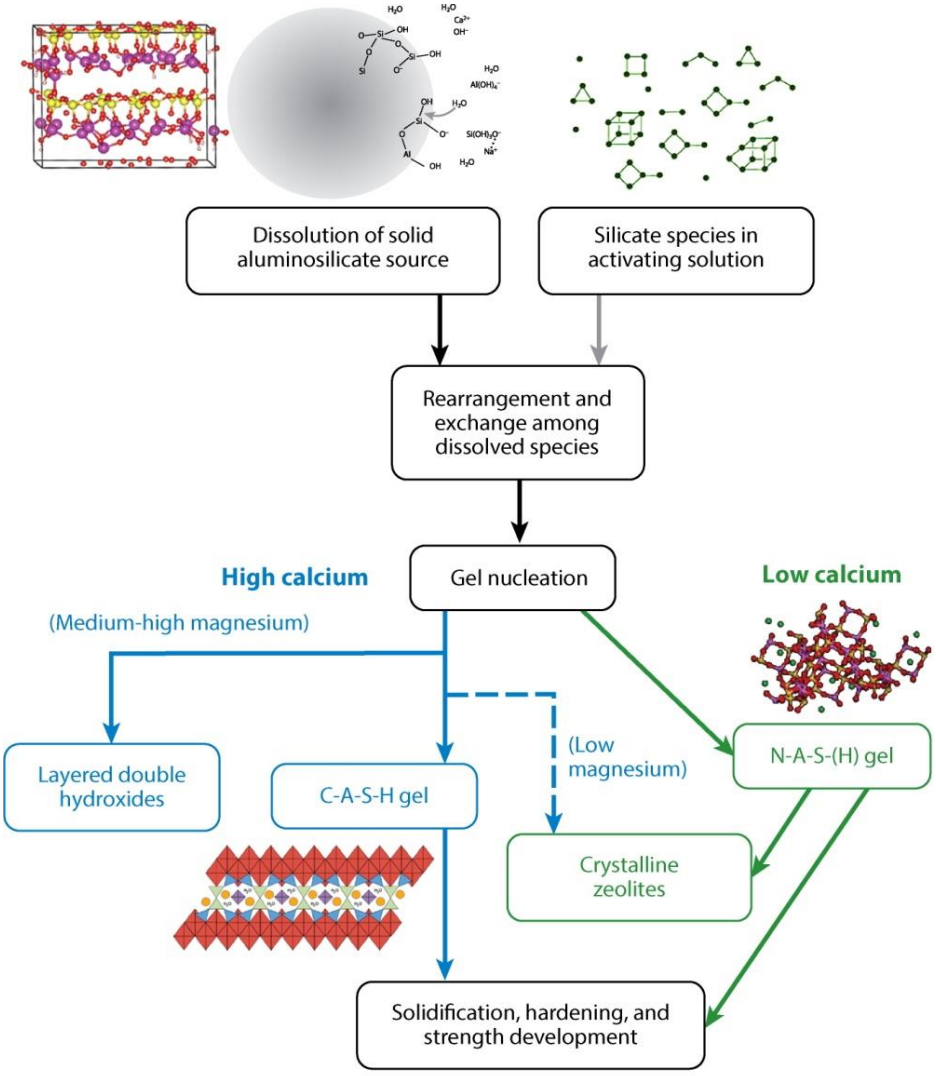

Figure III. Process and reaction products of alkaline activation of a solid aluminosilicate precursor. High-calcium systems react according to the left-hand (blue) pathway; low-calcium systems react according to the right-hand (green) pathway (Provis and Bernal, 2014).

[1] Abbreviations used in cement chemists are: S to represent SiO_2, A for Al_2O_3, C for CaO, N for Na_2O, K for K_2O, and H for H_2O.

The first of these gel types is represented as N-A-S-H, but can also show substitution of potassium (up to 100% replacement of sodium) or substitution of calcium for sodium, so a more complete description may be N,K-(C)-A-S-H. Furthermore the water is not a major structural component as it is in C-A-S-H-type gel (Allen et al., 2007). This gel is formed by silicon and aluminum, tetrahedrally coordinated with oxygen and randomly distributed, that intertwine forming a three-dimensional structure in which cavities are suitable to accommodate alkaline cations, to compensate for the deficit generated by electronegative charge presence of aluminum in tetrahedral coordination. N-A-S-H type gel can be also considered as a zeolites precursor (Davidovits, 1991; Provis et al., 2005), in effect zeolites can be revealed as secondary products of the reaction. Metakaolin and fly ashes (type F according to ASTM classification) belong to this first group.

In the rich-calcium AAMs, C-A-S-H gels are formed by layers of tetrahedrally coordinated silicate chains with a dreierketten structure, in which each chain containing (3*n*-1) tetrahedra for an integer value of *n*, as occur in the disordered tobermorite-like structure in OPC systems. The interlayer region contains Ca^{2+} cations, alkalis and the water of hydration that is chemically incorporated into the gel structure. Some alkali cations also balance the negative charge generated when Al^{3+} replaces Si^{4+} in the tetrahedral chain sites (Fernández-Jiménez et al., 2003; Myers et al., 2013). The second group is represented mainly by vitreous blast furnace slag (BFS). In fact, activation of BFS, takes place through a process of polymerization and crystallization of a main gel C-S-H (calcium silicate hydrate), similar to that obtained in hydration Portland cement, that incorporates a significant percentage of aluminum (Puertas et al., 2011).

IV. Alkali activated materials in construction industry

AAMs have been utilized on a significant scale in the construction of buildings and other civil infrastructure components since the 1950s in Western Europe, the 1960s in the former USSR and since the 1980s in Finland, China, Australia, the USA and other countries. The small scale tests and large scale industrial trials with alkaline cements (applications in areas such as hydroelectric engineering, roads, civil engineering and mining) have confirmed the high performance of the constructions made with such cements.

The efficiency and potential of these cements have been amply resumed by different researches (Brodko, 1999; Palomo et al., 2014; Provis and van Deventer, 2014a; Shi et al.,

2006). Furthermore a large number of private companies, such as Zeobond and Ceratech, have been engaging in the manufacture, commercialization and use of alkaline (primarily blast furnace slag) cement-based concrete, in a wide range of construction applications (Van Deventer et al., 2012).

In Lipetsk, Russia, several high-rise residential buildings (exceeding 20 floors) were built using different alkali activated BFS precast elements (exterior walls, floor slabs, stairways) by the industrial enterprise Tsentrmetallurgremont between 1986 and 1994. Other residential buildings were fabricated in Mariupol, Ukraine, in 1960, using alkali hydroxide and activated BFS precast blocks; in 1974 in Kraków, Poland, to build a storehouse using precast steel-reinforced alkali carbonate activated BFS concrete; in 1988 in Yinshan County, Hubei Province, China, to build a six-storey building (Shi et al., 2006). AAMs were also used in the construction of drainage collector (Odessa, Ukraine, in1966), roads (Magnitogorsk, Russia, in 1984); railway sleepers (Japan, Poland, Spain, since 1980), roofing tiles (Helsinki, Finland, in 1988), precast panels, bridge retaining walls, footpaths, pavement and ground works (Australia, produced by Zeobond Group, since 2006) (Provis and van Deventer, 2014a and the references therein). It was noted that the alkali activated cements and concretes, which have been placed into service, have been able to serve the purposes for which they were designed, without evident problems related to mechanical or chemical decay, surpassing OPC performances used in the same areas. Performance tests and indicated that the properties of cements and concretes depend on the raw materials used, service conditions and age.

The development of AAMs marketing, not in every case has been a success: complications related to water request, curing conditions and workability, have made in some cases AAMs less applicable than OPC. However, there is a growing body of evidence which speaks in favour of the usability, durability and marketability of alkali activated cements and concretes in civil infrastructure applications.

V. Alkali activated materials and conservation of Cultural Heritage

A rising interest on applicability of AAMs in the field of conservation of built Heritage was observed in the last few years, thanks to the versatility and potentiality of these materials. The experimentation and the use of unconventional materials could result convenient owing to the great variability of constructions, ancient but also contemporary, especially considering that, many architectures of the last century, mainly built in concrete, nowadays are became integral

part of built heritage. Surely the knowledge of basic properties of the new material is the first step and, in the case of AAMs, there is a substantial body of more or less recent literature (as listed in the previous paragraphs). Experimental studies of the properties of retrofitting materials are decisive to improve the knowledge of the whole restoration process.

Concerning applications in Cultural heritage one of the first studies on geopolymers has been conducted for the consolidation of terracotta structures (Hanzlíček et al., 2009). Geopolymer composites have been used as fixing and joining materials for reinforcement the unseen part of a Baroque statue, underlining the versatility of geopolymers both from workability point of view and to achieve a similar color shade of the original ceramic mass.

A more recent use regards the suitability of metakaolin-based geopolymers for the restoration of historic tiles (Geraldes et al., 2016). A chemical–mineralogical similitude to the ceramic body and a versatile range of physical properties have been obtained modifying the geopolymer formulation. Effectively, the results highlight that physical properties similar to those of the substrate, increase the compatibility parameters. Furthermore acting to prevent water evaporation allows a cracking reduction, thus to minimize the chances of poor adhesion to the substrate, as well as the disaggregation of the pastes when applied onto the tile. The problem of carbonation and the subsequent formation of highly soluble salts, has been solved by authors through desalination during the restoration process.

Metakaolin based geopolymers have been the object of a further work (Allali et al., 2016), aimed to develop a stable and durable coating mortars in which different amount of calcium hydroxide (lime) and calcium carbonate (calcareous sand) have been substituted to metakaolin.

AAMs fit for the purpose of stone consolidation or as restoration mortars has been also produced through mechanochemical activation of quartz and kaolin (Rescic et al., 2011). These starting materials have been modified by grinding at different times and by evaluating the reactivity degree through the study of the changes induced on their crystalline structure. In the authors' opinion, the mechanochemical activation process could achieve the result to reduce the use of alkaline solutions as activators until not harmful amounts for the monuments.

Alkaline activation has been also proposed in order to stabilize clay-rich soils used in earthen architecture (Elert et al., 2015; Elert et al., 2008). Clays from the Alhambra Formation (Spain) were undergone significant mineralogical and textural changes following long-term treatment with diluted alkaline solutions of $Ca(OH)_2$, NaOH and KOH at room temperature.

These improvements have been the result of the dissolution of clay minerals and their transformation into amorphous phases with cementing properties. However the tests represent preliminary laboratory outcomes and the authors suggest to monitor over extended periods of time test areas in historic earthen structures.

The production of pastes/mortars with properties suitable to repointing existing masonries (i.e., filling the most external part of mortar joints, lost due to deterioration processes) has been evaluated by (Sassoni et al., 2016) through the alkali-activation of recycled materials. The performances of brick wastes have been compared to those of traditional lime-based mortars through studies of porosity, water absorption and water vapor permeability. These tests have been considered fundamental for fulfilling the compatibility requirements with the masonry substrate, due to the possible reduction of water exchanges between masonry and the environment, and the subsequent degradation, after the restoration. The results have evidenced the formation of a large amount of efflorescences caused by an insufficient SiO_2/Al_2O_3 ratio. This produced an increase in water absorption and a decrease in water vapor permeability, thus to suggested a further optimization of the mix design to avoid harmful consequence for the historic mansonries. Furthermore better results have been obtained with a curing at 50°C, though preventing their use in open environments at room temperature.

Concluding this brief dissertation on AAMs and Cultural Heritage, metakaolin has been noted to be the most suitable and used precursor for the synthesis of AAMs, not only because a fairly pure and homogenous material is necessary, but also because owns properties such as the high level of resistance to a range of different acids and salt solutions, low shrinkage and low thermal conductivity (Duxson et al., 2007; Lee and van Deventer, 2007; Palomo et al., 1999a) that are of extreme importance in the restoration field. However some aspects were identified which deserve further research. These include the study of some physical properties, such as the thermal ones, but above all, the durability in open environments. It is worth to underline that hardly the positive outcome of the laboratory studies have been confirmed by in situ applications. Application on real cases could help to assess the validity of these promising materials.

Starting from the encouraging findings obtained in the above-mentioned studies, in this PhD Thesis, alkali-activated pastes, mortars and composites have been formulated and manufactured. Their structural, microstructural and physical-mechanical properties have been

studied in order to investigate their compatibility with existing materials belonging to Cultural Heritage. In particular the interaction with some ornamental stones, largely widespread in the Italian architecture, has been the central idea of all the work. The theme of reuse has been also investigated through the valorization of recycled starting materials deriving by quarrying of an Italian sandstone called Pietra Serena.

References

Ahmari, S., Zhang, L., 2012. Production of eco-friendly bricks from copper mine tailings through geopolymerization. Construction and Building Materials 29, 323-331.

Allali, F., Joussein, E., Kandri, N.I., Rossignol, S., 2016. The influence of calcium content on the performance of metakaolin-based geomaterials applied in mortars restoration. Materials and Design 103, 1-9.

Allen, A.J., Thomas, J.J., Jennings, H.M., 2007. Composition and density of nanoscale calcium–silicate–hydrate in cement. Nature materials 6, 311-316.

Avila-López, U., Almanza-Robles, J.M., Escalante-García, J.I., 2015. Investigation of novel waste glass and limestone binders using statistical methods. Construction and Building Materials 82, 296-303.

Bakharev, T., 2005a. Durability of geopolymer materials in sodium and magnesium sulfate solutions. Cement and Concrete Research 35, 1233-1246.

Bakharev, T., 2005b. Resistance of geopolymer materials to acid attack. Cement and Concrete Research 35, 658-670.

Barbosa, V.F., MacKenzie, K.J., 2003. Synthesis and thermal behaviour of potassium sialate geopolymers. Materials Letters 57, 1477-1482.

Barbosa, V.F.F., MacKenzie, K.J.D., Thaumaturgo, C., 2000. Synthesis and characterisation of materials based on inorganic polymers of alumina and silica: Sodium polysialate polymers. International Journal of Inorganic Materials 2, 309-317.

Bernal, S.A., Rodríguez, E.D., Kirchheim, A.P., Provis, J.L., 2016. Management and valorisation of wastes through use in producing alkali-activated cement materials. Journal of Chemical Technology and Biotechnology.

Brodko, O.A., 1999. Experience of explotation of the alkaline ements concrete. Proceedings of the Second International Conference on Alkaline Cements and Concrete, 657-684.

Buchwald, A., Hohmann, M., Posern, K., Brendler, E., 2009. The suitability of thermally activated illite/smectite clay as raw material for geopolymer binders. Applied Clay Science 46, 300-304.

Chen, J.-H., Huang, J.-S., Chang, Y.-W., 2009. A preliminary study of reservoir sludge as a raw material of inorganic polymers. Construction and Building Materials 23, 3264-3269.

Criado, M., Palomo, A., Fernández-Jiménez, A., 2005. Alkali activation of fly ashes. Part 1: Effect of curing conditions on the carbonation of the reaction products. Fuel 84, 2048-2054.

Davidovits, J., 1988. Geopolymer chemistry and properties, Geopolymer, pp. 25-48.

Davidovits, J., 1991. Geopolymers - Inorganic polymeric new materials. Journal of Thermal Analysis 37, 1633-1656.

Deja, J., 2002. Immobilization of Cr6+, Cd2+, Zn2+ and Pb2+ in alkali-activated slag binders. Cement and Concrete Research 32, 1971-1979.

Duxson, P., Fernández-Jiménez, A., Provis, J.L., Lukey, G.C., Palomo, A., van Deventer, J.S.J., 2006a. Geopolymer technology: the current state of the art. Journal of Materials Science 42, 2917-2933.

Duxson, P., Lukey, G.C., Separovic, F., Van Deventer, J.S.J., 2005a. Effect of alkali cations on aluminum incorporation in geopolymeric gels. Industrial and Engineering Chemistry Research 44, 832-839.

Duxson, P., Lukey, G.C., van Deventer, J.S., 2006b. Thermal evolution of metakaolin geopolymers: Part 1–Physical evolution. Journal of Non-Crystalline Solids 352, 5541-5555.

Duxson, P., Provis, J.L., 2008. Designing precursors for geopolymer cements. Journal of the American Ceramic Society 91, 3864-3869.

Duxson, P., Provis, J.L., Lukey, G.C., Mallicoat, S.W., Kriven, W.M., van Deventer, J.S.J., 2005b. Understanding the relationship between geopolymer composition, microstructure and mechanical properties. Colloids and Surfaces A: Physicochemical and Engineering Aspects 269, 47-58.

Duxson, P., Provis, J.L., Lukey, G.C., van Deventer, J.S.J., 2007. The role of inorganic polymer technology in the development of ‘green concrete’. Cement and Concrete Research 37, 1590-1597.

Elert, K., Pardo, E.S., Rodriguez-Navarro, C., 2015. Alkaline activation as an alternative method for the consolidation of earthen architecture. Journal of Cultural Heritage 16, 461-469.

Elert, K., Sebastián, E., Valverde, I., Rodriguez-Navarro, C., 2008. Alkaline treatment of clay minerals from the Alhambra Formation: Implications for the conservation of earthen architecture. Applied Clay Science 39, 122-132.

Elimbi, A., Tchakoute, H., Njopwouo, D., 2011. Effects of calcination temperature of kaolinite clays on the properties of geopolymer cements. Construction and Building Materials 25, 2805-2812.

Fernandez-Jimenez, A., García-Lodeiro, I., Palomo, A., 2007. Durability of alkali-activated fly ash cementitious materials. Journal of Materials Science 42, 3055-3065.

Fernández-Jiménez, A., Monzó, M., Vicent, M., Barba, A., Palomo, A., 2008. Alkaline activation of metakaolin-fly ash mixtures: Obtain of Zeoceramics and Zeocements. Microporous and Mesoporous Materials 108, 41-49.

Fernández-Jiménez, A., Palomo, A., 2005. Mid-infrared spectroscopic studies of alkali-activated fly ash structure. Microporous and Mesoporous Materials 86, 207-214.

Fernández-Jiménez, A., Palomo, A., Sobrados, I., Sanz, J., 2006. The role played by the reactive alumina content in the alkaline activation of fly ashes. Microporous and Mesoporous Materials 91, 111-119.

Fernández-Jiménez, A., Palomo, J.G., Puertas, F., 1999. Alkali-activated slag mortars: Mechanical strength behaviour. Cement and Concrete Research 29, 1313-1321.

Fernández-Jiménez, A., Palomo, A., Pastor, J.Y., Martin, A., 2008. New Cementitious Materials Based on Alkali-Activated Fly Ash: Performance at High Temperatures. Journal of the American Ceramic Society 91, 3308-3314.

Fernández-Jiménez, A., Pastor, J.Y., Martín, A., Palomo, A., 2010. High-Temperature Resistance in Alkali-Activated Cement. Journal of the American Ceramic Society 93, 3411-3417.

Fernández-Jiménez, A., Puertas, F., Sobrados, I., Sanz, J., 2003. Structure of calcium silicate hydrates formed in alkaline-activated slag: influence of the type of alkaline activator. Journal of the American Ceramic Society 86, 1389-1394.

Ferone, C., Colangelo, F., Cioffi, R., Montagnaro, F., Santoro, L., 2013. Use of reservoir clay sediments as raw materials for geopolymer binders. Advances in Applied Ceramics 112, 184-189.

Ferone, C., Liguori, B., Capasso, I., Colangelo, F., Cioffi, R., Cappelletto, E., Di Maggio, R., 2015. Thermally treated clay sediments as geopolymer source material. Applied Clay Science 107, 195-204.

Flatt, R.J., Roussel, N., Cheeseman, C.R., 2012. Concrete: An eco material that needs to be improved. Journal of the European Ceramic Society 32, 2787-2798.

Gasparini, E., Tarantino, S.C., Ghigna, P., Riccardi, M.P., Cedillo-González, E.I., Siligardi, C., Zema, M., 2013. Thermal dehydroxylation of kaolinite under isothermal conditions. Applied Clay Science 80-81, 417-425.

Geraldes, C.F.M., Lima, A.M., Delgado-Rodrigues, J., Mimoso, J.M., Pereira, S.R.M., 2016. Geopolymers as potential repair material in tiles conservation. Applied Physics A: Materials Science and Processing 122, 1-10.

Glukhovsky, V.D., 1959. Gruntosilikaty (Soil Silicates).

Habert, G., De Lacaillerie, J.D.E., Roussel, N., 2011. An environmental evaluation of geopolymer based concrete production: reviewing current research trends. Journal of Cleaner Production 19, 1229-1238.

Hanzlíček, T., Steinerová, M., Straka, P., Perná, I., Siegl, P., Švarcová, T., 2009. Reinforcement of the terracotta sculpture by geopolymer composite. Materials and Design 30, 3229-3234.

Hawa, A., Tonnayopas, D., Prachasaree, W., Taneerananon, P., 2013. Development and Performance Evaluation of Very High Early Strength Geopolymer for Rapid Road Repair. Advances in Materials Science and Engineering 2013, 9.

Horpibulsuk, S., Suksiripattanapong, C., Samingthong, W., Rachan, R., Arulrajah, A., 2015. Durability against Wetting–Drying Cycles of Water Treatment Sludge–Fly Ash Geopolymer and Water Treatment Sludge–Cement and Silty Clay–Cement Systems. Journal of Materials in Civil Engineering 28, 04015078.

Husbands, T.B., Malone, P.G., Wakeley, L.D., Engineers, U.S.A.C.o., Station, U.S.A.E.W.E., Program, C.P.A.R., 1994. Performance of Concretes Proportioned with Pyrament Blended Cement. U.S. Army Engineer Waterways Experiment Station.

Kong, D.L., Sanjayan, J.G., Sagoe-Crentsil, K., 2007. Comparative performance of geopolymers made with metakaolin and fly ash after exposure to elevated temperatures. Cement and Concrete Research 37, 1583-1589.

Krivenko, P., 1997. Alkaline cements: terminology, classification, aspects of durability, Proceedings of the 10th International Congress on the Chemistry of Cement, Gothenburg, Sweden, Amarkai and Congrex Göteborg, Gothenburg, Sweden, p. 6.

Krivenko, P., Kovalchuk, G., Palomo, A., FernÁndez-JimÉnez, A., 2007. Fly Ash Based Geocements: Genesis of Microstructure and Properties at Hydration-Dehydration Process, Brittle Matrix Composites 8, pp. 55-64.

Krivenko, P.V., Kovalchuk, G.Y., 2007. Directed synthesis of alkaline aluminosilicate minerals in a geocement matrix. Journal of Materials Science 42, 2944-2952.

Kühl, H., 1908. Slag Cement and Process of Making the Same.

Lancellotti, I., Kamseu, E., Michelazzi, M., Barbieri, L., Corradi, A., Leonelli, C., 2010. Chemical stability of geopolymers containing municipal solid waste incinerator fly ash. Waste Management 30, 673-679.

Lee, W.K.W., van Deventer, J.S.J., 2007. Chemical interactions between siliceous aggregates and low-Ca alkali-activated cements. Cement and Concrete Research 37, 844-855.

Li, C., Zhang, T., Wang, L., 2014. Mechanical properties and microstructure of alkali activated Pisha sandstone geopolymer composites. Construction and Building Materials 68, 233-239.

Makó, É., Frost, R.L., Kristóf, J., Horváth, E., 2001. The effect of quartz content on the mechanochemical activation of kaolinite. Journal of Colloid and Interface Science 244, 359-364.

Mejía, J.M., Mejía de Gutiérrez, R., Puertas, F., 2013. Rice husk ash as a source of silica in alkali-activated fly ash and granulated blast furnace slag systems. Materiales de Construcción 63, 361-375.

Myers, R.J., Bernal, S.A., San Nicolas, R., Provis, J.L., 2013. Generalized structural description of calcium–sodium aluminosilicate hydrate gels: the cross-linked substituted tobermorite model. Langmuir 29, 5294-5306.

Pacheco-Torgal, F., Castro-Gomes, J., Jalali, S., 2008a. Alkali-activated binders: A review. Part 1. Historical background, terminology, reaction mechanisms and hydration products. Construction and Building Materials 22, 1305-1314.

Pacheco-Torgal, F., Castro-Gomes, J., Jalali, S., 2008b. Alkali-activated binders: A review. Part 2. About materials and binders manufacture. Construction and Building Materials 22, 1315-1322.

Pacheco-Torgal, F., Castro-Gomes, J., Jalali, S., 2008c. Properties of tungsten mine waste geopolymeric binder. Construction and Building Materials 22, 1201-1211.

Pacheco-Torgal, F., Jalali, S., Castro Gomes, J.P., 2009. 13 - Utilization of mining wastes to produce geopolymer binders, Geopolymers. Woodhead Publishing, pp. 267-293.

Palomo, A., Blanco-Varela, M.T., Granizo, M.L., Puertas, F., Vazquez, T., Grutzeck, M.W., 1999a. Chemical stability of cementitious materials based on metakaolin. Cement and Concrete Research 29, 997-1004.

Palomo, A., Glasser, F., 1992. Chemically-bonded cementitious materials based on metakaolin. British ceramic. Transactions and journal 91, 107-112.

Palomo, A., Grutzeck, M.W., Blanco, M.T., 1999b. Alkali-activated fly ashes: A cement for the future. Cement and Concrete Research 29, 1323-1329.

Palomo, A., Krivenko, P., Garcia-Lodeiro, I., Kavalerova, E., Maltseva, O., Fernández-Jiménez, A., 2014. A review on alkaline activation: new analytical perspectives. Materiales de Construcción 64, e022.

Payá, J., Monzó, J., Borrachero, M.V., Tashima, M.M., 2014. Reuse of aluminosilicate industrial waste materials in the production of alkali-activated concrete binders, Handbook of Alkali-Activated Cements, Mortars and Concretes, pp. 487-518.

Provis, J.L., 2009. 19 - Immobilisation of toxic wastes in geopolymers, Geopolymers. Woodhead Publishing, pp. 421-440.

Provis, J.L., Bernal, S.A., 2014. Geopolymers and related alkali-activated materials, Annual Review of Materials Research, pp. 299-327.

Provis, J.L., Lukey, G.C., Van Deventer, J.S.J., 2005. Do geopolymers actually contain nanocrystalline zeolites? a reexamination of existing results. Chemistry of Materials 17, 3075-3085.

Provis, J.L., van Deventer, J.S., 2014a. Alkali activated materials. Springer.

Provis, J.L., Van Deventer, J.S.J., 2014b. Alkali Activated Materials: State-of-the-art Report, RILEM TC 224-AAM.

Puertas, F., Martínez-Ramírez, S., Alonso, S., Vázquez, T., 2000. Alkali-activated fly ash/slag cements: Strength behaviour and hydration products. Cement and Concrete Research 30, 1625-1632.

Puertas, F., Palacios, M., Manzano, H., Dolado, J.S., Rico, A., Rodríguez, J., 2011. A model for the C-A-S-H gel formed in alkali-activated slag cements. Journal of the European Ceramic Society 31, 2043-2056.

Puertas, F., Torres-Carrasco, M., 2014. Use of glass waste as an activator in the preparation of alkali-activated slag. Mechanical strength and paste characterisation. Cement and Concrete Research 57, 95-104.

Purdon, A.O., 1940. The action of alkalis on blast-furnace slag. J Soc Chem Ind 59, 191-202.

Rahier, H., Simons, W., Van Mele, B., Biesemans, M., 1997. Low-temperature synthesized aluminosilicate glasses: Part III Influence of the composition of the silicate solution on production, structure and properties. Journal of Materials Science 32, 2237-2247.

Rashad, A.M., 2013. Alkali-activated metakaolin: A short guide for civil Engineer – An overview. Construction and Building Materials 41, 751-765.

Rescic, S., Plescia, P., Cossari, P., Tempesta, E., Capitani, D., Proietti, N., Fratini, F., Mecchi, A., 2011. Mechano-chemical activation: an ecological safety process in the production of materials to stone conservation. Procedia Engineering 21, 1061-1071.

Ruiz-Santaquiteria, C., Fernández-Jiménez, A., Skibsted, J., Palomo, A., 2013. Clay reactivity: Production of alkali activated cements. Applied Clay Science 73, 11-16.

Sassoni, E., Pahlavan, P., Franzoni, E., Bignozzi, M.C., 2016. Valorization of brick waste by alkali-activation: A study on the possible use for masonry repointing. Ceramics International 42, 14685-14694.

Shi, C., Fernandez-Jimenez, A., 2006. Stabilization/solidification of hazardous and radioactive wastes with alkali-activated cements. Journal of hazardous materials 137, 1656-1663.

Shi, C., Jiménez, A.F., Palomo, A., 2011. New cements for the 21st century: The pursuit of an alternative to Portland cement. Cement and Concrete Research 41, 750-763.

Shi, C., Roy, D., Krivenko, P., 2006. Alkali-activated cements and concretes. CRC press.

Siddique, R., Klaus, J., 2009. Influence of metakaolin on the properties of mortar and concrete: A review. Applied Clay Science 43, 392-400.

Siemer, D.D., 2002. Hydroceramics, a "new" cementitious waste form material for U.S. defense-type reprocessing waste. Materials Research Innovations 6, 96-104.

Škvára, F., Jílek, T., Kopecký, L., 2005. Geopolymer materials based on fly ash. Ceram.-Silik 49, 195-204.

Sturm, P., Gluth, G.J.G., Brouwers, H.J.H., Kühne, H.C., 2016. Synthesizing one-part geopolymers from rice husk ash. Construction and Building Materials 124, 961-966.

Temuujin, J., Williams, R., Van Riessen, A., 2009. Effect of mechanical activation of fly ash on the properties of geopolymer cured at ambient temperature. Journal of Materials Processing Technology 209, 5276-5280.

Torres-Carrasco, M., Rodríguez-Puertas, C., Alonso, M.d.M., Puertas, F., 2015. Alkali activated slag cements using waste glass as alternative activators. Rheological behaviour. Boletín de la Sociedad Española de Cerámica y Vidrio 54, 45-57.

Turner, L.K., Collins, F.G., 2013. Carbon dioxide equivalent (CO2-e) emissions: A comparison between geopolymer and OPC cement concrete. Construction and Building Materials 43, 125-130.

Van Deventer, J.S.J., Provis, J.L., Duxson, P., 2012. Technical and commercial progress in the adoption of geopolymer cement. Minerals Engineering 29, 89-104.

Wastiels, J., Wu, X., Faignet, S., Patfoort, G., 1994. Mineral polymer based on fly ash. J RESOUR MANAGE TECHNOL 22, 135-141.

Weng, L., Sagoe-Crentsil, K., Brown, T., Song, S., 2005. Effects of aluminates on the formation of geopolymers. Materials Science and Engineering B: Solid-State Materials for Advanced Technology 117, 163-168.

Yang, K.-H., Lo, C.-W., Huang, J.-S., 2013. Production and properties of foamed reservoir sludge inorganic polymers. Cement and Concrete Composites 38, 50-56.

Zhang, Z., Yao, X., Wang, H., 2012. Potential application of geopolymers as protection coatings for marine concrete III. Field experiment. Applied Clay Science 67–68, 57-60.

Zuhua, Z., Xiao, Y., Huajun, Z., Yue, C., 2009. Role of water in the synthesis of calcined kaolin-based geopolymer. Applied Clay Science 43, 218-223.

CHAPTER 1

GEOPOLYMER BASED MORTARS WITH ORNAMENTAL STONE AGGREGATES

1.1. Introduction

Conservation practices make cultural heritage available to future generations. The maintenance of historic structures brings to the use of traditional materials and methods, but more and more frequently new ones are developed and proposed to safely preserve or restore monuments and artworks, including constructions manufactured in the last decades (Corradi et al., 2008; Valluzzi et al., 2014).

A new class of materials alternative to traditional binders, obtained by reaction of alkali with aluminosilicates, has been developed with a view towards reducing the CO_2 footprint of construction materials. Alkali activated materials (AAMs), including those called geopolymers, can exhibit a wide variety of properties and characteristics, depending on the raw material selection and processing conditions (Duxson et al., 2006; Provis, 2013; Provis and Bernal, 2014). They have therefore recently emerged as novel engineering materials with commercial and technological potential (Palomo et al., 2014; Van Deventer et al., 2012). They are prepared under mild processing conditions from inexpensive feedstocks, such as industrial wastes, like ground blast furnace slags and fly ashes, or calcined clays. Calcination of kaolin, normally carried out at temperatures between 600°C and 800°C, allows to obtain its dehydroxylated phase, metakaolinite (MK), that is considered to be a suitable precursor for geopolymer production due to its reactivity and predictable and tunable properties of the final geopolymer (Duxson et al., 2006; Siddique and Klaus, 2009). It has been shown that properties of geopolymers, such as high level of resistance to a range of different acids and salt solutions, low shrinkage and low thermal conductivity, are best achieved by MK-based geopolymers rather than fly ash-based ones (Duxson et al., 2007b; Palomo et al., 1999; Palomo and Glasser, 1992). Exploitation of these properties will depend on the development of applications in which the relatively high cost of metakaolin compared to fly ash is not a driving consideration and in which a fairly pure and homogenous material is necessary. Cultural Heritage, in the authors' opinion, could be one of the contexts in which geopolymer-based binders prepared from high-grade metakaolin can find application and in which the abovementioned properties are of extreme importance.

Geopolymers have frequently been proposed as binder phases in mortars (Arellano-Aguilar et al., 2014; Kamseu et al., 2014; Pelisser et al., 2013; Vasconcelos et al., 2011), while very few applications in cultural heritage are reported in literature (Elert et al., 2008; Hanzlíček et al., 2009). Due to the large variability and different typologies of masonry structures included in our cultural heritage, a specific knowledge of both the materials to be repaired and the restoration materials is required. Experimental studies of the properties of retrofitting materials are indeed decisive to improve the knowledge of the whole restoration process. Mortars used in restoration practices should respect the requirements of compatibility with the original material from the chemical, physical and mechanical points of view, including showing similar aesthetic features ((Van Balen et al., 2005) (ICOMOS Charter, 2004)). In detail, their mechanical behaviour should guarantee good adhesion to the substrate and the ability to adapt themselves to the masonry movements, being softer than the original material (Gulotta et al., 2013b; Lanas and Alvarez-Galindo, 2003). Naturally, the great variability of historical buildings and structures needs a case-by-case approach, where the use of unconventional materials might result convenient.

In this work, mortars (the term is used here to generally indicate a mixture of binder and aggregates) have been synthesized by using MK-based geopolymers as binder phase. The effects of a fluid slurry on the mechanical strength, binding capacity and chemical properties of the products are investigated. The study has been organized as follows:

- a high-grade kaolin has been selected as starting material in order to i) respect the high standard requested in the field of restoration of cultural heritage structures, and ii) have a convenient ‘reference system’;
- geopolymer binders have been prepared with different water/solid weight ratios. Maturation has been carried out at room temperature in order to simulate an outdoor setting;
- physico-chemical characterization of binders has been carried out by Fourier Transform Infrared Spectroscopy in Attenuated Total Reflectance (FTIR-ATR), powder X-ray Diffraction (XRD), Mercury Intrusion Porosimetry (MIP) and mechanical tests. Microstructural features and their variations with water/solid ratio have been analyzed in detail by Field Emission Scanning Electron Microscopy (FESEM) and discussed with respect to binding efficiency of geopolymer formulation;

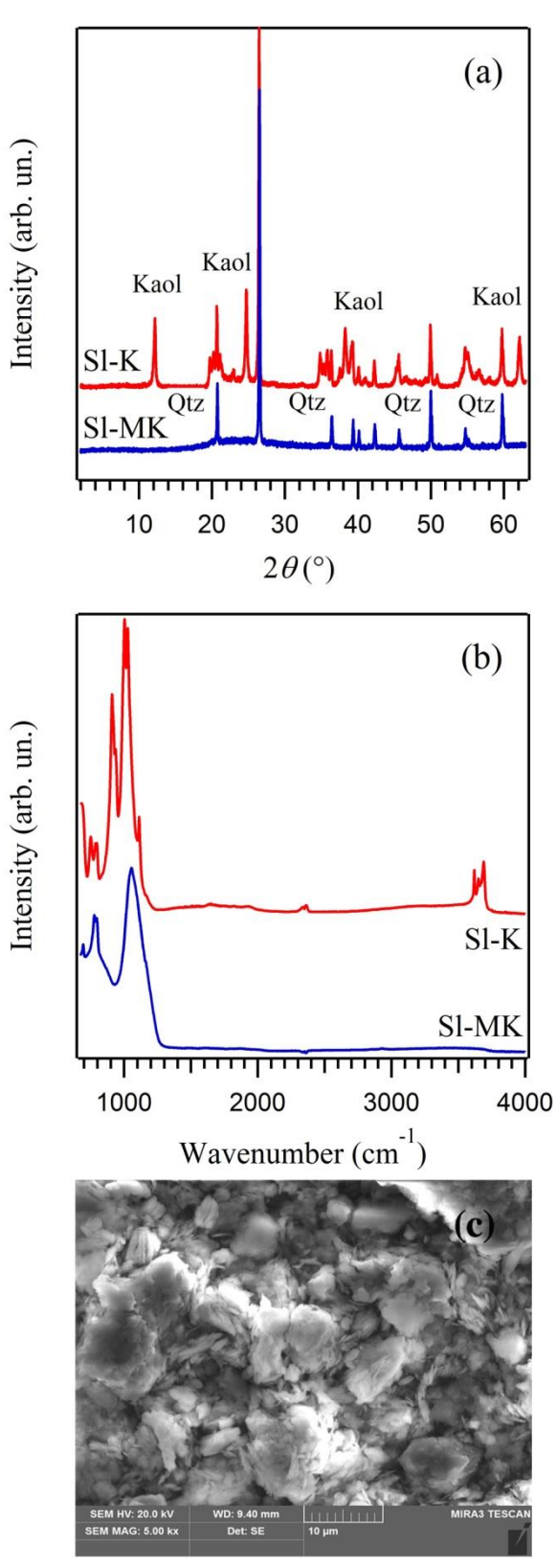

- geopolymer-based mortars have been synthesized by using i) standard sand and ii) powders from two different ornamental stones as aggregates;
- the effect on the final product of including fine size fraction (< 63 µm) of ornamental stones aggregates has been evaluated from the aesthetic and physico-chemical viewpoints.

1.2. Materials and methods

1.2.1 Sl-K kaolin

For this work, an industrial kaolin labelled Sl-K, deriving from the Seilitz kaolin deposits (Germany) and provided by Sibelco Italia S.p.A, was used. Sl-K is composed of 73 wt.% kaolinite and 27 wt.% quartz as determined by (Gasparini et al., 2013), who studied the dehydroxylation kinetics of this sample. Its chemical composition, determined by X-ray fluorescence (XRF), is: SiO_2 67.0%, Al_2O_3 31.5%, Fe_2O_3 0.32%, TiO_2 0.24%, CaO 0.12%, MgO 0.23%, K_2O 0.35%, and its measured ignition loss 10.02% (the theoretical value for pure kaolinite is 13.96%).

Figure 1.1 Characterization of Sl-K kaolin (red) and respective metakaolin (blue) obtained at 800°C. Sample names are reported in the figures. (a) XRD patterns. Main peaks are labelled. Kaol = Kaolinite; Qtz = Quartz; (b) FT-IR spectra; (c) SEM image of metakaolin.

The XRD pattern (Fig. 1.1a) of the untreated sample shows the presence of kaolinite and quarz only. The IR spectrum (Fig. 1.1b) displays intense and well-resolved absorption bands and

shows the four OH-stretching bands between 3600 and 3700 cm^{-1}. The double peak at around 750 cm^{-1} is indicative of the presence of quartz in the sample.

The kaolin powder was submitted to thermal treatment at 800°C for 2 hours to obtain the reactive metakaolin, hereafter labelled Sl-MK, characterized by a specific surface area of 12.04(5) m^2/g (the digit in parentheses indicates standard deviation), as measured by nitrogen adsorption BET analysis. The XRD pattern and IR spectrum of Sl-MK are reported in Figs. 1.1a and 1.1b, respectively. The XRD pattern shows the quartz peaks only. In the IR spectrum, all the OH stretching bands and those at 910 and 935 cm^{-1} related to Al-O-H have disappeared, the Si-O peaks have become a unique broad band centered at 1050 cm^{-1}. The micro-morphological features of Sl-MK metakaolin are shown in Fig. 1.1c. Metakaolinite plates are irregular in shape and characterized by discontinuous, embayed or lobed margins. This is a typical feature of kaolinite particles subjected to thermal treatment at temperature lower than 900°C (Schomburg, 1991). From SEM image, it is also evident that the metakaolinite plates are mostly condensed together.

A study making use of this kaolin clay to produce geopolymers has been reported by Gasparini et al. (2015).

1.2.2 Other materials

Sodium silicate solution supplied by Ingessil s.r.l. (Na_2O 14.37 wt%, SiO_2 29.54 wt%, H_2O 56.09 wt%) and NaOH pellets (Sigma-Aldrich, purity ≥ 98%) were used.

For the preparation of geopolymer-based mortars (see par. 1.2.3.2), a standard siliceous natural sand conforming to norm UNI-EN 196-1:2005, provided by Société Nouvelle du Littoral, and crushed ornamental stones were used as aggregates. Two varieties of Italian stones, Pietra di Angera and Pietra Serena (hereafter labelled PA and PS, respectively), mainly employed for decorative purposes, were selected. PA is a dolostone (yellow variety), and the sample used for this work comes from the collection of the Department of Earth and Environment Sciences of University of Pavia. PS, a sandstone characterized by low porosity and mainly composed of quartz, feldspars, micas and fragments of silicate and carbonatic rocks, was provided by Consorzio Pietra Serena of Firenzuola, Italy. Chemical compositions of these stones, determined by FESEM-EDAX energy dispersive spectrometry (EDS), are reported as oxides wt% in Table 1.1. Mineralogical description of the two stones is given by Cantisani et al. (2013) for PS and by Soggetti and Zezza (1983) for PA.

Table 1.1. Chemical compositions (wt%) of Pietra di Angera (PA) and Pietra Serena (PS).

Oxides	MgO	CaO	SiO_2	FeO	Al_2O_3	Na_2O	K_2O	SO_3	TiO_2	Total
PA	33(2)	64(2)	0.8(2)	2.2(1)	/	/	/	/	/	100(1)
PS	6.3(6)	5(1)	59(1)	6.2(5)	16(1)	2.9(7)	2.7(7)	0.5(2)	1.4(4)	100(1)

Standard deviations are in parentheses.

1.2.3 Sample preparation

1.2.3.1 Geopolymer binders

For the synthesis of geopolymer binders, the sodium silicate solution was modified by adding distilled water and dissolving solid sodium hydroxide; four different sodium silicate solutions were prepared with H_2O/Na_2O ranging between 10 and 20. Sl-MK was allowed to react with each of these solutions, in order to obtain, for all samples, the following molar ratios: SiO_2/Al_2O_3 = 3.7 and Al_2O_3/Na_2O = 1.04. In fact, a SiO_2/Al_2O_3 ratio of around 4 provides the MK-based geopolymers with the highest strength and without formation of crystalline zeolite-type phases, as reported in the literature (Duxson et al., 2005; Fletcher et al., 2005; Komnitsas and Zaharaki, 2007). In particular, SiO_2/Al_2O_3 ratio of 3.7 was selected in order to mature geopolymers at room temperature and obtain high values of mechanical resistance, as indicated by the compressive strength vs. composition contour plot reported in Fig. 1 of (Burciaga-Diaz et al., 2012). Different H_2O/Na_2O molar ratios were used with the aim of improving the slurry workability, and obtaining water/solid weight ratios between 0.33 and 0.66. Sample labels and water/solid ratios used for the synthesis are reported in Table 1.2.

Water/solid ratio is a variable that influences physical and mechanical behaviour of mortars and concrete. In case of concrete, compressive strength is inversely correlated to water/solid ratio through the Abrams' generalization law. Furthermore, a ratio between 0.30 and 0.40 reduces durability issues due to increasing of the porosity and development of hydration products (Aïtcin, 2003). In mortars, the increase of water content improves their workability, but eventually reduces the strength of hardened products. It was observed that the minimum water/solid ratio required to make a cement mortar workable is about 0.50 (Haach et al., 2011; Rao, 2001; Singh et al., 2015). In geopolymer synthesis, water results to have great effects on the development of geopolymer gels and on the properties of the final products. In terms of strength,

the minimization of water/solid ratio corresponds to an increase of compressive strength and to a reduction of permeability (Rashad, 2013; Van Deventer et al., 2012; Zhang et al., 2010).

Geopolymer binder samples were prepared by adding Sl-MK powder to the alkaline solutions and mixing for 10 minutes to form homogenous slurries. Mixing operations were performed by using a mechanical mixer, according to the European technical standard (UNI-EN 196-1:2005), under controlled conditions of temperature and relative humidity (20°C and 65% R.H., respectively). Samples were poured into prismatic steel moulds (4 × 4 × 16 cm^3) and compacted by mechanical vibration for 60s to remove entrained air. Specimens were cured in climatic room for 28 days at 20°C and 65% R.H. before testing. Three specimens for each geopolymer binder were prepared.

Table 1.2 Details of geopolymer binders

Sample	GpB_0.33	GpB_0.46	GpB_0.53	GpB_0.66
H_2O/Na_2O molar ratio	10	14	16	20
water/solid weight ratio	0.33	0.46	0.53	0.66
Si-O-T (cm^{-1})[a]	986	979	990	987
Relative peak area[a]	0.69(5)	0.68(5)	0.67(5)	0.63(5)
Compressive strength (MPa)	72(3)	66(4)	63(8)	59(4)
Flexural strength (MPa)	6.1(8)	4.9(1)	4.9(7)	3.6(5)
Porosity (%)	21.5	24.3	29.8	31.8
Median pore radius (μm)	0.0057	0.0052	0.0064	0.0076
Mass loss (%)[b]	18	19	19	20

Standard deviations are in parentheses.
[a]From FTIR spectroscopy. Si-O-T peak position is calculated from the first and second derivatives of the IR line. Relative peak area is calculated from the areas of the fitted Lorentian components of the main IR band as the ratio between the area of the Lorentian curve centred at 990 cm^{-1} and the area of the whole band (standard deviation from the fit).
[b]From TG analysis.

1.2.3.2 Geopolymer-based mortars

Three geopolymer-based mortars were prepared by mixing the geopolymer binder slurry GpB_0.66 with, respectively, standard sand (StS_GpM) and powders obtained by grinding PS (PS_GpM) and PA (PA_GpM).

Mortars were prepared in compliance with the requirements of UNI-EN 196-1:2005, but for StS_GpM, a binder/sand ratio of 1:2 (weight/weight) was used, thus giving a mortar with water/solid weight ratio of 0.23, whereas for mortars with crushed ornamental stones, PS_GpM and PA_GpM, a binder/aggregate ratio of 1:1 was used to obtain mortars with a water/solid weight ratio of 0.39. For these samples, the granulometric fraction smaller than 0.5 mm was used as aggregate in the preparation of mortars. Clayey fractions were also included to make the colour tone of the mortars similar to that of their respective stone.

Each paste was mixed for 10 minutes, poured into prismatic steel moulds (4 × 4 × 16 cm^3) and compacted by mechanical vibration for 60s. All samples were submitted to maturation phase in climatic room for 14 days at 20°C and 90% R.H., then were de-moulded and cured at the same conditions for other 14 days.

1.2.4 Sample Characterization

1.2.4.1 Powder X-ray Diffraction (XRD)

XRD analyses were carried out on all samples by using a Philips PW1800/10 X-ray diffractometer, equipped with a Cu anticathode and a graphite monochromator. Data were collected in the range 2-65° 2θ with an angular step of 0.01° 2θ and time per step of 5s.

1.2.4.2 Fourier Transform Infrared Spectroscopy in Attenuated Total Reflectance (FTIR-ATR)

FTIR-ATR spectra were collected at room temperature in the range of wavelength between 670 and 4000 cm^{-1} with 4 cm^{-1} resolution by means of a ThermoScientific Nicolet iN10 MX micro-spectrometer. Spectra, recorded in ATR with a liquid nitrogen-cooled mercury cadmium telluride array detector, were calculated by Fourier transformation of 256 interferometer scans and total scanning time of 90s. A germanium hemispherical internal reflection element (IRE) crystal with a diameter of 300 µm was used. The ATR accessory is mounted on the X-Y stage of the FTIR microscope, and the IRE crystal makes contact with the

sample via a force level with pressure of 2 Pa. A 150 × 150 μm^2 aperture size was used. IR spectra were recorded on the surface of compressed powder pellets of geopolymer binders.

1.2.4.3 Thermogravimetric analysis (TGA)

TG analyses were performed by using a TA instruments Hi-Res Modulated TGA 2950 Termogravimetric Analyzer. 15 mg of finely ground powders of geopolymer binders were heated in a Pt crucible at 10°C/min heating rate under nitrogen atmosphere in the temperature range 30-1000°C.

1.2.4.4 Field Emission Scanning Electron Microscopy (FESEM)

A Field Emission Scanning Electron Microscope TESCAN Mira 3 XMU-series, equipped with an EDAX energy dispersive spectrometer, was utilized to investigate samples textures from micrometric to nanometric scale. Analyses of the morphological features were performed on fracture surfaces of the specimens, obtained by placing thin splinters of material directly on the stab. Samples were covered by 5 nm carbon coating before being investigated to prevent charge built-up on electrically insulating sample surface. Images were collected using backscattered electron (BSE) and secondary electron (SE) at a working distance of 15.8 mm with an acceleration voltage of 20 kV and 30 kV. Microstructural observations at the nanometer scale were carried out by InBeam mode using a working distance of 5 mm. EDS analyses (on spots and on areas of 25 μm^2) were done with accelerating voltage of 20 kV, working distance of 15.8 mm, beam current of 20 µA and spot diameter of about 5 µA, acquiring for 100s per spot analysis. Chemical compositions were determined considering 100 wt% oxide content on an H_2O- and CO_2-free basis and are reported in Table 1.1.

1.2.4.5 Mercury intrusion porosimetry (MIP) and gas pycnometry

A Micrometrics Autopore IV 9500 series mercury intrusion porosimeter was used to analyze prismatic samples of approximately 1 × 2 × 2 cm^3. A pressure from 0.10 to 60000.00 psia was applied. Results are reported in Tables 1 and 3 for binders and mortars, respectively.

Densities of mortars were measured by a ULTRAPYC 1200e gas ultrapycnometer (Quantachrome Instruments, USA) and are reported in Table 1.3. Measurements were carried out in a sample chamber of 48.1 cm^3 and using nitrogen as pycnometric gas. For each sample,

density was obtained by averaging six measurements. Data accuracy is < ±0.02% and reproducibility is < ±0.01%. Stainless-steel spheres were used for instrument calibration.

1.2.4.6 Mechanical tests

Flexural strengths of geopolymers and mortars cured for 28 days were measured by the three point bending mode on 4 × 4 × 16 cm^3 prismatic specimens. Compressive strengths were measured using a Controls press equipped with a 250 kN load cell on residual pieces obtained from flexural tests according to UNI-EN 196-1:2005 (Methods of testing cement – Part 1: Determination of strength; 2005). Data are reported in Tables 1.2 and 1.3 for binder and mortars, respectively.

1.2.4.7 Colorimetry

Colorimetric measurements of geopolymer-based mortars and original ornamental stones were carried out by a Konica Minolta CM-2600d instrument. A spot of 6 mm in diameter was used. For each sample, six measurements were performed on different areas of the external surface. Values are reported in Table 1.3 and are expressed in the CIELAB (L*,a*,b*) colour coordinates system, where L* defines lightness and ranges from 0 (total absorption or black) to +100 (white), whereas a* and b* denote the green/red and blue/yellow values, respectively, both ranging between -60 and 60.

1.3. Results

1.3.1 MK-based geopolymer binders

1.3.1.1 Structural properties

No significant differences in the diffraction patterns of geopolymer binders with different water content were observed (Figure 1.2). XRD patterns of all samples show a broad hump between 20 and 35° 2θ, typical of the amorphous phase of geopolymers. The only crystalline phase revealed by XRD is quartz, which derives from the kaolin precursor and remains stable up to about 1000°C. No peaks associated with zeolite phases and soluble salts were detected.

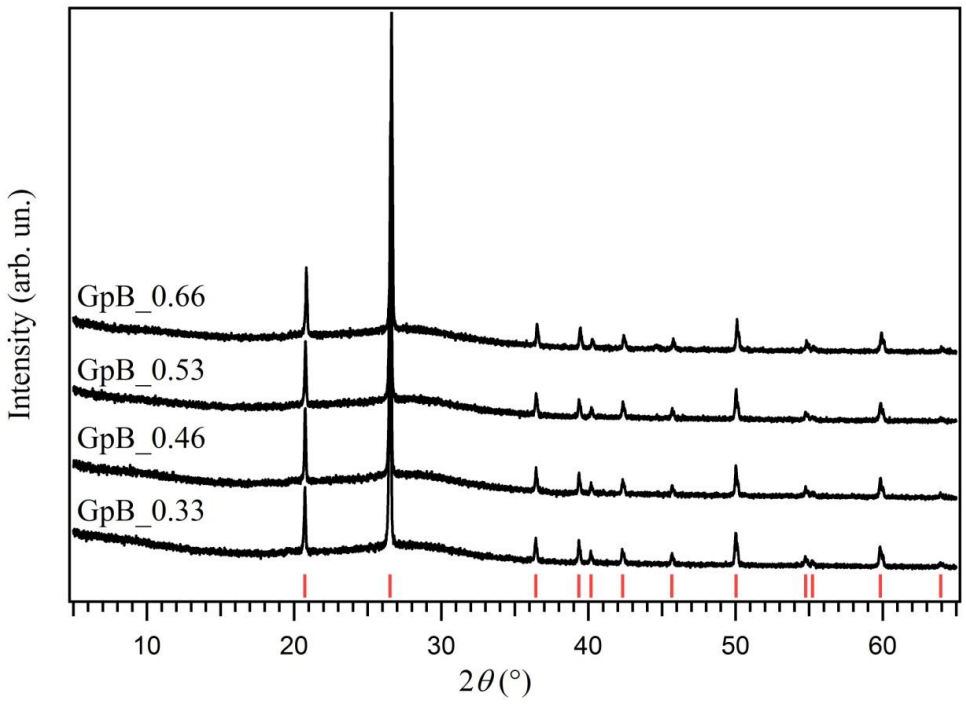

Figure 1.2. XRD patterns of geopolymer binders. Sample names are reported in the figure. Red lines indicate quartz peak positions.

As for XRD, also FTIR-ATR spectra of powders of geopolymer binders show similar features (Figure 1.3). A broad band centered at about 990 cm^{-1} (peak maxima calculated from first and second derivatives of the IR signal are reported in Table 1.2) represents the fingerprint of the aluminosilicate geopolymer phase and demonstrates the formation of the geopolymer network in all samples, as reported in many studies (Irfan Khan et al., 2015; Lee and Van Deventer, 2003; Lee and van Deventer, 2004). Peaks in this region are related to asymmetric stretching of the Si-O-T bonds, where T is Al or Si in tetrahedral coordination. This band has been fitted by using three Lorentian components: one for the aluminosilicate gel, one for metakaolinite and one for quartz. The fits, carried out by using the Multipeak Fitting package of Igor Pro 6.37, converged for the 4 formulations with nearly flat residuals curves. Fitted positions of peaks from metakaolinite and quartz are centered, respectively, at around 1050 and 1140 cm^{-1} for all samples, as expected. Peak from the aluminosilicate gel is centered at 990 cm^{-1}, as reported in literature. It is worth noting that the relative area of quartz peak is about 15% and constant for all samples, while relative areas of peaks from gel and metakaolinite show, with changing water content, slight variations which are opposite one to the other. From inset of Figure 1.3 and data in Table 1.2, it is evident how the relative area of peak from gel represents the largest part of the main peak area, and it decreases slightly with increasing the water content

in the geopolymer formulation. This may be interpreted as implying that there is a reduction in the actual amount of gel, and hence of reactivity, at high water/solid ratio. However, geopolymer relative peak area is large at water/solid ratio of 0.66, thus implying that the metakaolinite conversion is high, and likewise the gel binder amount.

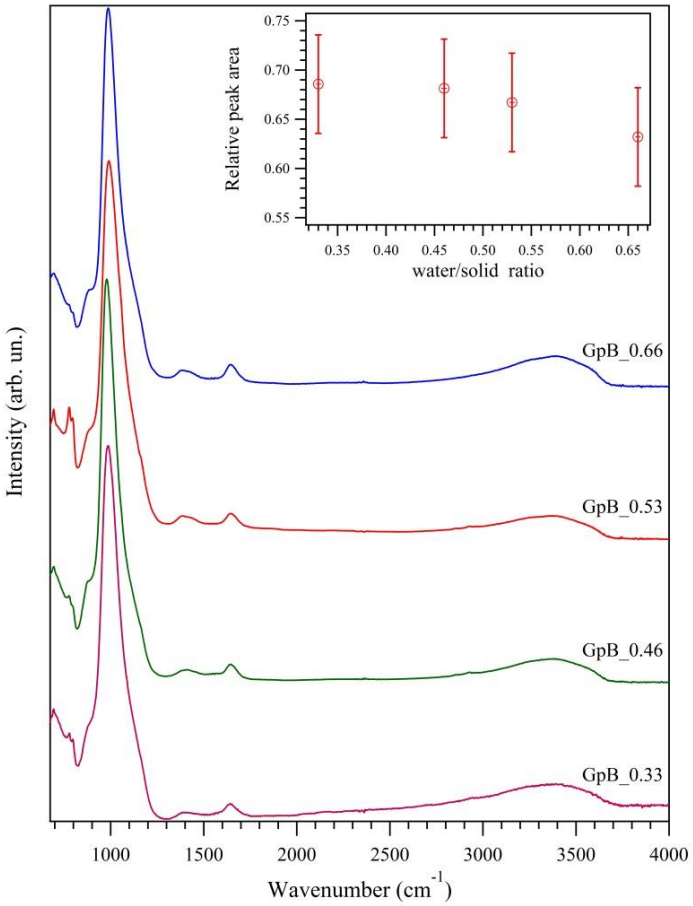

No features due to the presence of new crystalline phases are evident in the spectra but small bands at around 1400 cm^{-1} can be related to CO_3^{2-} stretching vibrations and thus reveal the formation of sodium carbonates. Sodium carbonate formation can be due to an excess of Na^+ cations that are mobile within pore network and, as water evaporates, are brought onto the surface and can then react with atmospheric CO_2.

Figure 1.3. FTIR spectra of geopolymer binders between 675 and 4000 cm^{-1}. In the inset: relative peak area of aluminosilicate gel as a function of the water/solid ratio.

Trona, $Na_3(HCO_3)(CO_3)\cdot 2H_2O$, and other sodium carbonates, such as thermonatrite, $Na_2CO_3\cdot H_2O$, have already been observed as efflorescence in geopolymers and, although they may sometimes coexist, the nature and extent of efflorescence is related to humidity conditions during curing (Criado et al., 2005; Krivenko and Kovalchuk, 2007; Xie and Kayali, 2014). No correlation between carbonate formation and water/solid ratio of geopolymers is noted. Samples have been cured in air-tight containers and carbonate peaks are not evident in spectra collected on the surface of the as-demoulded samples but start to appear ca. 4h after the samples are exposed to air. It must be noted that IR spectra have been measured in ATR mode with Ge crystal, which is very sensible to surface effects (calculated penetration depth at 45° and 1000 cm^{-1} is 0.65 μm). The amount of carbonates is very low and below XRD detection limit, and the only evidence of their presence is given by these IR peaks. However, the presence of potentially

harmful compounds, such as soluble salts, could influence the potential applicability of geopolymers in restoration and precautions have to be taken into account. In restoration practices, the development of soluble salts is a common issue and the possible formation of potential harmful products needs to be accurately investigated with respect to the substrates to be restored.

The presence of water in geopolymers is proved by the bands at around 3400 and 1640 cm^{-1}, related to OH asymmetric stretching and H-O-H bending vibrations of molecular water, respectively. Both bands, and in particular that ascribed to OH-stretching, are broad and indicate a large disorder of hydroxyl groups and water molecules. Further indications on the presence of water and hydroxyl groups are also inferred by TG analysis. All the geopolymers of this study show the TG pattern typically observed for MK-based geopolymers (Provis and Van Deventer, 2009). Weight loss due to dehydration of loose water begins above room temperature and continues up to 300°C, when the bulk of free water has evaporated. At this temperature the weight loss is of about 16-17% for all the samples, irrespective of the water/solid ratio used for the synthesis. In fact, the largest weight loss occurs below 200°C, as already observed in other studies (Barbosa and MacKenzie, 2003; Duxson et al., 2007a; Kong et al., 2008). Above 300°C and up to 800°C there is a further weight loss, which increases slightly from 1.6% for GpB_0.33 to 3.2% for GpB_0.66. Weight loss in this temperature range is attributed to dehydroxylation of chemically bound water, therefore the observed differences might suggest a difference in the amount of hydroxyls linked to the geopolymer gel.

Porosity of geopolymer binders increases from 21.5% to 31.8% with increasing the water/solid ratio from 0.33 to 0.66, as reported in Table 1.2. All samples are characterized by mesoporosity, with median pore radius ranging between 0.0057 and 0.0076 μm. Median pore radius increases with increasing the water/solid ratio.

1.3.1.2 Mechanical properties

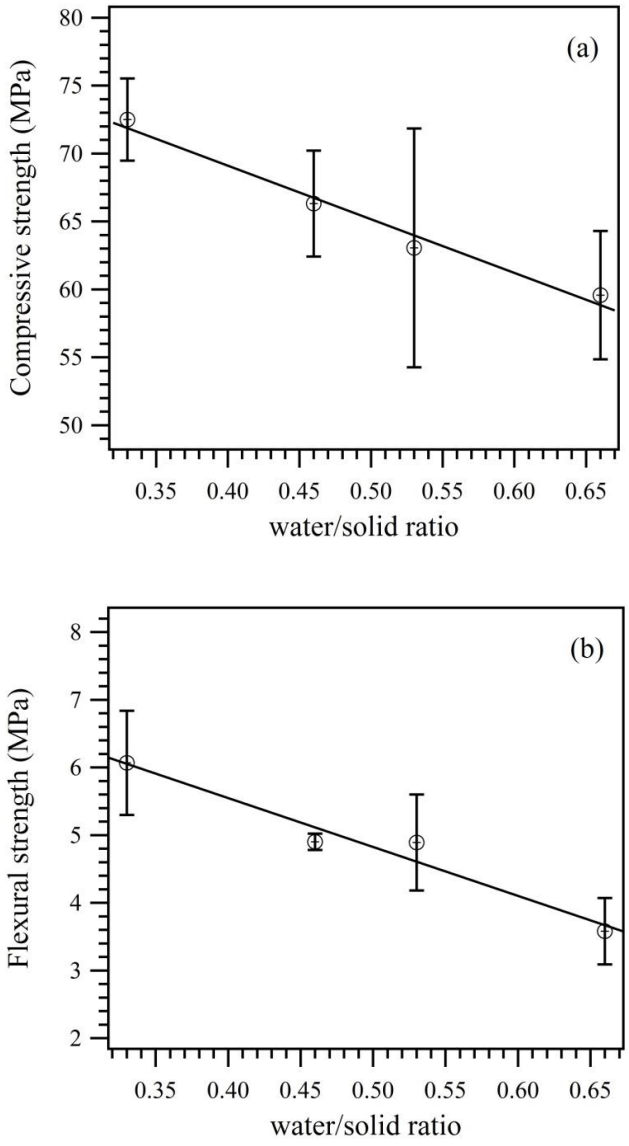

The mean values of three tests for flexural strength and six tests for compressive strength are reported in Table 1.2 and plotted in Figure 1.4. High values of compressive strength, between 72 MPa and 59 MPa, were obtained, with compressive resistance decreasing linearly with increasing the water/solid ratio. These values are higher than those reported in UNI-EN 998-2:2010 for masonry mortars, but similar to those reported in UNI-EN 206-1:2006 for high performance concrete (C 60/75). Considering the absence of aggregates in geopolymers, samples with low water content, such as GpB_0.33, could be preferentially chosen for structural applications.

Figure 1.4. (a) Compressive strength and (b) flexural strength in MPa of geopolymer binders as a function of the water/solid ratio. The average loads for compressive and flexural strengths, as measured by the press, are: GpB_0.33 = 116 kN and 2.4 kN; GpB_0.46 = 106 kN and 2.0 kN; GpB_0.53 = 101 kN and 2.0 kN; GpB_0.66 = 95 kN and 1.4 kN.

Flexural strength slightly decreases with increasing water with a maximum difference of 2.5 MPa between samples with 0.33 and 0.66 water/solid ratio, respectively. At the end of flexural strength tests, specimen section fractures appeared flat and orthogonal to traction direction, the same fracture mode found in ceramic materials. Flexural data are in accordance with those reported in literature for MK-based geopolymers. (Kamseu et al., 2014) found similar values for samples enriched with different percentages of fine aggregates. Furthermore, it has been demonstrated that flexural strength of MK-based geopolymers subject to aggressive media shows little or no variation (Palomo et al., 1999). Reduction of mechanical strength values with increasing water/solid ratio may be ascribed to the increase of porosity rather than to a reduction of MK conversion into geopolymer.

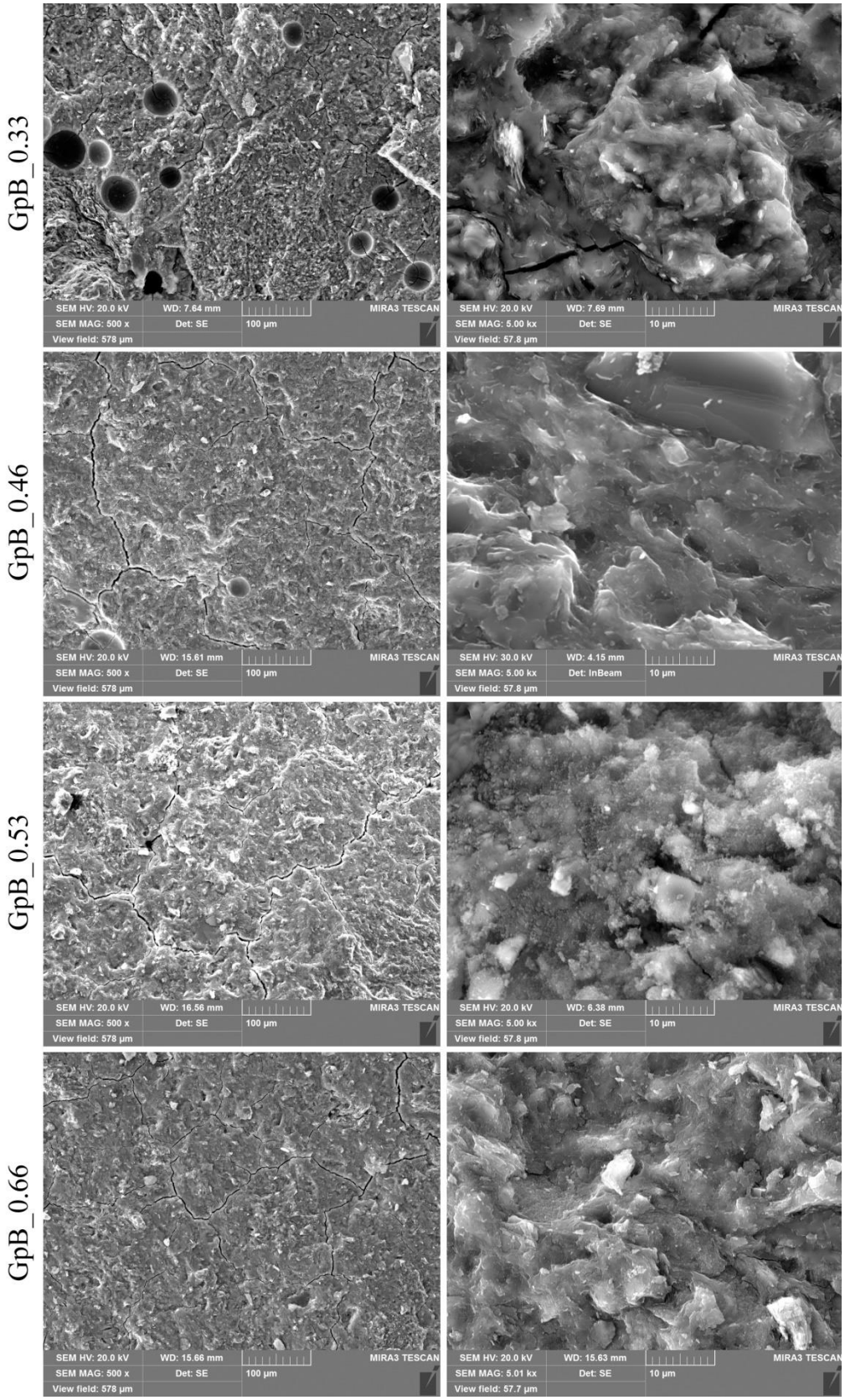

Figure 1.5. (Left panel) FESEM micrographs of geopolymer binders with different water/solid ratios at different magnifications. Each row refers to one sample, sample names are reported both on the left and on the right of the rows. Magnification 500x (left); 5Kx (right). Scale bar and magnification are showed in each image.

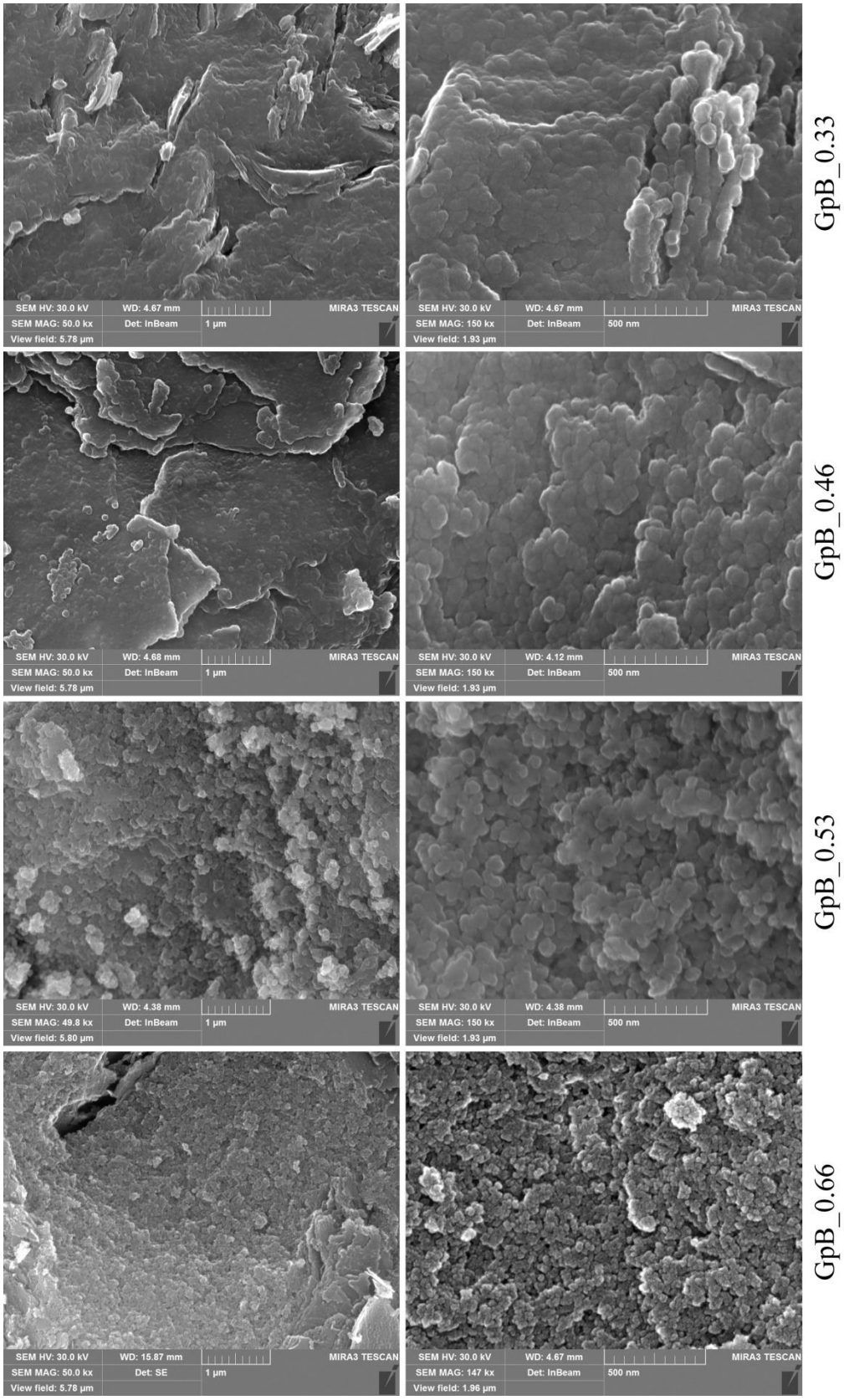

Figure 1.5. (Right panel). FESEM micrographs of geopolymer binders with different water/solid ratios at different magnifications. Each row refers to one sample, sample names are reported both on the left and on the right of the rows. Right panel: 50Kx (left); 150Kx (right). Scale bar and magnification are showed in each image.

The increase in water content has also extended the setting time of the samples. GpB_0.33 hardened after one day, while 10 days were necessary for GpB_0.66. However, after 28 days all specimens were suitably hardened to be used for mechanical tests.

1.3.1.3 Textural and microstructural properties

Differences in the morphology of the geopolymer binder matrices are hereafter analyzed based on high resolution SEM images at increasing magnifications. At low magnifications (500x and 5Kx) (Figure 1.5, left panel), the presence of porosity, porous size, matrix homogeneity and diffusion of micro-fractures network were taken into account. At 500x, the micrographs show, for all samples, a homogeneous and dense texture. In GpB_0.33, spherical voids of 50-70 micron in size are evident, probably due to air bubbles trapped in the gel during the synthesis. In any case, they contribute to the total porosity. At this length scale, a textural feature common to all samples is the presence of micro-sized defects, such as micro-voids, which may be ascribable to entrapped air, and micro-cracks due to sample cutting and vacuum extraction during sample preparation. At 5Kx, the amorphous features are confirmed. No crystalline phases and few unreacted or partially reacted MK particles are found. The morphological features of the binder matrix show little difference among the samples: an articulated and rough surface is always evident, although the irregularities are at a shorter length scale for GpB_0.53 and GpB_0.66 samples.

Analyses at higher magnifications (50Kx to 150Kx) display clearly the differences in the microstructural features of geopolymer binders with different water/solid formulations (Figure 1.5, right panel). At this length scale, the distribution of grains, the rounding of the spherical particles, the development degree and the compaction mode were investigated. At 50Kx, it is evident how the matrix of sample GpB_0.33 shows a tendency to organize itself into parallel layers, a morphological feature related to MK. At higher magnification (150 Kx), concatenated spherical particles, interconnected to create small clusters of aluminosilicate gel, become visible. The arrangement in parallel planes is still visible. Sample GpB_0.46 displays the same structural arrangement as GpB_0.33, with an increase in particle size. With increasing the water content (GpB_0.53 and GpB_0.66), particles become smaller than 50 nm and well confined into isolated elements. The matrix is made of ultra-fine particles, partially bonded together, and directionality disappears. An increase of matrix porosity is also evident, as confirmed by MIP measurements.

1.3.2 Geopolymer-based mortars

All geopolymer-based binders of this work show high mechanical strength and relatively high amount of aluminosilicate binding phase. Therefore, the most fluid (and hence workable) formulation, i.e. GpB_0.66, was used to prepare mortars. These were prepared using different materials: a sandstone (PS), a dolostone (PA) and standard sand. The latter was used to evaluate the binding capacity of the binder.

1.3.2.1 Structural properties

Diffraction patterns of mortars PS_GpM and PA_GpM are reported in Figure 1.6 and compared to those of original stones used as aggregates. For both samples, patterns show the peaks characteristics of quartz, deriving from the kaolin precursor, and of their respective aggregates, as expected. No efflorescence appears on mortar samples. XRD analyses, performed after 90 days from mortars synthesis, confirmed the absence of any new crystalline phases.

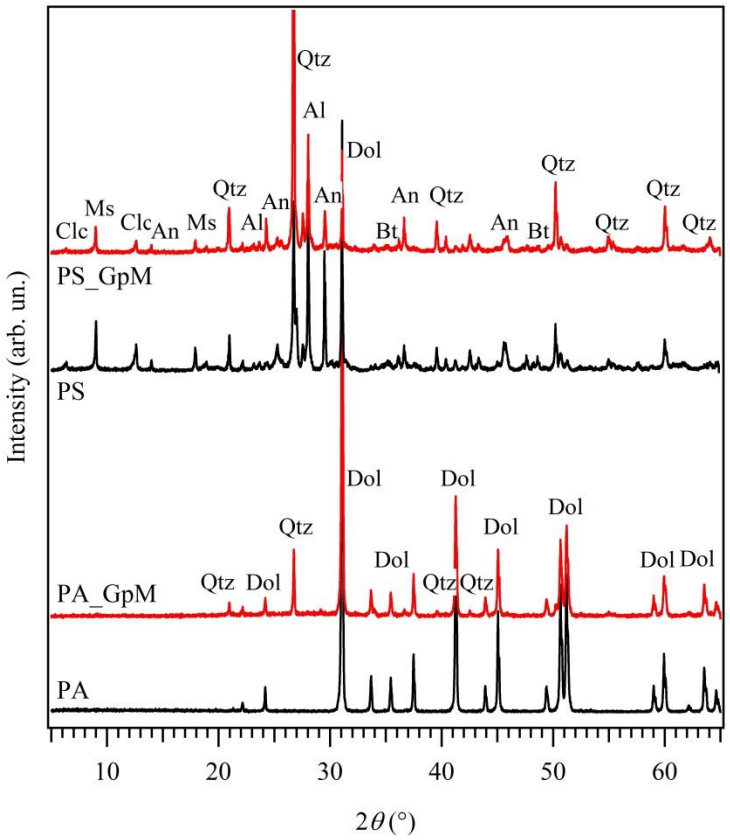

Figure 1.6. XRD patterns of geopolymer mortars (red) and respective ornamental stones used as aggregates (black). Ab = Albite; An = Anorthite; Bt = Biotite; Clc = Clinochlore; Dol = Dolomite; Ms = Muscovite; Qtz = Quartz.

The presence of aggregates rich in aluminum (in PS_GpM) and calcium (in PA_GpM) could help reduce carbonate formation, producing an increase of crosslinking in the geopolymer binder and reducing the mobility of alkalis, as already noted by (Kani et al., 2012). Densities of mortars, as measured by pycnometry (Table 1.3), are similar to those of their respective stones; this can be interpreted as a positive feature, if considering these materials for use in replacement practices. Moreover, such values are of the same order of magnitude of those reported for MK-based geopolymers of composition Si/Al = 1.9 ((Duxson et al., 2005).

Percent porosity of all mortars is nearly half that of the binder GpB_0.66, as expected (see data in Tables 1 and 3). However, while porosity of PA_GpM is similar to that of the "yellow" variety of PA, porosity of PS_GpM is higher than that of PS (Cantisani et al., 2013; Fratini et al., 2014). Pore size distributions of all mortars fall in the mesoporosity range and are reported in Figure 1.7, where are compared with that of the geopolymer binder GpB_0.66. While the binder and the mortar with standard sand show almost unimodal distributions with a sharp main peak, mortars with ornamental stones show broad and multimodal distributions. In all three cases, the main peak in the differential curves of mortars is shifted towards larger pore size than in the binder, and there are additional pores, which are greater in size. Differences in pore size distribution of mortars are expected considering the differences in type, quantity, granulometric distribution as well as porosity of aggregates themselves.

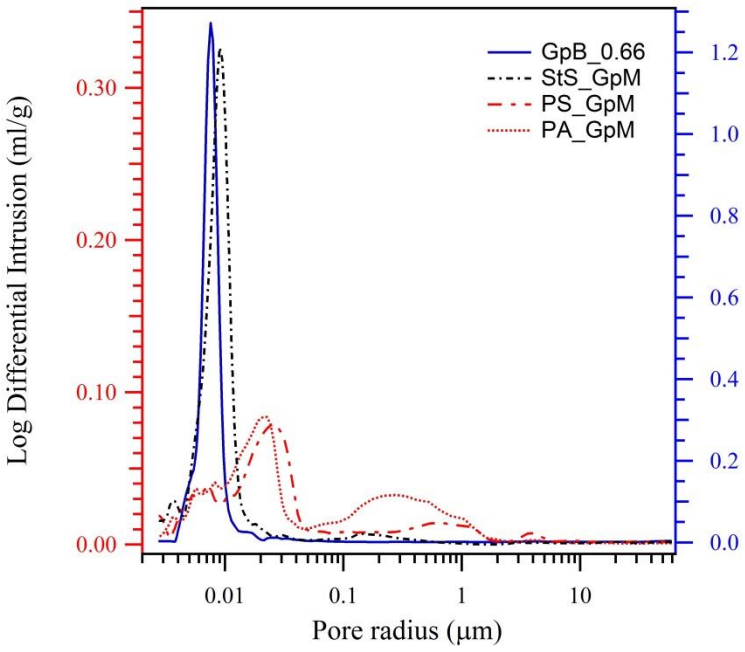

Figure 1.7. Pore distributions in geopolymer-based mortars as determined by MIP. Dotted line: StS_GpM; dot-dashed line: PS_GpM; dashed line: PA_GpM. Pore distribution in geopolymer binder GpB_0.66 is reported for comparison as solid line and refers to the right axis.

Differential curve for mortar StS_GpM, prepared with standard sand, exhibits a sharply defined peak in the 0.004 to 0.015 μm range, indicating a nearly unimodal distribution of pore sizes. The presence of a sharply defined intrusion peak in the differential curve indicates the intrusion of mercury throughout a pore network connected to the specimen surface. Therefore, the main intrusion peak observed here corresponds to the minimum throat dimension of an interconnected capillary network. In the other two mortars, the main band is large, displays many features and is centered at larger pore dimensions than StS_GpM. A second, more rounded peak appears at a larger pore size. In fact, the whole granulometric fraction smaller than 0.5 mm was used for the synthesis of PA_GpM and PS_GpM, including the fine size fraction (< 63 μm) of the crushed rock.

This favours binder compaction in the mortars and reduces the amount of low-size pores if compared to the standard mortar StS_GpM. Differential and cumulative intrusion curves for PA_GpM and PS_GpM clearly reveal how the global porosity is the result of the contribution of the porosity of both aggregates and geopolymer binder. In PS_GpM, the pore size distribution below 0.032 μm displays features similar to those generally observed for different varieties of PS sandstone (Cantisani et al., 2013; Fratini et al., 2014; Manganelli Del Fa, 1987). The same effect can be observed for the pore size distribution of PA_GpM, moreover, for this mortar, porosity of PA itself can contribute further to the porosity in the range between 0.1 and 1 μm (Soggetti and Zezza, 1983). The second rounded peak in the differential curve is usually attributed to larger pores present in the interfacial zone between aggregate and binder paste. In the differential curve of PA_GpM, this is more pronounced and broader than in the other two mortars, thus reflecting on the one side the aforementioned contribution of aggregates, but also a less linked interface between geopolymer gel and carbonate aggregates. Conversely, such porosity is reduced in StS_GpM and PS_GpM due to the reaction of geopolymer with siliceous aggregates.

A large porosity range distribution is particularly relevant in conservation issues in outdoor environments (Gulotta et al., 2013a). The low percentage porosity associated to large median pore radius of geopolymer-based mortars could be considered as a positive feature for possible restoration applications. Although this may not reduce or inhibit the decay of the original stone, it could offer better breathability and adaptability of mortar to the original substrate.

1.3.2.2 Mechanical properties

The results of mechanical tests on geopolymer-based mortars are reported in Table 1.3. No shrinkage of the gel during the curing was observed for all samples.

Table1. 1.3. Details of geopolymer mortars and ornamental stones used as aggregates.

Sample		StS_GpM	PA_GpM	PS_GpM	PA	PS
Compressive strength (MPa)[a]		75(2)	18(5)	21(3)	-	-
Flexural strength (MPa)[b]		9(1)	3.2(9)	3.6(8)	-	-
Porosity (%)		17.3	17.8	14.1	-	-
Median pore radius (µm)		0.009	0.0254	0.0243	-	-
Density (g/cm^3)		2.419(5)	2.767(7)	2.962(1)	2.706(5)	2.941(1)
Colorimetric CIELAB coordinates	L*	-	81.3(4)	73(1)	80.2(7)	62.2(7)
	a*	-	6.1(5)	-0.07(1)	7.2(1)	-0.45(5)
	b*	-	22(1)	3.9(4)	26.4(6)	5.5(1)

Standard deviations are in parentheses.
[a] The average loads, as measured by the press, are: StS_GpM = 119 kN; PA_GpM = 24 kN; PS_GpM = 29 kN.
[b] The average loads, as measured by the press, are: StS_GpM = 3.7 kN; PA_GpM = 6.8 kN; PS_GpM = 7.2 kN.

For StS_GpM, a compressive strength of 75(2) MPa was measured, comparable to the value obtained for the geopolymer binder GpB_0.33. This result encourages considering the use of a slight high amount of water rather than of plasticizers to improve fluidity and workability of a binder in restoration applications. With the use of plasticizers, (Pacheco-Torgal et al., 2011) obtained compressive strength values of up to 50 MPa. The flexural strength is higher compared to geopolymer binders. The average value of 9(1) MPa confirms how the addition of aggregates favors a decrease of fragility of the final product, which could bring benefits if used as retrofitting material. Observed flexural/compressive strength ratio of StS_GpM is similar to those reported for PS and PA (Cantisani et al., 2013; Fiumara et al., 1979; Soggetti and Zezza, 1983).

PS_GpM and PA_GpM show compressive strength lower than StS_GpM, but in agreement with those recommended in UNI-EN 998-2:2010 for the masonry mortars class M20. The mechanical tests results can be explained by considering the morphology (low sphericity grains) of aggregates and that fine powders have also be used. In detail, for PA_GpM, deleterious effect on strength of adding significant percentages (> 20%) of alkaline earth

carbonate minerals was already reported by Yip et al. (2008). For PS_GpM the fine aluminosilicate powders admixtures may play part in the geopolimerisation process, for example they may change local Al/Si ratio. The formation of nanometric neogenic crystals, which may have influenced the mechanical strength, has been observed by high magnification SEM (see par. *1.3.2.3*). Although the negative effect on mechanical properties, these findings suggest further studies on the use of PS itself as precursor in the synthesis of geopolymers.

1.3.2.3 Textural and microstructural properties

Mortar StS_GpM (Figure 1.8) has a quite compact microstructure, only few micro-fractures are observed within the mortar matrix or along the aggregates rims, likely due to cutting of the specimens for metallographic preparation. At high magnifications, the binder phase appears more homogeneous and compact if compared to that of the naked binder GpB_0.66. The spherical particles that compose the matrix show a particle size between 50 and 0.5 nm with a sub-rounded or rounded shape. The compaction of the mortar binder and its lower porosity with respect to the naked binder are due to the presence of aggregates.

In PS_GpM sample (Figure 1.9), aggregates are poorly sorted, as expected considering that powders have not be sieved, and are characterized by low sphericity grains, with an angular or sub angular shape. A more detailed analysis of microstructure of quartz and feldspar grains evidences an incipient dissolution; boundaries of these siliceous minerals show embayments at a few micron length scale. At the interaction zone with the matrix, mica rims are sharp and regular. Few needle-shaped crystals are observed in this sample. Their small crystal size made EDS analyses impossible; however, on the basis of their morphology, these crystals could be attributed to framework silicates zeolites or feldspathoids. It could be hypothesized that such neogenic crystals may be due to the fine size fraction of PS, which supplies soluble silico-aluminate phases. The availability of aluminum and silicon in solution may alter the Si/Al ratio on a local scale thus promoting zeolite crystallization.

PA_GpM (Figure 1.10) shows a network of micro-cracks in the binder matrix and along binder-aggregate interfaces. Cracks follow a preferential orientation starting from the grain rims and continuing in the binder with a radial trend. The particles size is poorly sorted, with a size ranging from coarse to very fine. The aggregates shape is from sub-angular to sub-rounded, with uneven rims with indentations where the binder phase fills the primary porosity. No microstructures associated with dissolution processes are observed. The boundary between aggregates and binder is sharp and well defined and follows grains irregularities. No structures

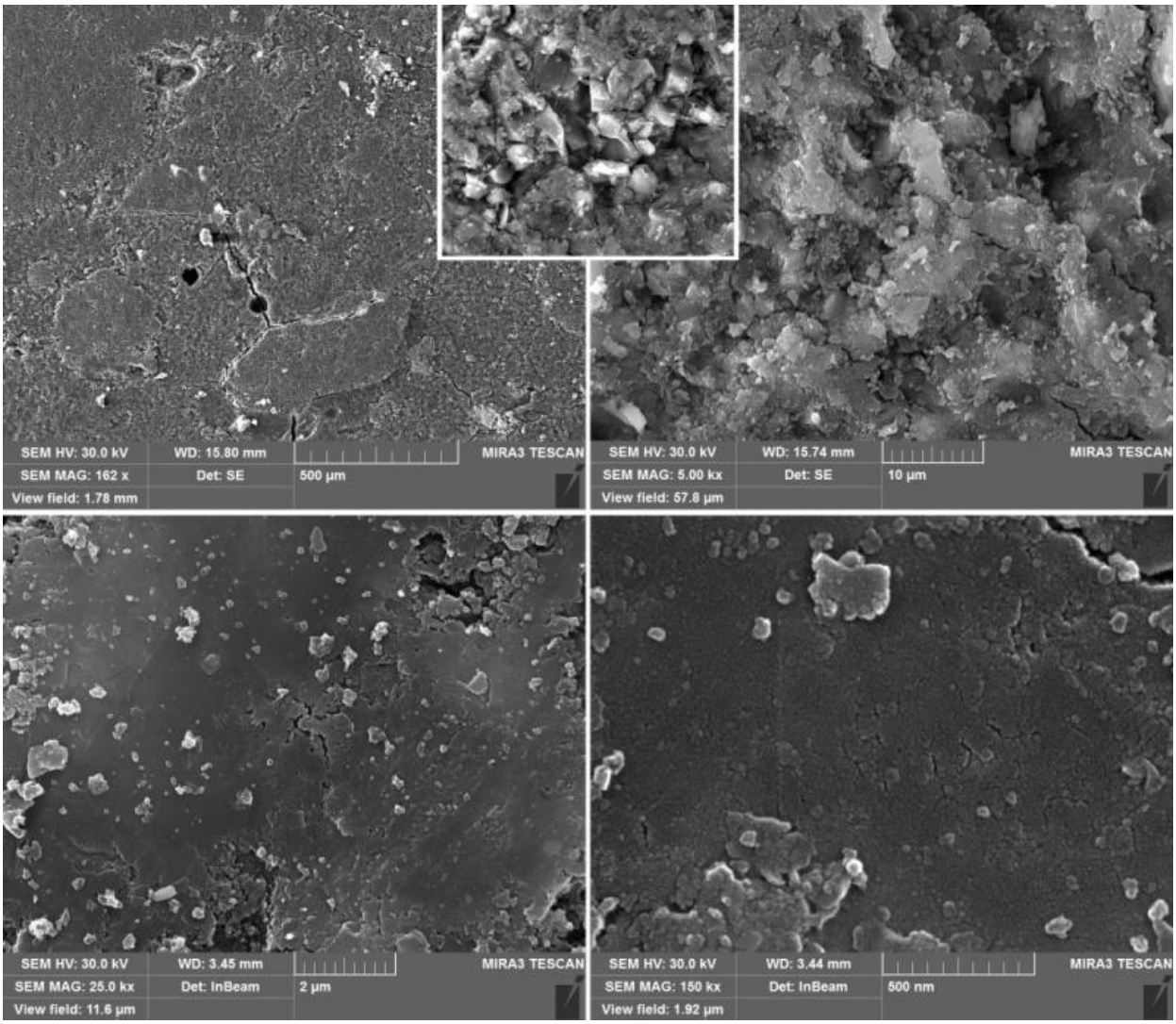

Figure 1.8. FESEM micrographs of geopolymer-based mortar StS_GpM at different magnification. In the inset: quartz grain included in matrix (magnification of 2.5Kx). Scale bar and magnification are showed in each image.

characteristic of C–S–H gel are observed. However, EDX analyses indicate Ca and Mg uptake of geopolymer gel around aggregates particles. Likely, Ca and Mg concentrations remain low enough to avoid the formation of C-S-H, as indicated by Yip et al. (2008).

1.3.2.4 Aesthetic compatibility

Mortars PS_GpM and PA_GpM, prepared with powders of PS and PA as mineral admixtures, may find application as decoration mortars or as sealing and repairing mortars for small gaps in masonries and stone artifacts. For these purposes, their aesthetic features should be similar to those of the original stone. Rock fines have been added to homogeneously color the resulting

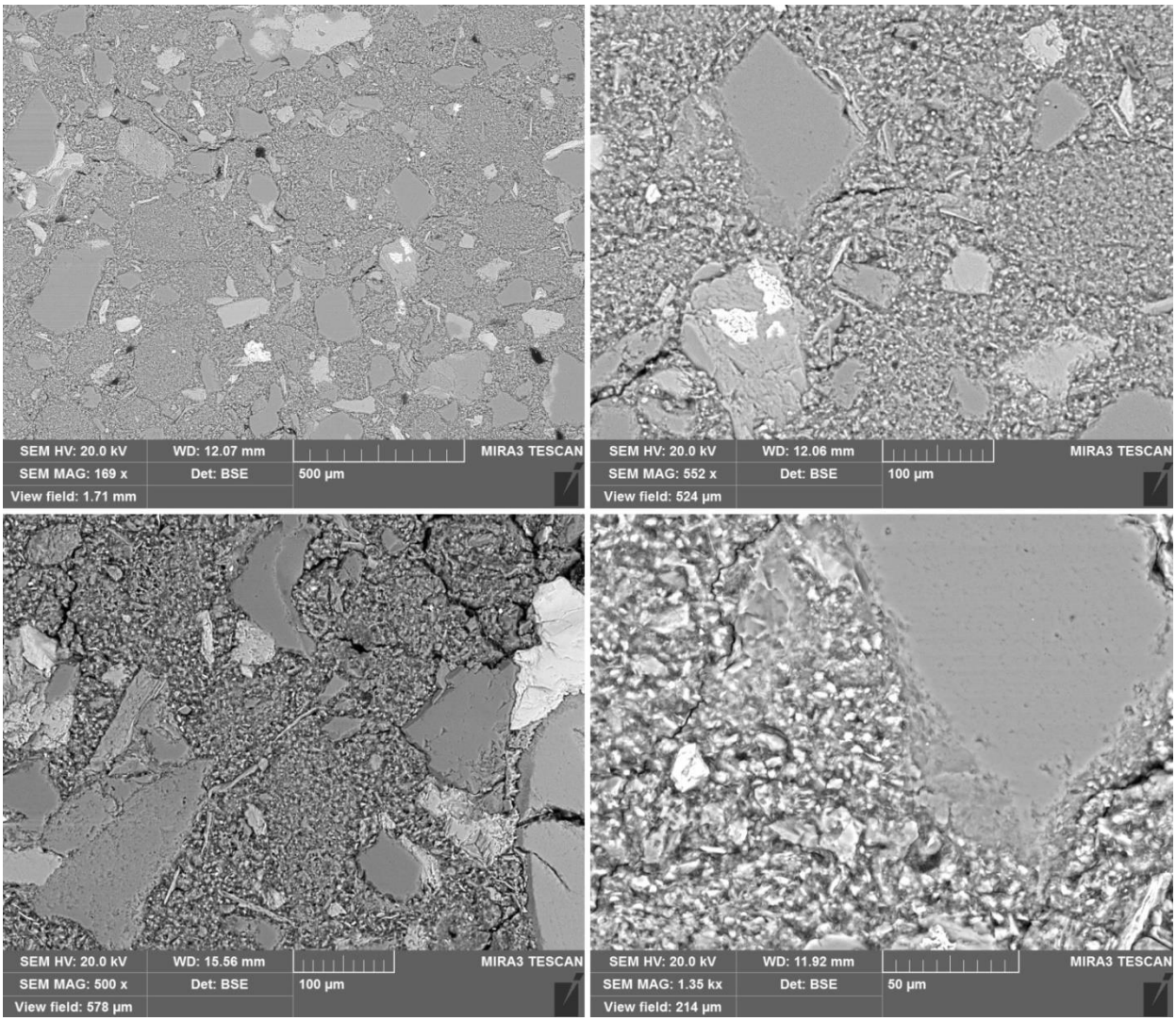

Figure 1.9. FESEM micrographs of geopolymer-based mortar PS_GpM at different magnifications. Scale bar and magnification are showed in each image.

mortar and colorimetric measurements performed. The average of six measurements of L*,a*,b* space for each sample is reported in Table 1.3. As expected, diluting rock powders into a white matrix results in a solid with nearly the same color hue and paler than the original rock. Difference in color hue angle, $h_{ab} = \tan^{-1}(b^*/a^*)$, is less than 1 for PA_GpM and about 4 for PS_GpM. The main differences are due to lightness ΔL^* and color saturation ΔC^*, which is −4.9 and −1.9 for PA_GpM, and PS_GpM, respectively. The color variation between stone references

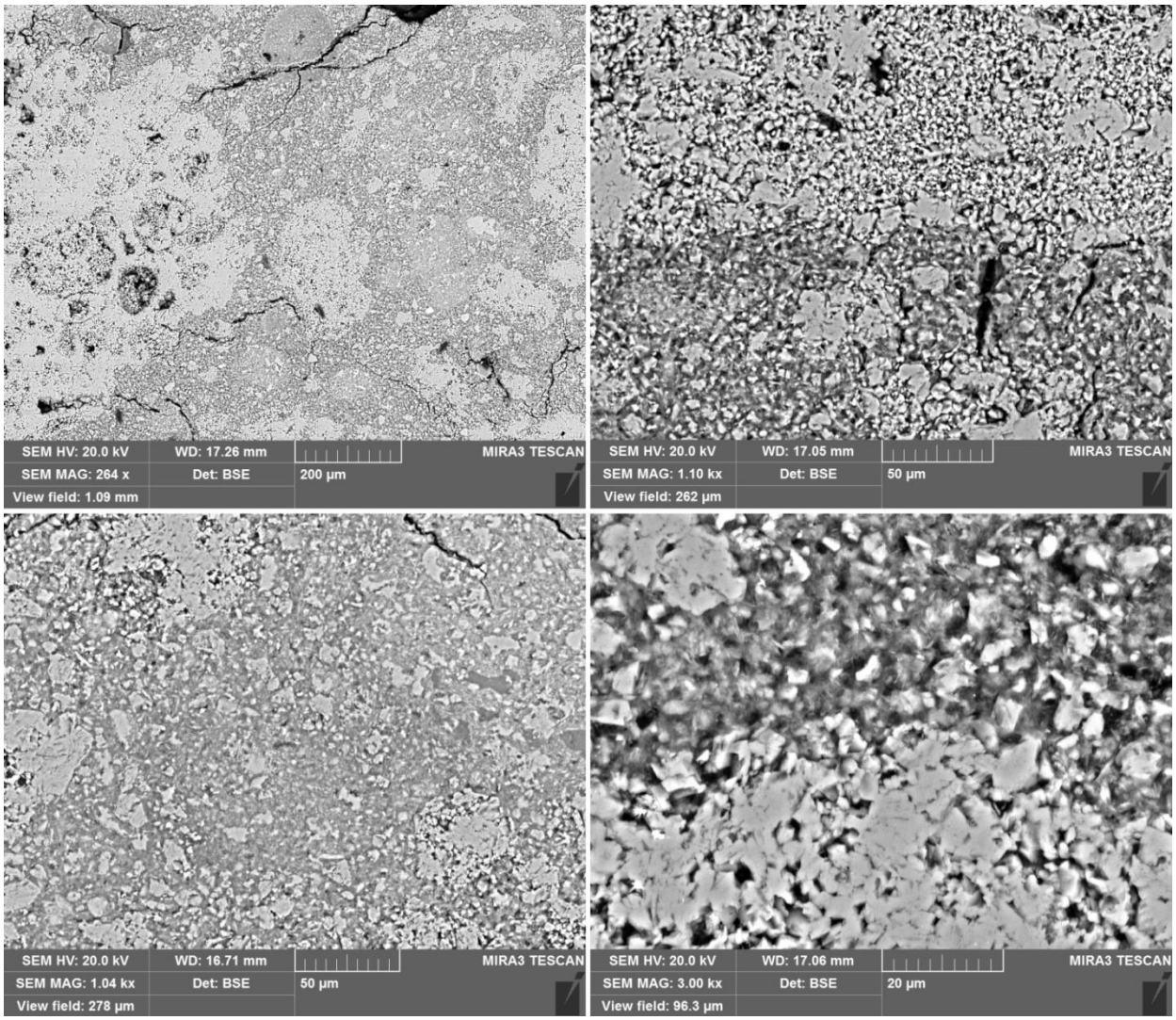

Figure 1.10. FESEM micrographs of geopolymer-based mortar PA_GpM at different magnifications. Scale bar and magnification are showed in each image.

and mortars has been evaluated by using the total color difference, expressed as $\Delta E = \text{sqrt}[(L^*_1-L^*_2)^2+(a^*_1-a^*_2)^2+(b^*_1-b^*_2)^2]$. In both cases, the difference in visual appearance of the samples is small, being $\Delta E = 5$ and 11 for PA_GpM and PS_GpM, respectively, but however distinguishable by human eye. These results confirm the purpose to obtain recognizable materials.

References

Aïtcin, P.C., 2003. The durability characteristics of high performance concrete: a review. Cement and Concrete Composites 25, 409-420.

Arellano-Aguilar, R., Burciaga-Díaz, O., Gorokhovsky, A., Escalante-García, J.I., 2014. Geopolymer mortars based on a low grade metakaolin: Effects of the chemical composition, temperature and aggregate:binder ratio. Construction and Building Materials 50, 642-648.

Barbosa, V.F.F., MacKenzie, K.J.D., 2003. Thermal behaviour of inorganic geopolymers and composites derived from sodium polysialate. Materials Research Bulletin 38, 319-331.

Burciaga-Diaz, O., Escalante-Garcia, J.I., Gorokhovsky, A., 2012. Geopolymers based on a coarse low-purity kaolin mineral: Mechanical strength as a function of the chemical composition and temperature. Cement and Concrete Composites 34, 18-24.

Cantisani, E., Garzonio, C.A., Ricci, M., Vettori, S., 2013. Relationships between the petrographical, physical and mechanical properties of some Italian sandstones. International Journal of Rock Mechanics and Mining Sciences 60, 321-332.

Corradi, M., Tedeschi, C., Binda, L., Borri, A., 2008. Experimental evaluation of shear and compression strength of masonry wall before and after reinforcement: Deep repointing. Construction and Building Materials 22, 463-472.

Criado, M., Palomo, A., Fernandezjimenez, A., 2005. Alkali activation of fly ashes. Part 1: Effect of curing conditions on the carbonation of the reaction products. Fuel 84, 2048-2054.

Duxson, P., Fernández-Jiménez, A., Provis, J.L., Lukey, G.C., Palomo, A., van Deventer, J.S.J., 2006. Geopolymer technology: the current state of the art. Journal of Materials Science 42, 2917-2933.

Duxson, P., Lukey, G.C., van Deventer, J.S.J., 2007a. Physical evolution of Na-geopolymer derived from metakaolin up to 1000 °C. Journal of Materials Science 42, 3044-3054.

Duxson, P., Provis, J.L., Lukey, G.C., Mallicoat, S.W., Kriven, W.M., Van Deventer, J.S., 2005. Understanding the relationship between geopolymer composition, microstructure and mechanical properties. Colloids and Surfaces A: Physicochemical and Engineering Aspects 269, 47-58.

Duxson, P., Provis, J.L., Lukey, G.C., van Deventer, J.S.J., 2007b. The role of inorganic polymer technology in the development of 'green concrete'. Cement and Concrete Research 37, 1590-1597.

Elert, K., Sebastián, E., Valverde, I., Rodriguez-Navarro, C., 2008. Alkaline treatment of clay minerals from the Alhambra Formation: Implications for the conservation of earthen architecture. Applied Clay Science 39, 122-132.

Fiumara, A., Riganti, V., Veniale, F., Zezza, U., 1979. (On the preservation treatments of the Angera stone). Geologia Applicata e Idrogeologia 14, 191-214.

Fletcher, R.A., MacKenzie, K.J.D., Nicholson, C.L., Shimada, S., 2005. The composition range of aluminosilicate geopolymers. Journal of the European Ceramic Society 25, 1471-1477.

Fratini, F., Pecchioni, E., Cantisani, E., Rescic, S., Vettori, S., 2014. Pietra Serena: the stone of the Renaissance. Geological Society, London, Special Publications 407, 173-186.

Gasparini, E., Tarantino, S.C., Conti, M., Biesuz, R., Ghigna, P., Auricchio, F., Riccardi, M.P., Zema, M., 2015. Geopolymers from low-T activated kaolin: Implications for the use of alunite-bearing raw materials. Applied Clay Science 114, 530-539.

Gasparini, E., Tarantino, S.C., Ghigna, P., Riccardi, M.P., Cedillo-González, E.I., Siligardi, C., Zema, M., 2013. Thermal dehydroxylation of kaolinite under isothermal conditions. Applied Clay Science 80-81, 417-425.

Gulotta, D., Bertoldi, M., Bortolotto, S., Fermo, P., Piazzalunga, A., Toniolo, L., 2013a. The Angera stone: A challenging conservation issue in the polluted environment of Milan (Italy). Environmental Earth Sciences 69, 1085-1094.

Gulotta, D., Goidanich, S., Tedeschi, C., Nijland, T.G., Toniolo, L., 2013b. Commercial NHL-containing mortars for the preservation of historical architecture. Part 1: Compositional and mechanical characterisation. Construction and Building Materials 38, 31-42.

Haach, V.G., Vasconcelos, G., Lourenço, P.B., 2011. Influence of aggregates grading and water/cement ratio in workability and hardened properties of mortars. Construction and Building Materials 25, 2980-2987.

Hanzlíček, T., Steinerová, M., Straka, P., Perná, I., Siegl, P., Švarcová, T., 2009. Reinforcement of the terracotta sculpture by geopolymer composite. Materials & Design 30, 3229-3234.

ICOMOS Charter, 2004. Principles for the Analysis, Conservation and Structural Restoration of Architectural Heritage - 2003. In: ICOMOS (Ed.), International Charters for Conservation and Restoration -Monument and Sites Volume I. Lipp GmbH, München.

Irfan Khan, M., Azizli, K., Sufian, S., Man, Z., 2015. Sodium silicate-free geopolymers as coating materials: Effects of Na/Al and water/solid ratios on adhesion strength. Ceramics International 41, 2794-2805.

Kamseu, E., Cannio, M., Obonyo, E.A., Tobias, F., Bignozzi, M.C., Sglavo, V.M., Leonelli, C., 2014. Metakaolin-based inorganic polymer composite: Effects of fine aggregate composition and structure on porosity evolution, microstructure and mechanical properties. Cement and Concrete Composites 53, 258-269.

Kani, E.N., Allahverdi, A., Provis, J.L., 2012. Efflorescence control in geopolymer binders based on natural pozzolan. Cement and Concrete Composites 34, 25-33.

Komnitsas, K., Zaharaki, D., 2007. Geopolymerisation: A review and prospects for the minerals industry. Minerals Engineering 20, 1261-1277.

Kong, D.L.Y., Sanjayan, J.G., Sagoe-Crentsil, K., 2008. Factors affecting the performance of metakaolin geopolymers exposed to elevated temperatures. Journal of Materials Science 43, 824-831.

Krivenko, P.V., Kovalchuk, G.Y., 2007. Directed synthesis of alkaline aluminosilicate minerals in a geocement matrix. Journal of Materials Science 42, 2944-2952.

Lanas, J., Alvarez-Galindo, J.I., 2003. Masonry repair lime-based mortars: factors affecting the mechanical behavior. Cement and Concrete Research 33, 1867-1876.

Lee, W., Van Deventer, J., 2003. Use of infrared spectroscopy to study geopolymerization of heterogeneous amorphous aluminosilicates. Langmuir 19, 8726-8734.

Lee, W.K.W., van Deventer, J.S.J., 2004. The interface between natural siliceous aggregates and geopolymers. Cement and Concrete Research 34, 195-206.

Manganelli Del Fa, C., 1987. Pietra serena e pietraforte: le arenarie utilizzate nell'architettura fiorentina. Alterazione, restauro, conservazione, Il progetto di restauro e alcune realizzazioni. Edizioni kappa, pp. 108-115.

Pacheco-Torgal, F., Moura, D., Ding, Y., Jalali, S., 2011. Composition, strength and workability of alkali-activated metakaolin based mortars. Construction and Building Materials 25, 3732-3745.

Palomo, A., Blanco-Varela, M.T., Granizo, M.L., Puertas, F., Vazquez, T., Grutzeck, M.W., 1999. Chemical stability of cementitious materials based on metakaolin. Cement and Concrete Research 29, 997-1004.

Palomo, A., Glasser, F., 1992. Chemically-bonded cementitious materials based on metakaolin. British ceramic. Transactions and journal 91, 107-112.

Palomo, A., Krivenko, P., Garcia-Lodeiro, I., Kavalerova, E., Maltseva, O., Fernández-Jiménez, A., 2014. A review on alkaline activation: new analytical perspectives. Materiales de Construcción 64, e022.

Pelisser, F., Guerrino, E.L., Menger, M., Michel, M.D., Labrincha, J.A., 2013. Micromechanical characterization of metakaolin-based geopolymers. Construction and Building Materials 49, 547-553.

Provis, J.L., 2013. Geopolymers and other alkali activated materials: why, how, and what? Materials and Structures 47, 11-25.

Provis, J.L., Bernal, S.A., 2014. Geopolymers and Related Alkali-Activated Materials. Annual Review of Materials Research 44, 299-327.

Provis, J.L., Van Deventer, J.S.J., 2009. Geopolymers: structures, processing, properties and industrial applications. Elsevier.

Rao, G.A., 2001. Generalization of Abrams' law for cement mortars. Cement and Concrete Research 31, 495-502.

Rashad, A.M., 2013. Alkali-activated metakaolin: A short guide for civil Engineer – An overview. Construction and Building Materials 41, 751-765.

Schomburg, J., 1991. Thermal reactions of clay minerals: their significance as “archaeological thermometers” in ancient potteries. Applied Clay Science 6, 215-220.

Siddique, R., Klaus, J., 2009. Influence of metakaolin on the properties of mortar and concrete: A review. Applied Clay Science 43, 392-400.

Singh, S.B., Munjal, P., Thammishetti, N., 2015. Role of water/cement ratio on strength development of cement mortar. Journal of Building Engineering 4, 94-100.

Soggetti, F., Zezza, U., 1983. (Possibility of exploitation and technical properties of the Angera stone, Lago Maggiore). Geologia Applicata e Idrogeologia 18, 81-93.

Valluzzi, M.R., Modena, C., de Felice, G., 2014. Current practice and open issues in strengthening historical buildings with composites. Materials and Structures 47, 1971-1985.

Van Balen, K., Papayianni, I., Van Hees, R., Binda, L., Waldum, A., 2005. Introduction to requirements for and functions and properties of repair mortars. Materials and Structures 38, 781-785.

Van Deventer, J.S.J., Provis, J.L., Duxson, P., 2012. Technical and commercial progress in the adoption of geopolymer cement. Minerals Engineering 29, 89-104.

Vasconcelos, E., Fernandes, S., Barroso de Aguiar, J.L., Pacheco-Torgal, F., 2011. Concrete retrofitting using metakaolin geopolymer mortars and CFRP. Construction and Building Materials 25, 3213-3221.

Xie, J., Kayali, O., 2014. Effect of initial water content and curing moisture conditions on the development of fly ash-based geopolymers in heat and ambient temperature. Construction and Building Materials 67, Part A, 20-28.

Yip, C.K., Provis, J.L., Lukey, G.C., van Deventer, J.S.J., 2008. Carbonate mineral addition to metakaolin-based geopolymers. Cement and Concrete Composites 30, 979-985.

Zhang, Z., Yao, X., Zhu, H., 2010. Potential application of geopolymers as protection coatings for marine concreteI. Basic properties. Applied Clay Science 49, 1-6.

CHAPTER 2

COMPOSITE OF ALKALI ACTIVATED MATERIALS AND NATURAL AND ARTIFICIAL STONES

2.1. Introduction

In the last decades, a range of promising novel materials, such as the commonly designated alkali-activated materials (AAMs) (Pacheco-Torgal et al., 2008; Palomo et al., 2014; Provis et al., 2015) have attracted the attention of the scientific community, particularly in the field of civil engineering, due to their low carbon footprint (Van Deventer et al., 2012), excellent mechanical properties and high resistance to heat and acids (Bakharev, 2005a, b; Palomo et al., 1999; Shi et al., 2011; Temuujin et al., 2011). AAMs derived by low-in-calcium precursors are known as geopolymers (hereafter labeled GPs) (Provis and Bernal, 2014). Their potential applicability in the field of conservation of Cultural Heritage has been little explored so far. Some studies have been conducted specifically for the consolidation of terracotta structures (Hanzlíček et al., 2009), earthen architectures (Elert et al., 2015; Elert et al., 2008) and conservation of stones (Rescic et al., 2011). However, it is worth exploring whether these materials may find application for conserving and treating ancient but also contemporary art and architecture, as well as natural and artificial stone objects. Several different applications could be suggested: alkali-activated materials could, for example, be used to patch exposed renders, fill in gaps, repoint masonry joints, but also as adhesives or sealants.

For a proper assessment of the suitability of the material to be used in the protection of cultural monuments, it is necessary to define the elementary criteria, which must be evaluated. Obviously, the knowledge of basic properties of the new material is the first step and there is a substantial body of more or less recent literature describing AAMs, in particular metakaolin-based (hereafter MK) geopolymers (Duxson et al., 2005; Pacheco-Torgal et al., 2011; Pelisser et al., 2013; Rashad, 2013; Wang et al., 2005).

Materials for conservation should guarantee functional and aesthetic compatibility with the remaining old materials and the whole construction. Compatibility depends on the support features, hence mechanical compatibility should be tuned to each particular case and formulation of the materials must be studied also in function of destination of use. Due to the large variability and different typologies of masonry structures included in our cultural heritage, a specific

knowledge of both the materials to be repaired and the restoration materials is required. Different methodologies, aimed at evaluating the coating performances, have been carried out to study the interface both on natural and artificial stones (Cappelletti et al., 2015a; Cappelletti et al., 2015b). The study of the interaction between the new and historical materials, which includes chemical, compositional and textural analyses of the boundary between the original and the new material is a fundamental prerequisite in order to assess the suitability and applicability of new restoration materials. Therefore, in this work the interaction between MK-based geopolymers and different substrates has been evaluated. Three ornamental stones widely used in the historic Italian architecture have been selected: Pietra Serena (sandstone), Pietra of Angera (dolostone) and Pietra of Noto (limestone). Widespread construction materials, namely commercial cement, one historical lime mortar and handcrafted red brick have also been included in the study.

2.2. Materials and methods

2.2.1 Materials

Three varieties of stones, widely used for decorative purpose, and representative of the historic architecture of northern, central and southern parts of Italy, were used for this study. In addition to those, some common construction materials were also selected.

Pietra Serena was provided by Casone Group of Firenzuola, Italy. It is a sandstone composed of quartz (40%), feldspars (20%), calcite (10%), micas and fragments of sedimentary (mainly carbonatic), volcanic and metamorphic rocks in terrigenous matrix (30%), as observed by modal analysis in thin section. Pietra di Angera is a dolostone (yellow variety), composed by dolomite and subordinates contents of clay minerals (< 5 %). The samples used in this work come from the collection of the Department of Earth and Environment Sciences of University of Pavia. These also included a historic and decorative stone artifact, which comes from the balustrade of the central courtyard of University of Pavia building and was provided after restoration works. Blocks of Pietra di Noto, a yellowish organogenic limestone, constituted by bioclasts (40%) with a micritic matrix (60%) and characterized by high porosity, were made available by the Department of Civil and Environmental Engineering of Polytechnique University of Milan. The same Department also provided a historical mortar sample. Concrete samples were obtained using starting materials provided by Holcim Ltd. Brick blocks also come from the collection of the Department of Earth and Environment Sciences of University of Pavia.

Chemical compositions of all materials, as determined by FESEM-EDAX energy dispersive spectrometry (EDS), are reported in Table 2.1. Mineralogical descriptions of the natural stones are given in (Alessandrini et al., 1992; Anania et al., 2012; Bargossi et al., 2004; Cantisani et al., 2013; Fiumara et al., 1979; La Russa et al., 2011; Soggetti and Zezza, 1983; Veniale et al., 2001).

Table 2.1 Chemical compositions (wt%) of Pietra Serena, Pietra di Angera, Pietra di Noto, red brick and concrete.

Oxides	Pietra Serena	Pietra di Angera	Pietra di Angera (historic)	Pietra di Noto	Brick	Concrete
MgO	6.3(6)	33(2)	37(7)	2.1(2)	4(2)	4(3)
CaO	5(1)	64(2)	53(7)	96(1)	14(6)	46(19)
SiO_2	59(1)	0.8(2)	1(1)	2(1)	49(5)	26(16)
FeO	6.2(5)	2.2(1)	0.5(1)	-	7(2)	8(7)
Al_2O_3	16(1)	-	0.3(2)	-	21(2)	11(8)
Na_2O	2.9(7)	-	5(3)	-	4(2)	2(1)
SO_3	0.5(2)	-	4(3)	-	0.5(2)	1.5(1)
K_2O	2.7(7)	-	0.2(1)	-	1.5(5)	0.4(2)
TiO_2	1.4(4)	-	-	-	-	-
Total	100(1)	100(1)	100(2)	100(1)	100(2)	100(7)

Standard deviations are in parentheses.

2.2.2 Geopolymer starting materials and synthesis

Geopolymers were synthesized starting from a high-quality kaolin, used as aluminosilicate source, and a sodium silicate solution as alkaline activator. The kaolin, labeled Sl-K, was supplied by Sibelco Italia S.p.A. and derives from the Seilitz kaolin deposits (Germany). It is composed of 73 wt% kaolinite and 23 wt% quartz. More information about its characterization is given in (Gasparini et al., 2015). To obtain the reactive metakaolin (Sl-MK), the kaolin powder was heated at 800°C for 2 hours (Gasparini et al., 2013). The sodium silicate solution (containing Na_2O 14.37 wt%, SiO_2 29.54 wt%, H_2O 56.09 wt%) was provided by Ingessil s.r.l. It was altered by adding distilled water and dissolving solid sodium hydroxide (NaOH, purity ≥ 98%) in order to obtain GP binders characterized by the following molar ratios:

SiO_2/Al_2O_3 = 3.7, Al_2O_3/Na_2O = 1.04 and H_2O/Na_2O = 1. One GP binder characterized by H_2O/Na_2O molar ratio of 20 (hereafter labeled GP20) was prepared and used for tests in association with the historic element made of Pietra di Angera. The Sl-MK powder was then mixed to the alkaline solution and stirred for 10 minutes by using a mechanical mixer to form a homogenous slurry. Mixing operations were performed under controlled conditions of temperature and relative humidity (20°C and 65% R.H., respectively).

2.2.3 Sample preparation and characterization

GP slurries were poured on material surfaces and cured in climatic room for 28 days at 20°C and 65% R.H. before being demolded. Samples were cut and sections analyzed by using optical and electron scanning microscopes. Microtextural investigations were performed using a stereomicroscope Olympus SZ61. A Field Emission Scanning Electron Microscope TESCAN Mira 3 XMU-series, equipped with an EDAX energy dispersive spectrometer, was used to determine microstructural features and the gradient concentration of elements across the interfaces between materials and GP. Samples were covered by 5 nm carbon coating before being investigated to prevent charge built-up on electrically insulating sample surface. Images were collected using backscattered electron (BSE) at a working distance of 15.8 mm with an acceleration voltage of 20 kV. EDS spot analyses were done with accelerating voltage of 20 kV, working distance of 15.8 mm, beam current of 20 µA and spot diameter of about 5 µm, acquiring for 100s per spot analysis. Chemical compositions were determined considering 100 wt% oxide content on an H_2O- and CO_2-free basis.

2.3. Results and Discussions

2.3.1 Stereomicroscope observations

Macroscopic structural features common to all samples can be observed from the stereomicroscope photo (Figure 2.1 both for natural stones and artificial building materials): the contact regions are evident and allow to globally evaluate the interaction between the materials. In all samples, a reaction layer (labeled as “rim” in the images) is visible between the GP binder and each material. Even at such low enlargement factors, it is possible to appreciate that the binder entered the superficial porosity of the materials ensuring good adhesion between the two. In the GP matrix, it is possible to observe unreacted metakaolin, which appears as particles with a darker tone than the matrix.

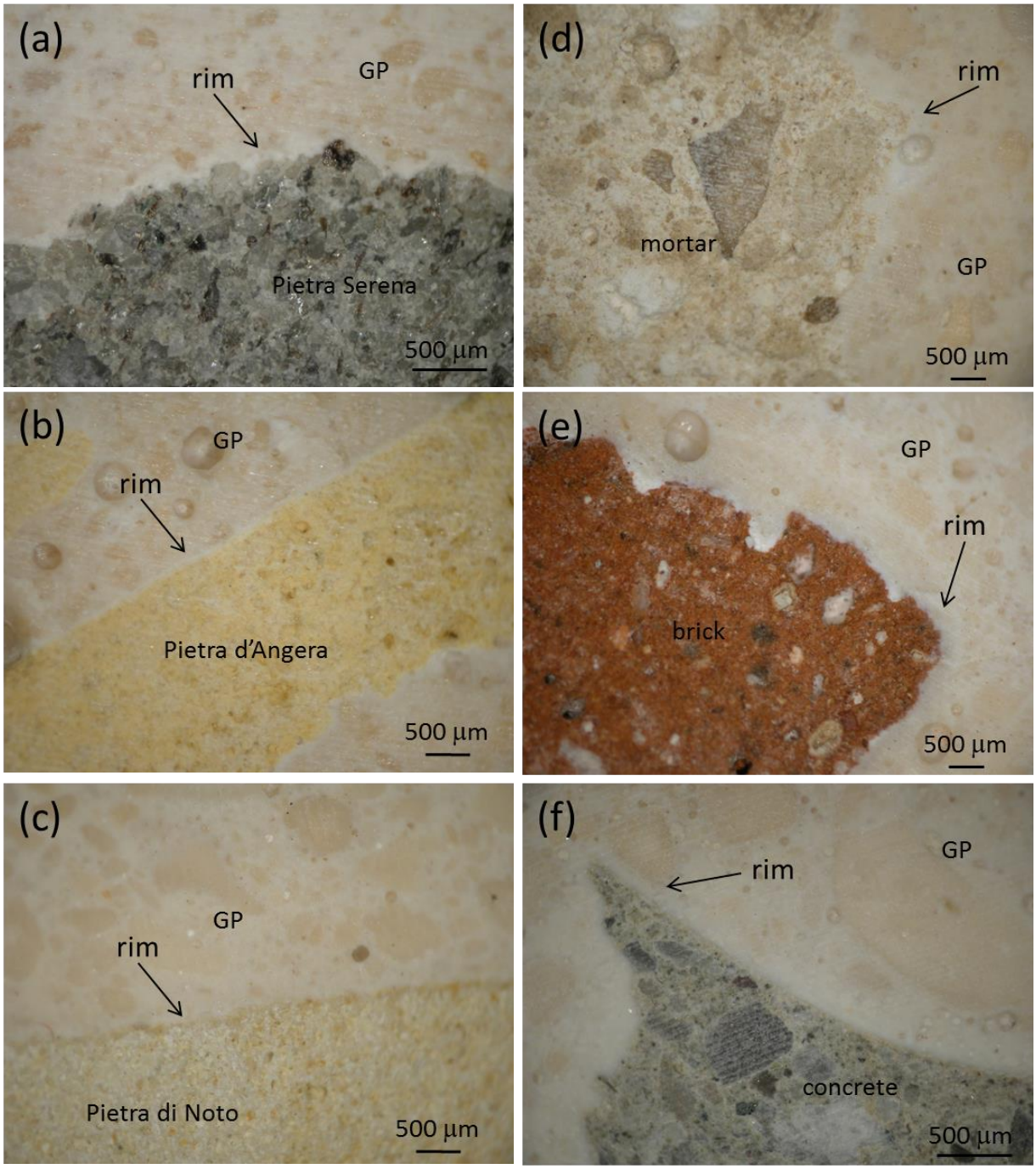

Figure 2.1. Stereomicroscope images of samples prepared with natural ornamental stones: a) Pietra Serena; b) Pietra di Angera; c) Pietra di Noto. Stereomicroscope images of samples prepared with artificial building materials: d) historic mortar; e) red brick; f) concrete. The rims are indicated by arrows. Graphic scale is reported in each image.

At the boundary between Pietra Serena and the GP, evidences of the reaction of the stone with alkalis in the slurry are recognizable: all the superficial mineral grains have rounded and not well defined borders, thus indicating partial dissolution during geopolymerization processes

(Figure 2.1a). The same border alteration is less evident in Pietra di Angera and Pietra di Noto (Figure 2.1b and 2.1c) at this observation scale.

Concerning the artificial building materials, a reaction layer is evident in all samples (Figure. 2.1d-f), and it is particularly thick between geopolymer and the lime-based mortar (Figure 2.1d).

2.3.2 SEM-EDS investigations

Microstructural features of GP binder at the interface with the different substrates have been analyzed by FE-SEM at different magnifications. The developed texture results from the chemical reaction processes responsible for geopolymer formation and for the interaction with the natural and artificial substrates. Texture analysis can then be used to develop a better understanding of the aforementioned mechanisms of reaction and to provide key insights into relating textural features to mechanical performances.

2.3.2.1 Natural stones – Pietra Serena

Interface between Pietra Serena and GP is showed in Figure 2.2a. Materials seem well bonded together. GP binder follows the stone profile and no cracks are evident at the interface. Fractures orthogonal to interface, observed within GP matrix, are probably due to cutting of the specimens for metallographic preparation. GP matrix has a quite compact microstructure with pores of ca. 50 μm in diameter. Lighter areas in the matrix are attributed to partially unreacted metakaolin.

At higher magnification (Figure. 2.2b and 2.2c), the interaction between siliceous aggregates and the highly alkaline solution resulted in a partial dissolution of quartz and mica grains, which show rounded and unraveled shapes, respectively.

However, no crystalline interfacial products are present, but an intermediate zone, which is of darker color in BSE images, thus suggesting a difference in composition, can be appreciated along the contact area and for 500 μm in depth into the GP matrix. This might be due to dissolution of siliceous aggregates that modifies the SiO_2/Al_2O_3 ratio locally, and at the same time promotes the geopolymerization on the stone surface. Another evidence of the partial dissolution of Pietra Serena is the presence of stone relicts inside the GP matrix, as shown in Figure 2.2d.

Furthermore, EDX analyses of this area (Table 2.2; labels as reported in Figure 2.2d) prove the presence of calcium deriving from Pietra Serena in the GP binder. The presence of calcium is probably due to the water flow during the first steps of geopolymerization. However, an average concentration of CaO wt% of less than 2.0(7) wt% is too low to favor the formation of C-S-H phases, as already indicated by (Yip et al., 2008), but enough to improve the adhesive mechanical strength.

2.3.2.2 Natural stones – Pietra di Angera

In Figure 2.3a, it can be seen how the GP binder well entered the superficial porosity of the stone, thus enhancing the contact the two materials suggesting a good adhesion between the two materials. An about 50 μm dark layer developed inside the GP at the contact with Pietra di Angera meaning that the two materials reacted once they were put together. Calcium can take part in the geopolimerization process and therefore its presence can affect the final products. It is important to evaluate its concentration along the borders and especially in the reaction layer. Different features due to the interaction of Pietra di Angera and the GP binder can be observed in Fig. 2.3c. EDX semi-quantitative analyses were performed in different spots on the area in Figure 2.3c and results are reported in Table 2.2.

Point analyses PA1, PA2 and PA3 correspond to reaction products. PA1 and PA2 are located on the alteration rim of a dolomite grain, while in the spot corresponding to PA3 the dolomite relict is not present anymore, but a new round phase is evident. The calcium diffusion is also evident looking at Figure 2.3c where calcium rich vein is present inside the geopolymer matrix. The composition of the reaction layer must be evaluated in order to understand which new phases developed. In Figure 2.3d, it is possible to observe is a reacted dolomite grain from Pietra di Angera giving new reaction by-products. Microchemical analyses were performed on both the new phases and the area surrounding them in order to observe how elements concentration varied in the different areas. Results are reported in Table 2.2. It is than possible to state that dolomite, which is the main mineral phase in Pietra di Angera, reacts with geopolymer slurry and gives an intermediate product richer in CaO than the geopolymer surrounding the dolomite relict. A coronitic structure is also evident.

Table 2.2 EDS analyses performed on samples prepared with natural stones expressed as wt%.

Point analyses	Na_2O	MgO	Al_2O_3	SiO_2	SO_3	K_2O	CaO	FeO
PS1	4.29	0.56	28.33	63.04	0.34	0.51	2.34	0.59
PS2	4.72	0.62	27.00	63.64	0.35	0.58	2.60	0.48
PS3	4.52	0.51	28.56	62.79	0.30	0.60	2.14	0.59
PS4	6.69	0.36	22.64	67.63	0.28	0.57	1.08	0.76
PA1	7.65	3.29	13.62	41.94	-	0.42	33.07	-
PA2	6.29	3.85	9.96	50.95	-	0.28	28.66	-
PA3	8.18	1.90	18.95	46.79	-	0.41	23.76	-
PA4	9.13	3.58	20.62	59.00	-	0.66	7.02	-
PA5	7.50	2.77	10.19	26.14	-	0.33	53.07	-
PA6	7.63	3.28	13.35	48.04	0.37	0.49	26.56	0.29
PA7	9.08	2.58	16.41	59.93	0.33	0.64	10.65	0.38
PA8	5.45	5.84	9.45	34.01	0.14	0.33	44.29	0.49
PAh1	14.99	1.40	16.85	59.05	3.30	0.92	3.17	0.32
PAh2	10.13	1.10	18.01	64.00	1.67	1.23	3.30	0.55
PAh3	13.01	1.09	22.64	52.50	6.79	0.85	2.49	0.62
PAh4	10.97	0.84	18.91	62.30	2.63	0.97	2.88	0.50
PAh6	10.04	0.93	11.88	69.26	3.31	0.79	3.28	0.51
PAh7	12.12	1.03	19.73	59.99	2.23	1.00	3.40	0.51
PN1	12.44	1.02	17.53	64.18	-	-	4.83	-
PN2	12.41	0.55	20.79	63.47	-	-	2.78	-
PN3	13.76	0.74	18.18	62.62	-	-	4.71	-
PN4	13.46	0.40	19.20	64.26	-	-	2.67	-
PN5	16.64	0.36	22.56	59.08	-	-	1.36	-
PN6	15.63	0.47	21.80	59.52	-	-	2.58	-
PN7	14.52	0.38	18.23	64.58	-	-	2.29	-
PN8	14.86	0.39	20.10	62.21	-	-	2.44	-
PN9	16.85	0.44	19.50	60.53	-	-	2.68	-
PN10	11.17	0.41	27.73	59.22	-	-	1.48	-

Note: labels indicate spot analyses as displayed in Fig. 2.2d (PS); Figs. 2.3c and 2.3d (PA); Fig. 2.4b (PAh); Fig. 2.5b (PN). For PAh and PN, analyses are performed along the transects indicated by red lines in the figures and go from the stone to the binder.

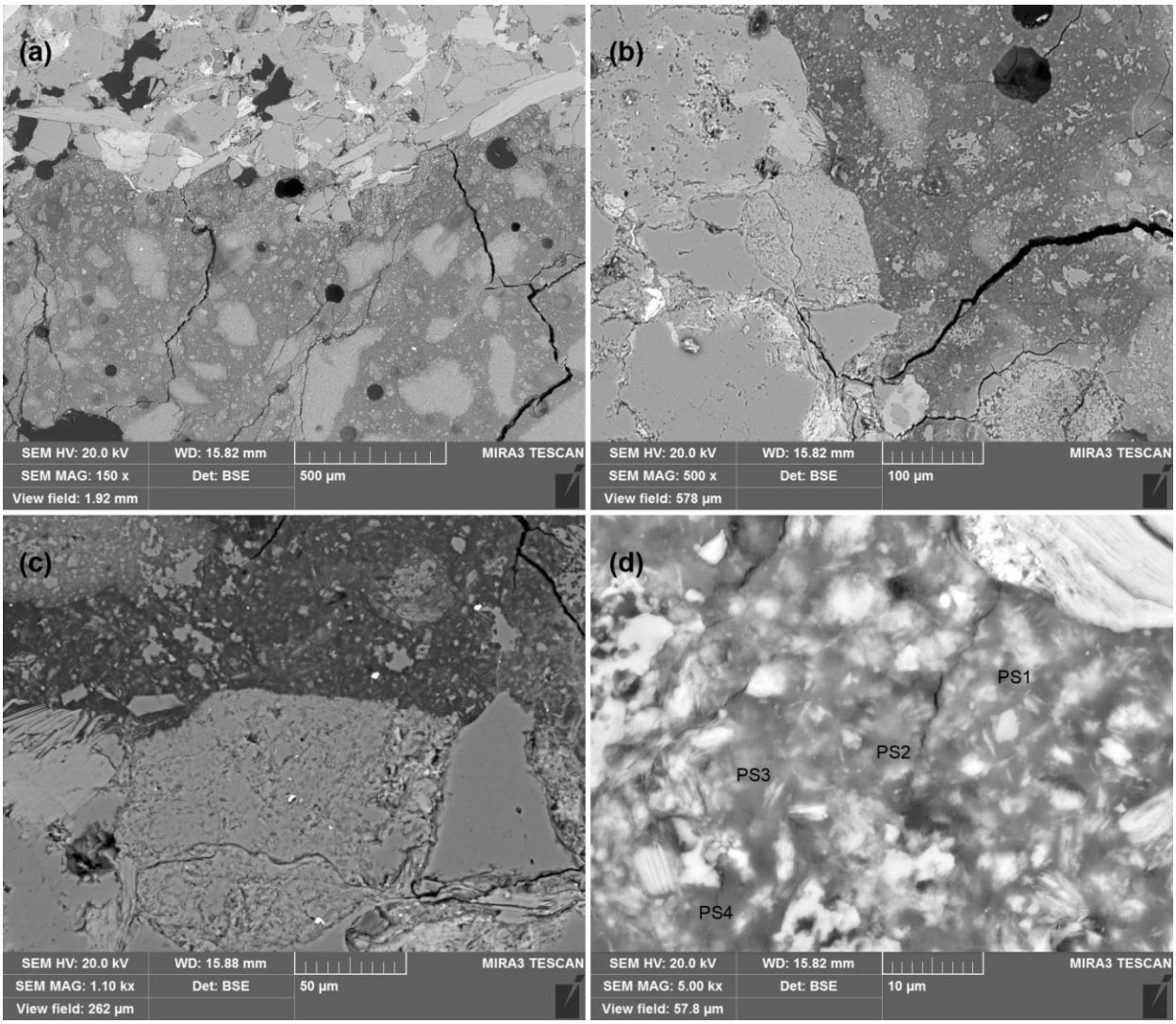

Figure 2.2. FESEM micrographs of sample prepared with Pietra Serena at different magnifications: (a) 150x; (b) 500x; (c) 1.10kx; (d) 5.00kx. Labels PS1 to PS4 in Fig. 2.2d refer to spot analyses reported in Table 2.2.

2.3.2.3 Natural stones – Historic Pietra di Angera

The interaction between a historic decorative stone element made in Pietra di Angera and a fluid GP binder was also evaluated. The sample was originally exposed to an outdoor environment. Chemical analyses carried out on the stone by FESEM-EDAX (Table 2.1) showed the presence of SO_3, concentrated in some areas, that possibly refers to the chemical decay of the stone due to the atmospheric pollutants. Polluted environments influence the conservation of carbonatic stones increasing the susceptibility to decay in outdoor conditions (Bugini and Folli, 2008; Török et al., 2011). Among pollutants, sulfur oxides produce sulfation of substrate especially for poor durable stones like Pietra di Angera (Gulotta et al., 2013).

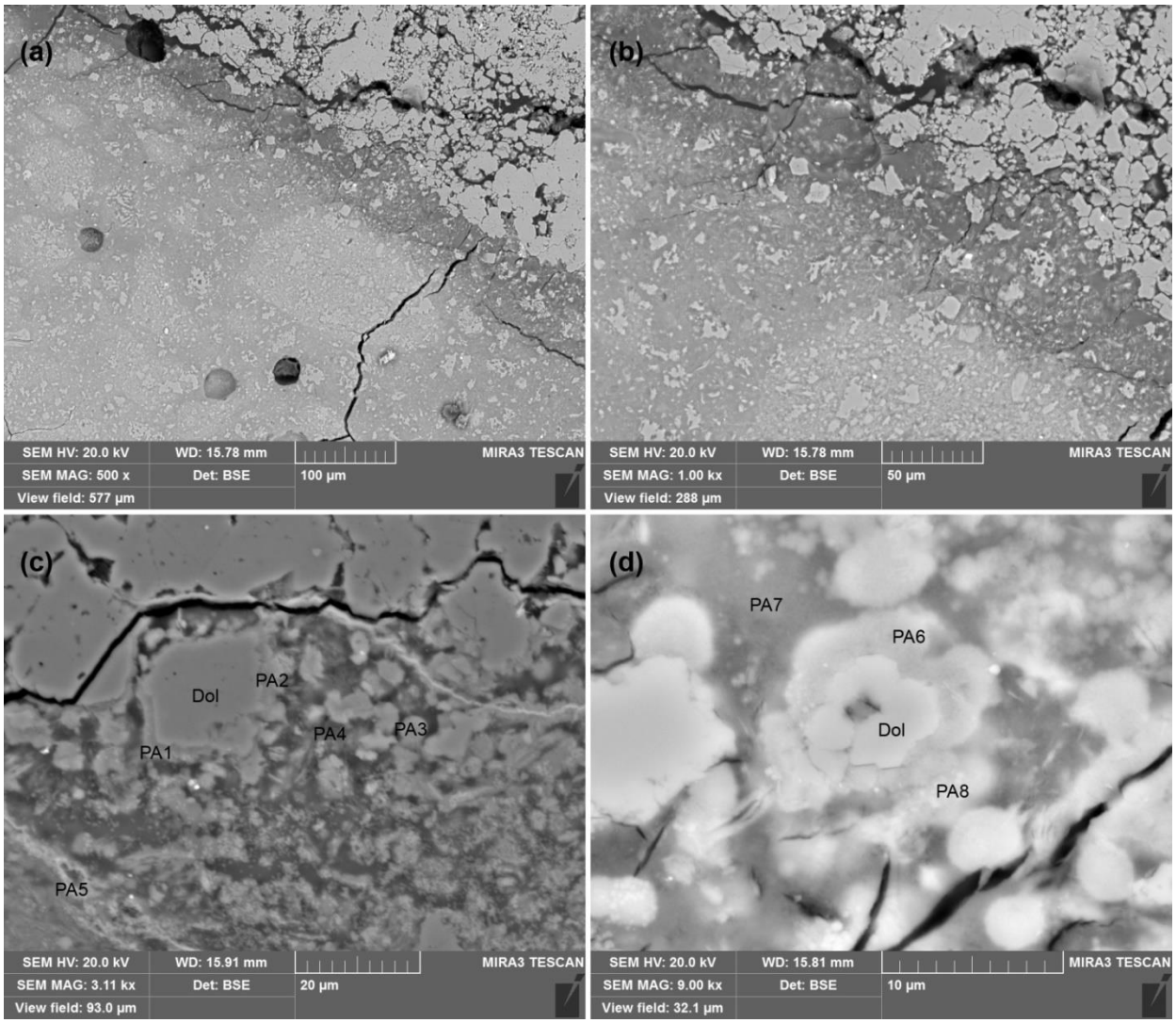

Figure 2.3. FESEM micrographs of sample prepared with Pietra di Angera at different magnifications. (a) 500x; (b) 1.00kx; (c) 3.11kx; (d) 9.00kx. Labels PA1 to PA8 in Fig. 2.3c and 2.3d refer to spot analyses reported in Table 2.2.

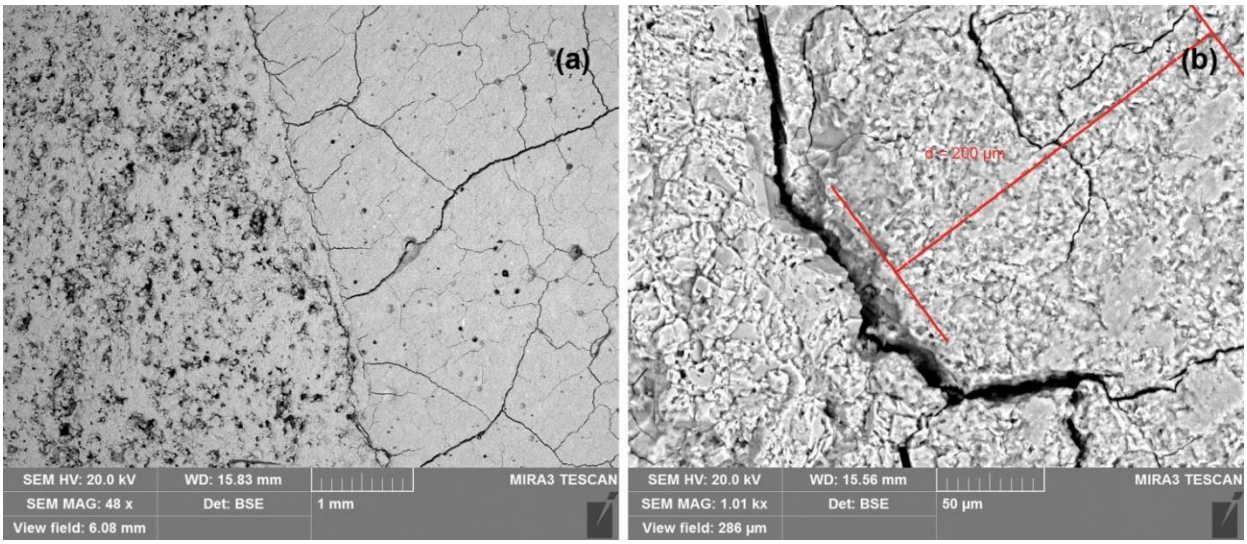

Figure 2.4. FESEM micrographs of sample prepared with the decorative element of Pietra di Angera at different magnifications. (a) 48x; (b) 1.00kx. Chemical analyses along the transect shown by the red line are reported in Table 2.2.

The interface zone (Figure 2.4a) shows that GP binder is less bonded to the stone with respect to the sample in which the quarry element of Pietra di Angera was used. Furthermore, GP matrix is widely fractured, with cracks (from few μm to 1-2 mm long) probably due both to the water loss during the curing and to sample preparation procedures. In Figure 2.4b, a transect about 200 μm long and perpendicular to the contact zone indicates the points (labeled PAh1 to PAh7 in Table 2.2) where microchemical analyses of the GP matrix were performed. The results show the presence in the matrix of SO_3 and CaO with average values of 3(2) wt% and 3(1) wt%, respectively. The diffusion of these elements in the matrix is attributed to the water contained in the alkaline solution that flows through the stone pores during the first phases of geopolymerization. However, no new phases such as thenardite or ettringite were observed in the binder. Sulfur may remain trapped in the amorphous network of GP gel, without giving rise to potentially harmful by-products (Rodriguez-Navarro et al., 2000). Consequently, the trapping function of GP can be positively considered in conservation practices.

2.3.2.4 Natural stones – Pietra di Noto

Interface between Pietra di Noto and GP is showed in Figure 2.5a. A good adhesion between the two materials can be observed, probably due to the high porosity and the rough profile of the stone. This allows the GP binder to better permeate (for about 500 μm) the stone, assuring a physical interlock and improving the adhesion between the two. Different authors relate the adhesion property to the roughness degree of the substrate (Garbacz et al., 2006), to the porosity of binder (Barroso De Aguiar and Cruz, 1998), and to the presence of the aggregates and their morphology (Caliskan and Karihaloo, 2004). In conservation practices, a good adhesion between the substrate and the binder could reduce the possibility of decay due to water infiltration. In this work, the high porosity of Pietra di Noto could increase the cohesive strength influencing positively the adhesion performances. However, the porosity of the stone facilitates the migration of water contained in the slurry into the stone causing a crack-rich region (about 1 mm wide) from the interface zone within the GP matrix.

Microchemical analyses of the GP matrix were performed along a 1 mm long transect perpendicular to the contact zone, as shown in Figure 2.5b. Analyses are reported in Table 2.2 and named PN1 to PN10. No reaction layers can be appreciated. A decrease in CaO wt% values from 4.8 to 1.3 wt% suggests the diffusion of calcium into the matrix with the same modalities as described for the other stone types.

In all natural samples described above (par. 2.3.2.1 to 2.3.2.4), GP contains some calcium, although it was synthesized from a Ca-free precursor such as metakaolin. The presence of this element into the geopolymer must be due to the interaction between the different carbonates contained in all the stones mentioned above and the geopolymer itself. Water contained in the geopolymer slurry allows calcium cations to migrate from the rock to the geopolymer. This in turn may likely affect its formation reaction and its final mechanical and physical properties.

Furthermore, stereomicroscope observations and elemental chemical analyses do not reveal the presence of efflorescence both on geopolymer matrix and on the stones. The use of an alkali-rich solution as activator for geopolymerization could affect the potential applicability of GP in restoration. However, the presence of calcium in GP gel can help to reduce carbonate formation, as already noted by Najafi Kani et al (2012).

2.3.2.5 Artificial construction materials – Red brick

A thin and discontinuous dark layer characterizes the interaction zone between red brick and GP binder as shown in Figure 2.6a. Fractures orthogonal and parallel to the interface are observed within the GP matrix. The former may be ascribed to preparation of specimens for the analysis; the latter are likely due to shrinkage of the binder caused by migration of water from GP into the brick. Anyway, close to the interaction zone, the GP matrix has a quite compact microstructure and profile of the brick facilitate the adhesion between the two materials. At higher magnification the rough, (Figure 2.6b) deteriorated and reacted crystals are evident at the interaction zone. This could be either due to interaction with alkalis or to high temperature processes in brick production.

Microchemical analyses were performed in GP matrix along an about 1 mm transect. Aluminum and silicon in red bricks increases the SiO_2/Al_2O_3 ratio at local scale promoting the geopolymerization next to the interface. SiO_2/Al_2O_3 varies from 3.5(1) to 2.9(4) moving from interface (the dark layer) to GP matrix. Detected CaO wt% values varies from 2.7 wt% to 1.2 wt%, with an average value of 1.8(6) wt%. Calcium values found in this sample are lower than the average ones found in other samples prepared both with natural stones and artificial building materials.

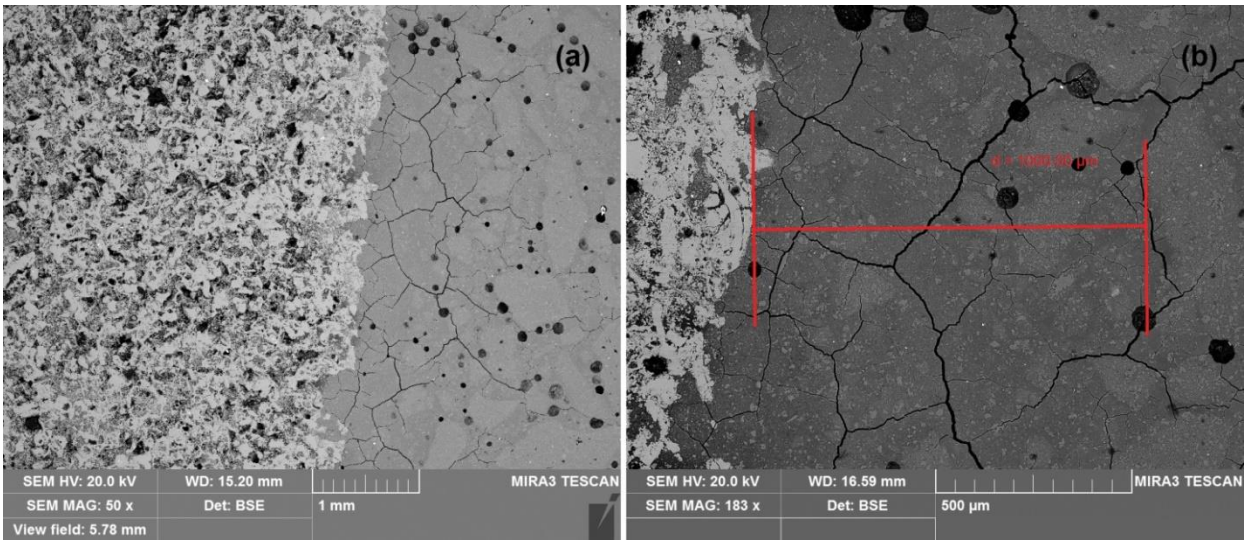

Figure 2.5. FESEM micrographs of sample prepared with Pietra di Noto at different magnifications. (a) 50x; (b) 183x. Chemical analyses along the transect shown by the red line are reported in Table 2.2.

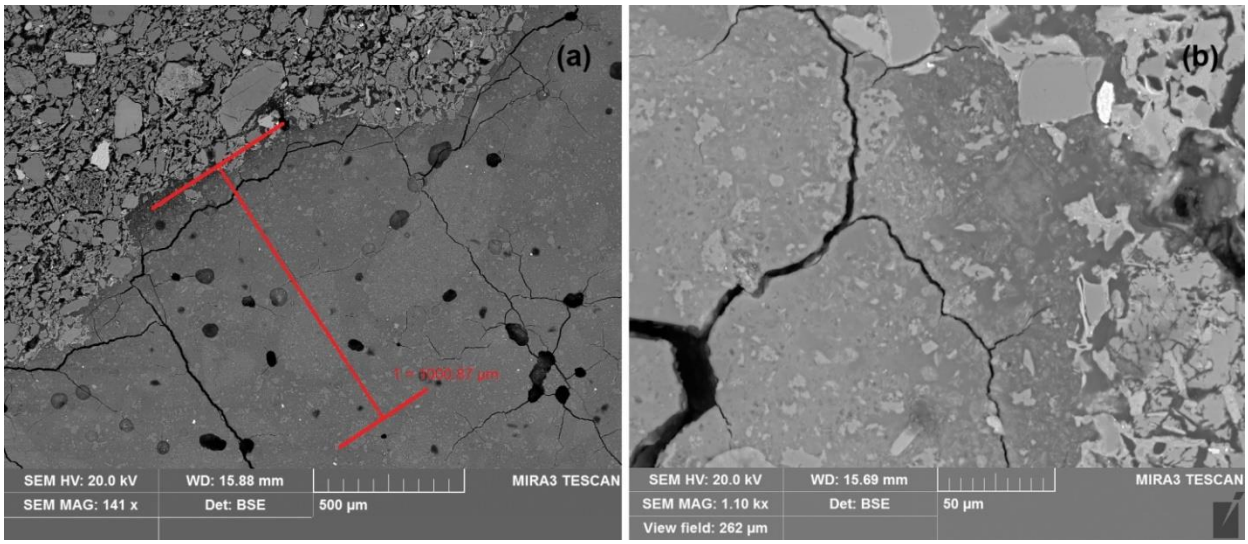

Figure 2.6. FESEM micrographs of samples prepared with a red brick at different magnifications: (a) 141x; (b) 1.10kx.

2.3.2.6 Artificial construction materials – Historic Mortar

In this work, the use of a historic mortar allowed the study of the interaction of GP with the closest material in terms of properties and destination of use. In Figure 2.7a, an evident reaction layer can be seen at the interface between the two materials. The reaction layer is continuous and runs along the contact interface. Geopolymer matrix appears homogeneous and no cracks can be observed at the interface. The geopolymer texture changes moving away from the contact with the mortar and becomes more homogeneous with less metakaolin and mortar relicts inside the matrix (Figure 2.7b). Looking at the interface at higher magnifications (Figure 2.7c and 2.7d), different reaction layers can be recognized. Point analyses performed in the area

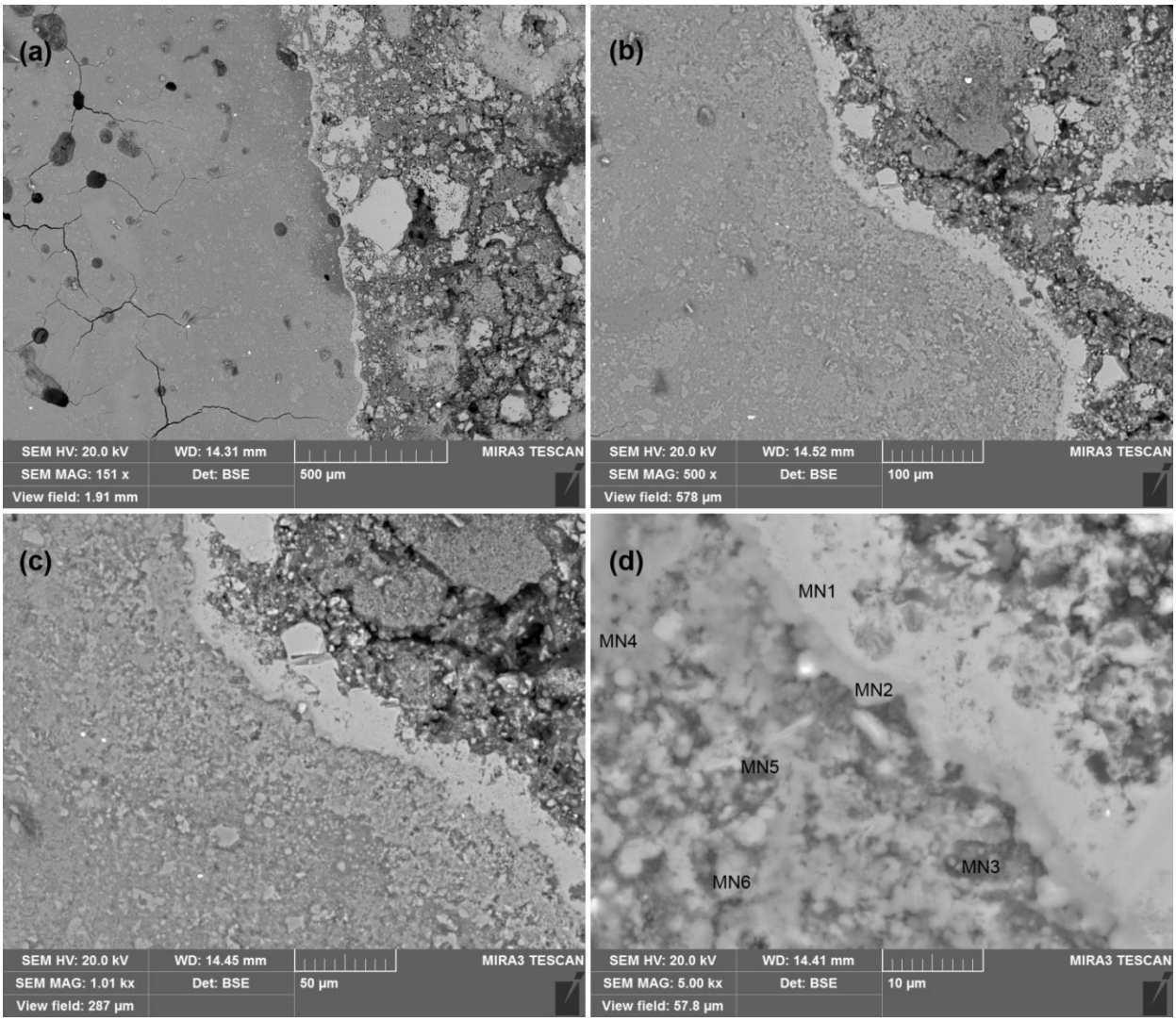

Figure 2.7. FESEM micrographs of sample prepared with a historic mortar at different magnifications: (a) 250x; (b) 644x; (c) 1.10kx; (d) 5.00kx. Labels MN1 to MN6 in Fig. 2.7d refer to spot analyses reported in Table 2.3.

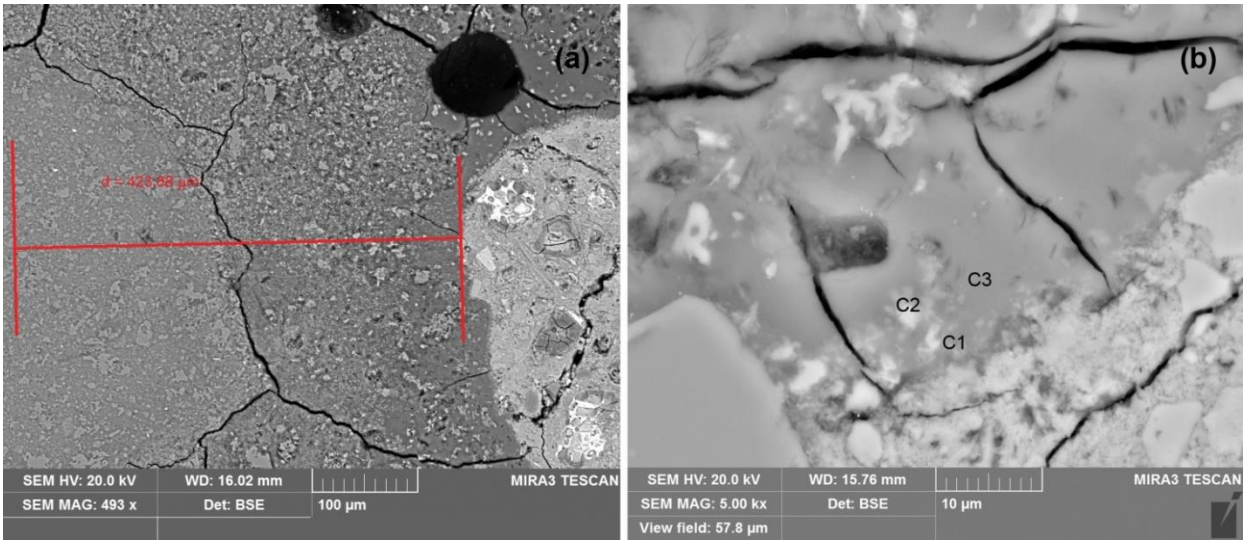

Figure 2.8. FESEM micrographs of sample prepared with concrete at different magnifications: (a) 493x; (b) 5.00kx. Labels C1 to C8 in Fig. 2.8b refer to spot analyses reported in Table 2.3.

shown in Figure 2.7d are reported in Table 2.3. Going from the mortar (upper right) to the GP, the first layer, 10 to 15 μm wide, is completely made up of calcium carbonate (Ca is 94.07 wt% at MN1) and appears be quite compact and homogeneous, and grows from the mortar. It is like geopolymer corroded and dissolved the mortar allowing new phases to precipitate. The second one, 2 to 5 μm wide, is darker than the first one. SiO_2, Al_2O_3 and CaO concentrations at MN2 spot analysis reveal the presence of C-A-S-H gel formed as a reaction by-product. A third reaction layer, about 100 μm large, is found inside the GP matrix (point analyses MN3, MN4, MN5). It appears less homogeneous than the others, and mainly formed by new rounded phases. The presence of different reaction layers rich in calcium could improve the mechanical properties at interfaces between the two materials.

Table 2.3. EDS analyses performed on samples prepared with artificial building materials expressed as wt%.

Point analyses	Na_2O	MgO	Al_2O_3	SiO_2	SO_3	K_2O	CaO
MN1	1.06	0.86	1.01	2.46	0.39	0.16	94.7
MN2	11.21	1.66	14.25	40.23	0.19	0.41	32.04
MN3	7.55	0.94	21.33	60.04	0.35	0.66	9.11
MN4	10.76	1.38	17.26	51.60	0.31	0.43	18.26
MN5	6.94	1.15	16.02	50.38	0.40	0.60	24.51
MN6	10.02	1.25	17.17	46.79	0.27	0.43	24.07
C1	9.49	3.01	19.40	58.31	0.97	0.53	8.24
C2	8.50	1.43	19.23	54.72	0.87	0.50	14.75
C3	8.08	0.98	21.80	62.62	0.94	0.54	5.03

Note: labels as in Figs. 2.7d (MN) and 2.8b (C).

2.3.2.7 Artificial construction materials – Concrete

Adhesion between geopolymer and concrete is good as shown in Figure 2.8a. There is no reaction layer between the two materials, but GP matrix becomes more homogeneous when moving away from the contact surface with concrete, highlighting three different textural areas. However, microchemical analyses performed on three areas of 100 μm^2 along the transect shown in figure, reveal no differences in SiO_2/Al_2O_3 ratio. Cracks due to sample preparation can be noticed both in matrix and in concrete. The interaction zone was analyzed at higher

magnification (5kx) (Figure 2.8b). Analyses were performed on three spots labeled C1 (close to the interface), C2 (on the brightest spot) and C3 (on GP matrix) and reported in Table 2.3. According to the chemical analyses, the SiO_2/Al_2O_3 ratio remains constant at around 2.9(1) wt% in all points. A fairly high calcium content was observed in all analyzed points and it affected in two ways the geopolymerization reaction. In C1 and C2, new phases developed, characterized by rounded shapes, like the ones found in the third reaction layer of the sample prepared with the historic mortar. In the matrix (C3), calcium modifies the composition of the gel, which approaches that of calcium silico-aluminate hydrate (C-A-S-H) gels.

References

Alessandrini, G., Bocci, A., Bugini, R., Emmi, D., Peruzzi, R., Realini, M., 1992. Stone materials of Noto (Syracuse) and their decay, Proceedings of the 7th International Congress on Deterioration and Conservation of Stone: held in Lisbon, Portugal, 15-18 June 1992. Laboratório Nacional de Engenharia Civil, pp. 11-20.

Anania, L., Badalà, A., Barone, G., Belfiore, C.M., Calabrò, C., La Russa, M.F., Mazzoleni, P., Pezzino, A., 2012. The stones in monumental masonry buildings of the "Val di Noto" area: New data on the relationships between petrographic characters and physical–mechanical properties. Construction and Building Materials 33, 122-132.

Bakharev, T., 2005a. Durability of geopolymer materials in sodium and magnesium sulfate solutions. Cement and Concrete Research 35, 1233-1246.

Bakharev, T., 2005b. Resistance of geopolymer materials to acid attack. Cement and Concrete Research 35, 658-670.

Bargossi, G.M., Gamberini, F., Gasparotto, G., Grillini, G.C., Marocchi, M., 2004. Dimension and ornamental stones from the Tosco-Romagnolo and Bolognese Apennine. Periodico di Mineralogia-LXXIII, special, 171-195.

Barroso De Aguiar, J., Cruz, M.D., 1998. A study of the adhesion between hydraulic mortars and concrete. Journal of adhesion science and technology 12, 1243-1251.

Bugini, R., Folli, L., 2008. Stones used in Milan architecture. Materiales de Construcción 58, 33-50.

Caliskan, S., Karihaloo, B.L., 2004. Effect of surface roughness, type and size of model aggregates on the bond strength of aggregate/mortar interface. Interface Science 12, 361-374.

Cantisani, E., Garzonio, C.A., Ricci, M., Vettori, S., 2013. Relationships between the petrographical, physical and mechanical properties of some Italian sandstones. International Journal of Rock Mechanics and Mining Sciences 60, 321-332.

Cappelletti, G., Fermo, P., Camiloni, M., 2015a. Smart hybrid coatings for natural stones conservation. Progress in Organic Coatings 78, 511-516.

Cappelletti, G., Fermo, P., Pino, F., Pargoletti, E., Pecchioni, E., Fratini, F., Ruffolo, S.A., La Russa, M.F., 2015b. On the role of hydrophobic Si-based protective coatings in limiting mortar deterioration. Environmental Science and Pollution Research 22, 17733-17743.

Duxson, P., Mallicoat, S., Lukey, G., Kriven, W., van Deventer, J.S., 2005. Microstructural Characterisation of Metakaolin-Based Geopolymers. Advances in Ceramic Matrix Composites X, Volume 165, 71-85.

Elert, K., Pardo, E.S., Rodriguez-Navarro, C., 2015. Alkaline activation as an alternative method for the consolidation of earthen architecture. Journal of Cultural Heritage 16, 461-469.

Elert, K., Sebastián, E., Valverde, I., Rodriguez-Navarro, C., 2008. Alkaline treatment of clay minerals from the Alhambra Formation: Implications for the conservation of earthen architecture. Applied Clay Science 39, 122-132.

Fiumara, A., Riganti, V., Veniale, F., Zezza, U., 1979. (On the preservation treatments of the Angera stone). Geologia Applicata e Idrogeologia 14, 191-214.

Garbacz, A., Courard, L., Kostana, K., 2006. Characterization of concrete surface roughness and its relation to adhesion in repair systems. Materials Characterization 56, 281-289.

Gasparini, E., Tarantino, S.C., Conti, M., Biesuz, R., Ghigna, P., Auricchio, F., Riccardi, M.P., Zema, M., 2015. Geopolymers from low-T activated kaolin: Implications for the use of alunite-bearing raw materials. Applied Clay Science 114, 530-539.

Gasparini, E., Tarantino, S.C., Ghigna, P., Riccardi, M.P., Cedillo-González, E.I., Siligardi, C., Zema, M., 2013. Thermal dehydroxylation of kaolinite under isothermal conditions. Applied Clay Science 80-81, 417-425.

Gulotta, D., Bertoldi, M., Bortolotto, S., Fermo, P., Piazzalunga, A., Toniolo, L., 2013. The Angera stone: A challenging conservation issue in the polluted environment of Milan (Italy). Environmental Earth Sciences 69, 1085-1094.

Hanzlíček, T., Steinerová, M., Straka, P., Perná, I., Siegl, P., Švarcová, T., 2009. Reinforcement of the terracotta sculpture by geopolymer composite. Materials & Design 30, 3229-3234.

Kani, E.N., Allahverdi, A., Provis, J.L., 2012. Efflorescence control in geopolymer binders based on natural pozzolan. Cement and Concrete Composites 34, 25-33.

La Russa, M.F., Barone, G., Belfiore, C.M., Mazzoleni, P., Pezzino, A., 2011. Application of protective products to “Noto” calcarenite (south-eastern Sicily): a case study for the conservation of stone materials. Environmental Earth Sciences 62, 1263-1272.

Pacheco-Torgal, F., Castro-Gomes, J., Jalali, S., 2008. Alkali-activated binders: A review. Construction and Building Materials 22, 1305-1314.

Pacheco-Torgal, F., Moura, D., Ding, Y., Jalali, S., 2011. Composition, strength and workability of alkali-activated metakaolin based mortars. Construction and Building Materials 25, 3732-3745.

Palomo, A., Blanco-Varela, M.T., Granizo, M.L., Puertas, F., Vazquez, T., Grutzeck, M.W., 1999. Chemical stability of cementitious materials based on metakaolin. Cement and Concrete Research 29, 997-1004.

Palomo, A., Krivenko, P., Garcia-Lodeiro, I., Kavalerova, E., Maltseva, O., Fernández-Jiménez, A., 2014. A review on alkaline activation: new analytical perspectives. Materiales de Construcción 64, e022.

Pelisser, F., Guerrino, E.L., Menger, M., Michel, M.D., Labrincha, J.A., 2013. Micromechanical characterization of metakaolin-based geopolymers. Construction and Building Materials 49, 547-553.

Provis, J.L., Bernal, S.A., 2014. Geopolymers and related alkali-activated materials, Annual Review of Materials Research, pp. 299-327.

Provis, J.L., Palomo, A., Shi, C., 2015. Advances in understanding alkali-activated materials. Cement and Concrete Research 78, Part A, 110-125.

Rashad, A.M., 2013. Alkali-activated metakaolin: A short guide for civil Engineer – An overview. Construction and Building Materials 41, 751-765.

Rescic, S., Plescia, P., Cossari, P., Tempesta, E., Capitani, D., Proietti, N., Fratini, F., Mecchi, A., 2011. Mechano-chemical activation: an ecological safety process in the production of materials to stone conservation. Procedia Engineering 21, 1061-1071.

Rodriguez-Navarro, C., Doehne, E., Sebastian, E., 2000. How does sodium sulfate crystallize? Implications for the decay and testing of building materials. Cement and Concrete Research 30, 1527-1534.

Shi, C., Jiménez, A.F., Palomo, A., 2011. New cements for the 21st century: The pursuit of an alternative to Portland cement. Cement and Concrete Research 41, 750-763.

Soggetti, F., Zezza, U., 1983. (Possibility of exploitation and technical properties of the Angera stone, Lago Maggiore). Geologia Applicata e Idrogeologia 18, 81-93.

Temuujin, J., Rickard, W., Lee, M., van Riessen, A., 2011. Preparation and thermal properties of fire resistant metakaolin-based geopolymer-type coatings. Journal of Non-Crystalline Solids 357, 1399-1404.

Török, Á., Licha, T., Simon, K., Siegesmund, S., 2011. Urban and rural limestone weathering; the contribution of dust to black crust formation. Environmental Earth Sciences 63, 675-693.

Van Deventer, J.S.J., Provis, J.L., Duxson, P., 2012. Technical and commercial progress in the adoption of geopolymer cement. Minerals Engineering 29, 89-104.

Veniale, F., Setti, M., Rodriguez-Navarro, C., Lodola, S., 2001. Role of clay constituents in stone decay processes. Materiales de Construcción 51, 163-182.

Wang, H., Li, H., Yan, F., 2005. Synthesis and mechanical properties of metakaolinite-based geopolymer. Colloids and Surfaces A: Physicochemical and Engineering Aspects 268, 1-6.

Yip, C.K., Provis, J.L., Lukey, G.C., van Deventer, J.S.J., 2008. Carbonate mineral addition to metakaolin-based geopolymers. Cement and Concrete Composites 30, 979-985.

CHAPTER 3

CEMENTS FROM PIETRA SERENA SEWAGE SLUDGE IN MATRICES OF FLY ASHES AND METAKAOLIN

3.1. Introduction

Pietra Serena is a bluish-gray sandstone mainly quarried in the district of Firenzuola (Appenine, North East of Florence, Italy), which belongs to the Marnoso-Arenacea formation (Banchelli et al., 1997; Cantisani et al., 2013; Malesani et al., 2003). The proximity of the quarries to Tuscan cities and towns have made Pietra Serena one of the most mined and used (mainly for decorative purposes) stones of the Italian architecture from Renaissance until nowadays (Fratini et al., 2014). A problem related to its cultivation, and generally common to all stone processing, is the production of waste materials, such as the sewage sludge obtained by the cutting of stone blocks. While the coarser fractions of quarrying wastes can be reused in construction industries (Akbulut and Gürer, 2007; Felekoglu, 2007), sewage sludge has a low commercial value and needs precise requirements for its suitable disposal. Furthermore, appropriate disposal sites must be found, otherwise harmful manifestations to the environment would also be induced. Reuse, rather than disposal, would be the ideal solution. Suitability of alkaline activation process applied to sewage sludge is here addressed.

Many studies on alkali activated materials (AAMs) as alternatives to traditional construction materials, such as mortars or Ordinary Portland Cement (OPC), have been realized with a view towards reducing the CO_2 footprint (Duxson et al., 2007; Pacheco-Torgal et al., 2008). Furthermore, a growing interest for the themes of sustainability and reuse of waste materials has been observed. In fact wastes derived by various human activities, until now under-utilized or simply dismissed, start to be valorised by the alkaline activation, producing economic and environmental benefits (Bernal et al., 2016; Payá et al., 2014).

The synthesis of AAMs require the employment of two main compounds: an alkaline activator, generally in aqueous solution, and a precursor sufficiently rich in reactive silica and alumina, mainly available as amorphous phase (Provis and Bernal, 2014). Among the calcined clays, metakaolin represents one of the most studied precursors, due to its high reactivity and the good properties in terms of resistance and durability of the final products (Clausi et al., 2016; Duxson et al., 2006; Gasparini et al., 2015; Palomo et al., 1999a; Siddique and Klaus, 2009).

Among the industrial by-products instead, largely used are the blast furnace slags from iron-making processes, and the fly ashes (FA) from coal combustion power plant. In literature, many studies on their characterization and on the performances of pastes, mortars and concrete can be found (Duxson and Provis, 2008; Fernández-Jiménez and Palomo, 2005; Palomo et al., 1999b; Puertas et al., 2000; Rashad, 2014). Slags and/or fly ashes can be further combined with secondary raw materials to maximise the conversion of wastes into novel resources (Horpibulsuk et al., 2015; Rakhimova and Rakhimov, 2015; Ruiz-Santaquiteria et al., 2013).

Studies concerning the identification of other potential secondary raw precursors in the synthesis of AAMs have been recently collected in thorough reviews (Bernal et al., 2016; Payá et al., 2014). Works on the use of sewage sludge and reservoir sludge as raw materials are reported (Ferone et al., 2013; Yang et al., 2013). Few researches have instead explored sandstone rocks as precursors in the alkaline activation process, achieving encouraging results by transforming the product of soil erosions into resource to produce cements (Dong et al., 2014; Li et al., 2014).

In this paper, the opportunity to reuse the sewage sludge derived from the production of the Pietra Serena sandstone in the synthesis of AAMs has been tested for the first time. A synergic use with a fly ash (FA) class F and a high-quality metakaolin is also proposed with the aim to produce valid construction materials. To this purpose, the work has been organized as follows:

- Pietra Serena sewage sludge, untreated and heated at 800 °C for two hours, FA and metakaolin have been characterized by X-ray Fluorescence (XRF), Fourier Transform Infrared Spectroscopy (FTIR), X-ray Powder Diffraction (XRPD), Thermogravimetry and Differential Thermal Analysis (TG-DTA) and laser granulometry;
- the sewage sludge have been mixed in different weight ratios with FA and metakaolin, respectively, and allowed to react with a sodium hydroxide solution. Samples have been cured at 85 °C at 100% Relative Humidity (R.H.) conditions. The use of FA has allowed the synthesis of AAMs exclusively composed by recycled raw materials, while metakaolin has been used to evaluate the possibility to use Pietra Serena sewage sludge in specific application fields as those of replacement or restoration;
- the hardened products obtained from the different mixtures have been characterized from the mechanical viewpoints;
- samples that returned the best mechanical behaviors have been submitted to physico-chemical and microstructural characterizations by XRPD, FTIR, Scanning Electron Microscopy (SEM) and colorimetry;

- results have been discussed with respect to the role of the sewage sludge in the AAMs synthesis.

3.2. Experimental

3.2.1 Selection and characterization of the starting materials

Sewage sludge of Pietra Serena (hereafter labelled only sPS) were provided by Pietra Serena Group S.r.l. of Firenzuola (Italy) and used after drying at 100 ºC for 24 hours in oven. The FA from a thermo-electric power plant located in Teruel (Spain) and classified as Class F in the ASTM C 618 normative were used after milling for 1 hour at 1200 rpm. The kaolin, labelled Sl-K, was provided by Sibelco Italia S.p.A. and derives from the Seilitz kaolin deposits (Germany). More information about its characterization and uses is reported in prior researches (Clausi et al., 2016; Gasparini et al., 2013). Sl-K was submitted to thermal treatment at 800 °C for 2 hours to obtain the reactive metakaolin (hereafter called Sl-MK).

The chemical compositions of the three starting materials were determined by X-ray fluorescence (XRF) using a PHILIPS PW1004 X-ray spectrometer with a Sc-Mo X-ray generator tube and are reported in Table 3.1. The lost on ignition (L.o.I.), determined by mass loss up to 1000 °C, is also reported in the table.

Table 3.1 Chemical composition (wt%) of Pietra Serena sewage sludge (sPS), fly ash (FA) and kaolin (Sl-K).

Oxides	SiO_2	Al_2O_3	$Fe2O_3$	CaO	MgO	SO_3	Na_2O	K_2O	TiO_2	Other	L.o.I.[a]
sPS	43.50	8.28	2.44	19.53	4.19	0.18	1.46	1.74	0.42	0.25	18
FA	39.03	27.06	19.50	6.40	1.04	1.76	0.16	1.41	0.96	0.85	1.82
Sl-K	67.00	31.50	0.32	0.12	0.23	-	-	0.35	0.24	-	10

[a]L.o.I.: weight loss after calcination at 1000 C for one hour.

sPS were also thermally treated at 800 °C for 2 hours, the same temperature used to produce Sl-MK, and used as starting material in the experimentation (labelled sPS_{800}).

TG-DTA measurements were performed on sPS by using a TA instruments Q600 and reported in Figure 3.1. 40 mg of sample powder were heated in a Pt crucible at 5 °C/min heating

rate under nitrogen atmosphere in the temperature range 26-1000 °C, using Al_2O_3 as reference material. A total weight loss of 16.5% was detected: 0.5% was ascribed to the adsorbed or weakly bonded water in the range 26-200 °C; a weight loss of 1.5% at around 500 °C was attributed to the dehydroxilation of chlorite group minerals; in the range between 700 and 800 °C, a weight loss of 14.5% was due to the CO_2 loss of carbonates. The endothermic peak close to 573 °C corresponds to the conversion of polymorphic transition phase from α-quartz to β-quartz.

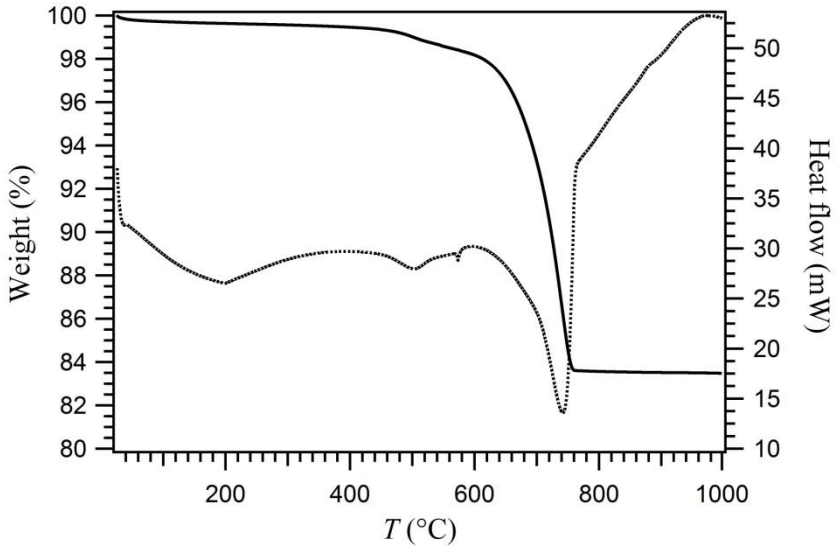

Figure 3.1. TG (black curve) and DTA (black dotted curve) of Pietra Serena sewage sludge (sPS).

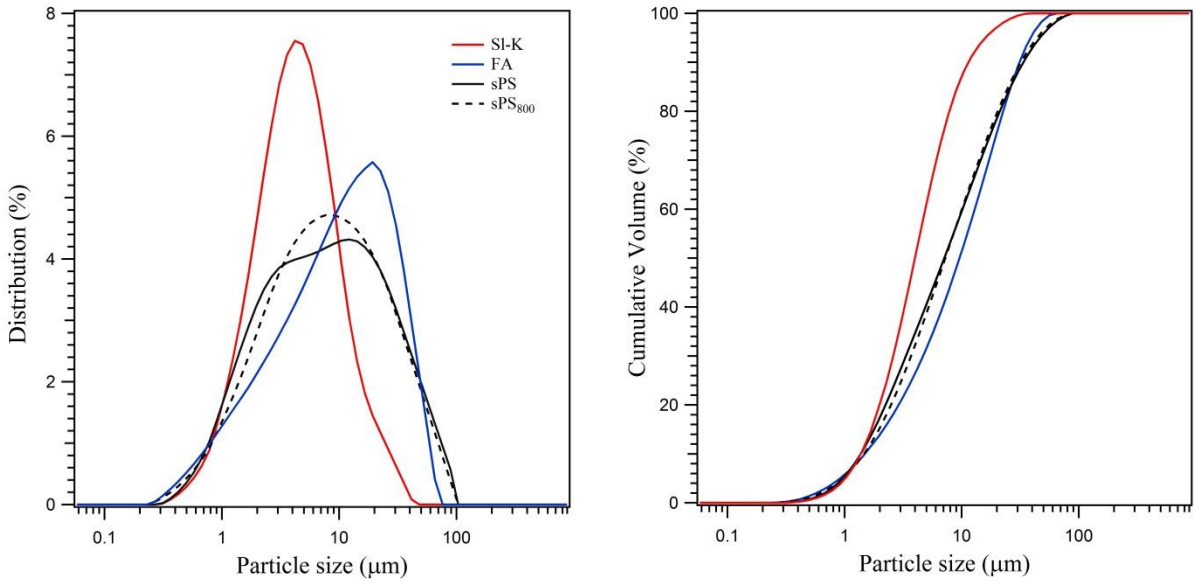

Figure 3.2. Granulometry distribution of the Pietra Serena sewage sludge untreated (sPS) (black line) and annealed at 800°C for 2hours (sPS_{800}) (black dotted line), fly ashes (FA) (blu line) and metakaolin (Sl-MK) (red line).

The particle size distribution of the four starting materials was analysed by laser granulometry using a laser diffractometer SYMPATEC with a measuring range of 0.05-875 µm and is showed in Figure 3.2. A unimodal distribution was observed for all materials with the particle size distribution ranging from 0.3 µm and 45 µm for Sl-MK, between 0.3 µm and 90 µm for sPS and sPS_{800}, and between 0.25 µm and 65 µm for FA.

XRPD analyses were carried out by using a BRUKER-AXS D8 ADVANCE X-ray diffractomer and collected with CuK α1,α2 radiation in the range 5-60º 2θ with an angular step size of 0.012º 2θ and time per step of 0.5 s. FA were constituted mainly by a vitreous phase and some crystalline phases (quartz, mullite and hematite), while Sl-MK pattern showed quartz as the only crystalline phase and a hump related to the amorphous phase between 20° and 35° 2θ (Figure 3.3a). In sPS, the crystalline phases detected were clinochlore, muscovite, quartz, albite, anorthite, calcite and dolomite; in sPS_{800} pattern, the carbonates decomposition was confirmed by the presence of lime (CaO) and periclase (MgO) and the disappearance of dolomite and calcite. Disappearance of clinochlore peaks was also observed (Figure 3.3b).

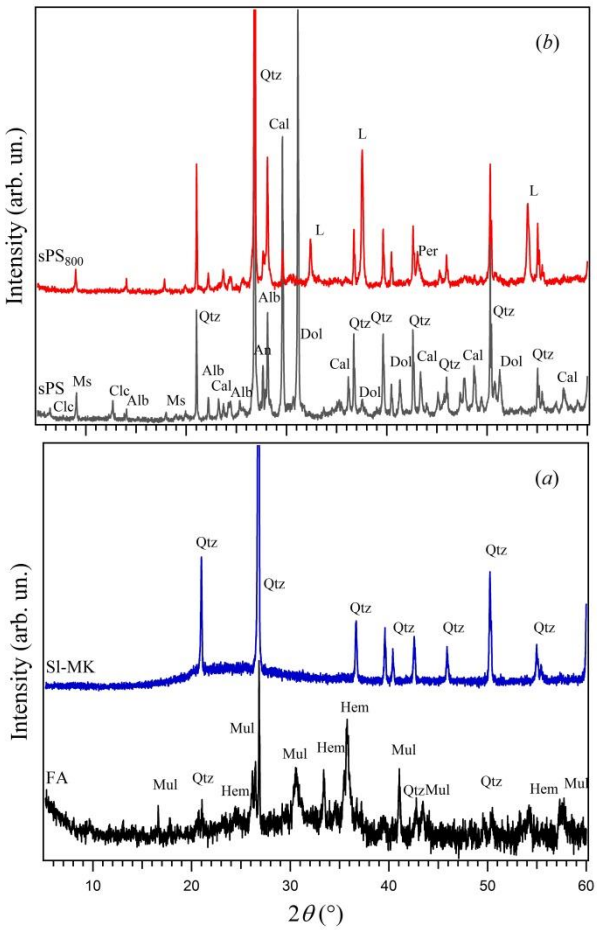

Figure 3.3. (a) XRPD patterns of FA and Sl-MK; (b) XRPD patterns of sPS and sPS_{800}. Alb = Albite; An = Anorthite; Cal = Calcite; Clc = Clinochlore; Dol = Dolomite; Hem = Hematite; L=Lime; Ms = Muscovite; Mul = Mullite; Per= Periclase; Qtz = Quartz .

3.2.2 Sample preparation and characterization

Powders of the starting materials were mixed in different weight proportions and added to sodium hydroxide solutions (NaOH 8M and 12M) obtained by dissolving pellets of sodium hydroxide (supplied by Sigma-Aldrich Co.; purity of 99 wt. %) in deionised water. The slurries were mixed for 3 minutes by using a mechanical mixer before being poured in 1 × 1 × 6 cm^3 prismatic steel moulds and compacted by mechanical vibrations for 60s to remove the entrained air. For each formulation, the liquid/solid weight ratio was chosen in order to guarantee the minimum workability of the slurry and to allow its pouring in the moulds. Specimens were cured at 85 °C for 5 or 20 hours in sealed vessels to ensure 100% R.H. conditions. At the end of the curing, specimens were demoulded and frozen in acetone and ethanol before being stored at room temperature. Information about the labels, the starting materials proportions and the synthesis parameters of each sample are reported in Table 3.2.

Flexural and compressive strengths of the resulting materials were measured after one day of curing using an IBERTEST AUTOTEST-200/10 SW test frame. Flexural strengths were calculated as the average value of six measurements, while the average compressive strengths values were measured on twelve specimens.

Selected samples were characterized by XRPD, FTIR, SEM and colorimetric analyses. FTIR spectra were obtained by analysing, at room temperature, pellets containing 1.0 mg of crushed sample and 300 mg of KBr by a Thermo Scientific NICOLET 6700 spectrometer. The range of wavelength collected was between 400 and 4000 cm^{-1} with 4 cm^{-1} of resolution. Spectra were calculated by Fourier transformation of 64 interferometer scans and total scanning time of 23s.

SEM JEOL JSM 5400, equipped with an OXFORD LINK-ISIS-EDX energy dispersive X-ray spectrometer, was utilized to investigate the microstructure of samples. Analyses were performed, in vacuum mode, on fracture surfaces of the specimens covered by carbon coating. Images were collected using secondary electron (SE) at a working distance of 15 mm with an acceleration voltage of 20 kV. EDS analyses (on spots) were done with accelerating voltage of 20 kV, working distance of 15 mm and beam current of 20 µA and acquiring for 30s per spot analysis. Chemical compositions were determined considering 100 wt% oxide content on an H_2O- and CO_2-free basis.

Colorimetric analyses were performed on the external surface of samples and were carried out by a Konica Minolta CM-2600d instrument. A spot of 6 mm in diameter was used. For each sample, the average value of three measurements was expressed in the CIELAB (L*,

a*, b*) colour coordinates system, where L* defines lightness and ranges from 0 (total absorption or black) to +100 (white), whereas a* and b* denote the green/red and blue/yellow values, respectively, both ranging between -60 and 60.

3.3. Results and discussion

3.3.1 Mechanical properties

The average values of flexural and compressive strengths are reported in Table 3.2 and plotted in Figure 3.4. The first evident finding is the difference between the strength values of sPS_100 and sPS_{800}_100: sPS_{800}_100 exhibits a compressive strength of 18.1(7) MPa, a value higher by 5 times that of 3.6(2) MPa achieved for sPS_100. The explanation of their different behaviors could lie in calcium reactivity of sPS and sPS_{800}, respectively. In the former, calcium is mostly found as carbonate ($CaCO_3$) or plagioclase crystalline phases, which have a low level of reactivity, while in sPS_{800}, calcium is present mainly in the form of highly reactive oxide (CaO) that may enhance the mechanical performance of the final material. An analogous process can be observed in systems as those formed with blast furnace slag that generate, due to the hydraulic activity, a more reactive material than those obtained in the absence of calcium (Puertas et al., 2000; Yip et al., 2005; Zhang et al., 2013). Furthermore, the presence of CaO in sPS_{800}_100 also implies an increase of the liquid/solid ratio to obtain the same workability of sPS_100. Concerning sPS_100, similar values of strength were obtained using a sandstone rock as starting material (Li et al., 2014), anyway the very low strength value implies that silica and alumina present in the raw material did not take part in the polymerization reaction. When part of the sPS sludge are replaced by metakaolin, higher values of both flexural and compressive strength are observed, thus implying that the resulting strength is mainly due to Sl-MK. In particular, resistance values increase with decreasing sPS contents. Taking into account MK_100 and sPS_MK_50/50, the mechanical strength values are exactly halved (decreasing from 16.1(6) MPa to 8.0(2) MPa and from 3.9(1) MPa to 2.2(1) MPa for compressive and flexural strength, respectively). This confirmes both the absence in the sPS of reactive compounds capable of reacting with the Sl-MK, both its inefficiency if considered as filler.

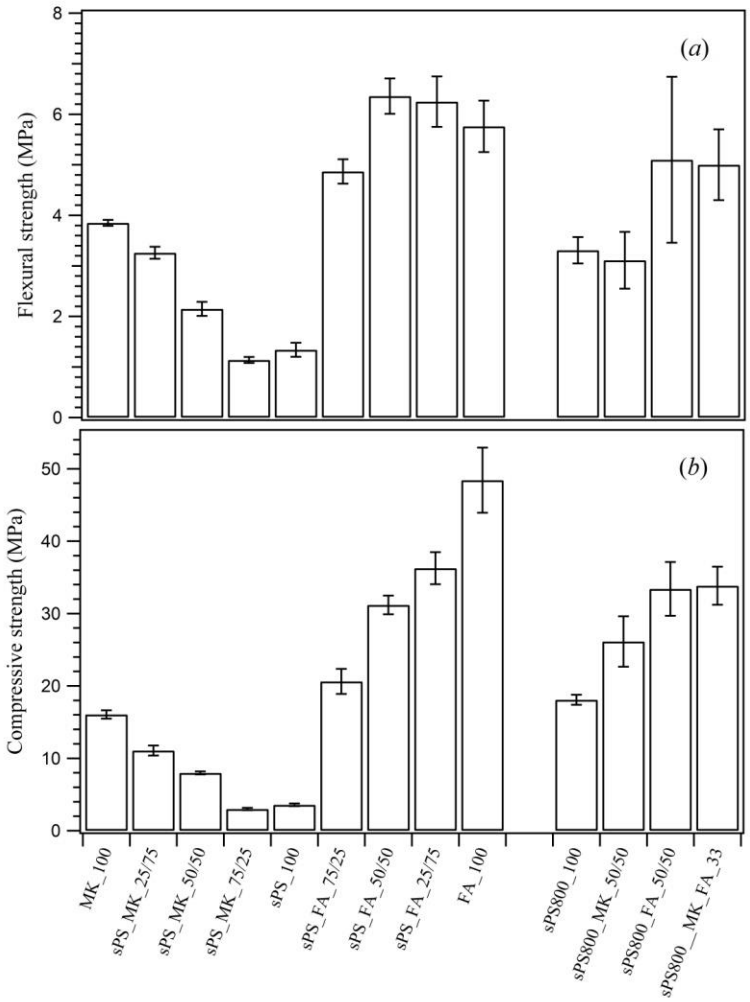

Figure 3.4. (a) Flexural strength and (b) compressive strength of the different alkali-activated specimens.

The mix prepared by using in the same proportions Sl-MK and sPS_{800} (sPS_{800}_MK_50/50) shows instead a considerable value of compressive strength (26(3) MPa) and flexural strength similar to those reported in literature for metakaolin based materials (Palomo et al., 1999a). This confirms the role of calcium in the reaction, contributing to develop a metakaolin based material with an appreciable strength after only one day of curing. It also to be noted that being Sl-MK and sPS_{800} heated at the same temperature, their synergic use may also be convenient from the economic standpoint, as only one synchronous thermal cycle can be carried out.

The compressive strengths of materials produced by the mixtures between FA and sPS show values among 36(2) MPa and 21(2) MPa, values that increased with increasing FA amount. An opposite trend is measured for the flexural strength that exhibits the highest value in sPS_FA_50/50 (6.4(4) MPa). A compressive and a flexural strength of 33(4) MPa and 5(2) MPa

Table 3.2. Details of AAMs

Sample	Starting materials weight proportion [a]	NaOH solution (M)	liquid/solid weight ratio	Curing time [b]	Compressive strength (MPa)	Flexural strength (MPa)	Colorimetric CIELAB coordinates		
							L*	a*	b*
MK_100	Sl-MK (1)	12	0.80	5h	16.1(6)	3.9(1)	88(1)	0.6(3)	5.6(5)
sPS_MK_25/75	sPS/Sl-MK (1:3)	12	0.70	5h	11.1(7)	3.3(1)	-	-	-
sPS_MK_50/50	sPS/Sl-MK (1:1)	12	0.60	5h	8.0(2)	2.2(1)	-	-	-
sPS_MK_75/25	sPS/Sl-MK (3:1)	12	0.60	5h	3.0(2)	1.1(1)	-	-	-
sPS_100	sPS (1)	8	0.35	20h	3.6(2)	1.3(1)	77.1(9)	0.06(4)	5.6(1)
sPS_FA_75/25	sPS/FA(3:1)	8	0.28	20h	21(2)	4.9(2)	-	-	-
sPS_FA_50/50	sPS/FA(1:1)	8	0.28	20h	31(1)	6.4(4)	55(1)	-0.15(5)	2.3(2)
sPS_FA_25/75	sPS/FA(1:3)	8	0.28	20h	36(2)	6.3(5)	-	-	-
FA_100	FA(1)	8	0.28	20h	48(4)	5.8(5)	45(1)	-0.11(6)	2.5(6)
sPS_{800}_100	sPS_{800} (1)	8	0.50	20h	18.1(7)	3.3(3)	69(1)	8.3(1)	19.5(5)
sPS_{800}_MK_50/50	sPS_{800}/Sl-MK (1:1)	8	0.60	20h	26(3)	3.1(6)	78.6(1)	5.05(2)	12.1(1)
sPS_{800}_FA_50_50	sPS_{800}/FA (1:1)	8	0.40	20h	33(4)	5(2)	56.2(5)	0.33(1)	2.3(2)
sPS_{800}_MK_FA_33	sPS_{800}/Sl-MK/FA (1:1:1)	8	0.50	20h	34(3)	5.0(7)	65.0(1)	0.60(1)	6.8(1)
PS sandstone							62.2(7)	-0.45(5)	5.5(1)

Standard deviations are in parentheses.
[a] sPS: Pietra Serena sewage sludges; Sl-MK: Metakaolin; FA: Fly ashes; sPS800: Pietra Serena sewage sludges annealed at 800°Cfor 2 hour.
[b] A curing temperature of 85°C was used for all samples.

respectively is observed in sPS_{800}_FA_50/50. These values underline that no significant strength differences occurr using sPS and sPS_{800}. Both treated and untreated sludge seem interact with FA, contributing to the strength values, but indeed FA do play an important role in the gain of mechanical strength for the large availability of reactive silicon and aluminium that could be transformed in gel when in contact with the alkaline solution. In all cases, all the results obtained by the mixtures with FA could be employed as binders in construction industry, even if a preferable use of sPS could be considered to avoid the sludge heating and therefore further production costs.

The mechanical strength of the activated material obtained by mixing in the same proportions FA, sPS_{800} and Sl-MK achieves good values of compressive and flexural strength equal to 34(3) Mpa and 5.0(7) MPa respectively. A mixture in which metakaolin and fly ashes are used in the same ratio, was already noted to improve the compressive strength compared with the results obtained using only metakaolin (Fernández-Jiménez et al., 2008).

3.3.2 Structural properties

A study of the structural and microstructural properties was performed on the samples that have developed the highest mechanical strength values.

The mineralogical composition of samples after the alkaline activation is displayed in Figure 3.5. In the XRD pattern of sPS_100 is worth highlighting the disappearance of peaks related to dolomite that may be due to the dissolution processes in the NaOH solution. It was noted that dolomite dissolution increases at temperatures similar to those used for the curing, promoting the development of brucite ($Mg(OH)_2$) (García et al., 2003), that effectively is also detected (peaks around 18° and 38° 2θ). The formation of pirssonite, a hydrated sodium calcium carbonate, already identified as secondary product of alkaline activation (Puertas et al., 2000), is revealed. The other crystalline phases detected are the same of sPS, highlighting the low reactivity of the sludge.

sPS_{800}_100 pattern shows the presence of portlandite ($Ca(OH)_2$) due to CaO hydration process (peaks at around 18°, 34° and 50° 2θ), and tobermorite. The presence of peaks at around 11°, 29° and 45° 2θ indicates the development of poorly crystalline calcium silicate hydrate (C-S-H) phases (Richardson, 2004; Taylor, 1997) as main reaction product of the heated sPS hydration , thus clarifying the increase of the mechanical strength.

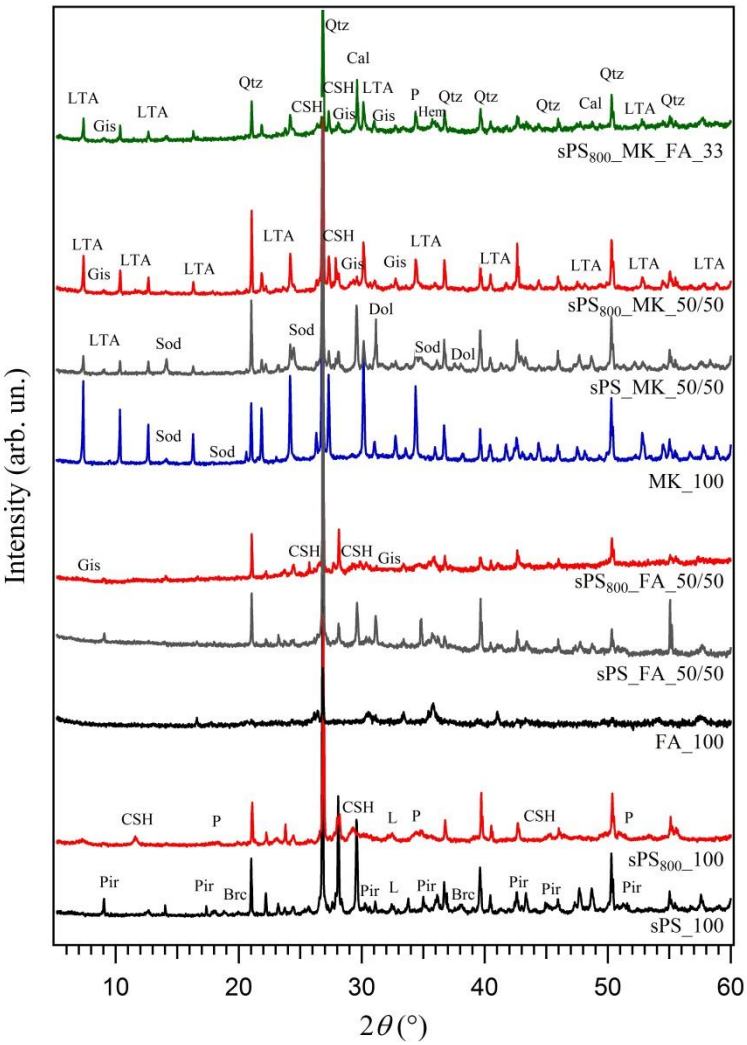

Figure 3.5. XRPD patterns of alkali activated materials. The label of each pattern is indicated in figure. Brc = Brucite; Cal = Calcite; CSH = C-S-H gel; Dol = Dolomite; Gis = Gismondine; L=Lime; P = Portlandite; Pir = Pirssonite; Sod = Sodalite; Qtz = Quartz; LTA = Zeolite A. The peaks not indexed are the same indicated in XRPD patterns in Fig. 3-3 for the starting materials.

XRD patterns from all the other samples present a hump, indicative of the amorphous gel development, in the 25-35° 2θ range. Peaks related to the presence of crystalline zeolite species are also evident. In particular zeolite A and sodalite are detected in Sl-MK based samples, while gismondine is revealed in the samples prepared using sPS_{800}. The zeolites identified in this work are in accordance with those reported in other studies (e.g., (Bernal et al., 2010; Katz, 1998; Provis et al., 2005)).

Pattern of sPS_MK_50/50 shows a lower crystallinity if compared to that of MK_100, The presence of still recognizable peaks related to sPS underlines, one more time, the low reactivity of sPS. In particular, peaks from dolomite are still present indicating that it did not undergo to the dissolution process contrarily to what occurrs in sPS_100. The same behaviour is observed in sPS_FA_50/50 pattern, in which exclusively the peaks characteristics of FA and sPS are detected.

In the binary o ternary mixtures containing sPS_{800}, the characteristics peaks of C-S-H are broad and not very intense, thus making their identification more difficult and less certain. The presence of the broad and amorphous hump from 25° to 35° 2θ and the calcium silicate hydrate (C–S–H) gels, indicates that the geopolymeric reaction and the hydration reaction occurred at the same time. In sPS_{800}_MK_FA_33, the presence of portlandite and calcium carbonate ($CaCO_3$)

are detected. They are probably produced by the hydration reaction of lime present in sPS_{800} and by the carbonation processes of calcium-based compounds after the curing process.

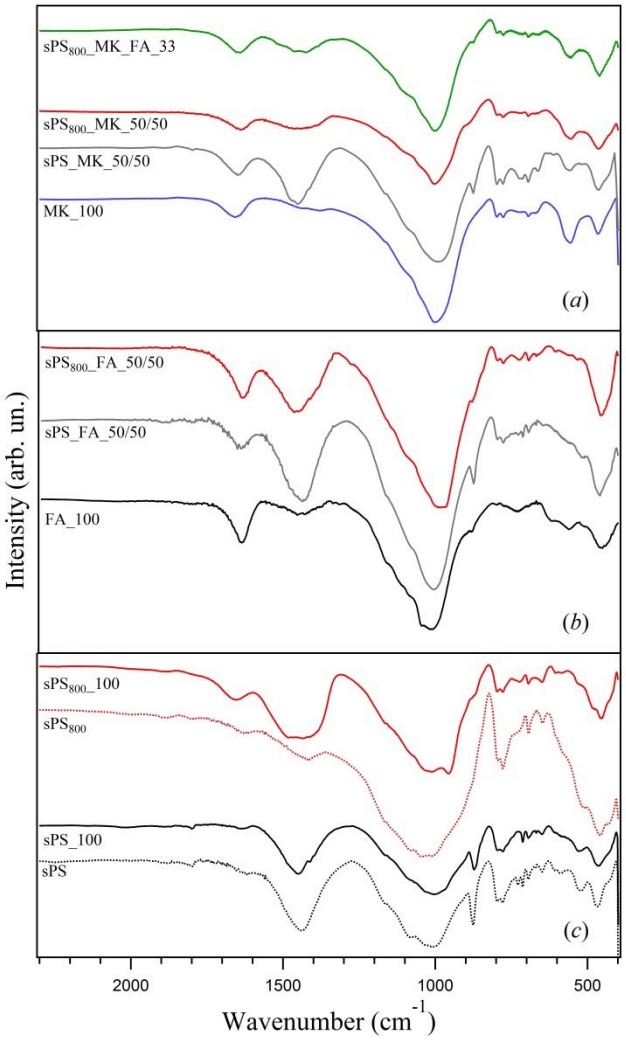

FTIR analyses are reported in Figure 3.6a-c. All Sl-MK and FA based samples (Figure 3.6a-b), after the alkali activation reaction, show one peak around 450 cm^{-1}, associated to Si-O-Si bending vibrations, and a broad band, centered between 990 cm^{-1} and 1010 cm^{-1}, related to asymmetric stretching of the Si-O-T bonds, where T is Al or Si in tetrahedral coordination. This region represents the marker of the aluminosilicate phase and indicates the formation of the amorphous gel, as reported in literature (Fernández-Jiménez and Palomo, 2005; Lee and Van Deventer, 2003).

Figure 3.6. FTIR spectra: (a) MK_100; sPS_MK_50/50; sPS_{800}_MK_50/50; sPS_{800}_MK_FA_33 (b) FA_100; sPS_FA_50/50; sPS_{800}_ FA_50/50; (c) sPS; sPS_100; sPS_{800}; sPS_{800}_100.

The position of this band seems to depend mainly on the Si/Al ratio of the formed product. The shift to lower frequencies is due both to the increase in the tetrahedral aluminium amount (Fernández-Jiménez et al., 2006) and to the presence of calcium in the gel (both binary and ternary mixtures sPS_{800},FA, Sl-MK). The band at 780-790 cm^{-1} corresponds to quartz, while the presence of water is indicated by the humps at around 1640 cm^{-1}, ascribable to H-O-H bending vibrations. The presence of carbonates is identified by the bands around 1450 cm^{-1} (CO_3^{2-} stretching vibrations) and the other C-O vibrations at 875$cm^{-1}$and 710 cm^{-1} (Hughes et al., 1995). Figure 3.6c shows the spectra of sPS_100 and sPS_{800}_100 in which sPS and sPS_{800} are reported for comparison. sPS and sPS_100 spectra exhibit similar features. The presence of carbonates is related both to the presence of calcite and sodium calcium carbonate. In particular, sodium carbonates can be considered as secondary products formed by the large amount of Na^+

cations, not chemically bonded, available to react with atmospheric CO_2 during the curing (Criado et al., 2005; Puertas et al., 2006) due to the low reactivity of sPS in alkaline solution. The main peak at 1000 cm^{-1} cannot be related to amorphous aluminosilicate structure rather to quartz and silicate minerals. A clear change in the main band is instead noted comparing sPS_{800} and sPS_{800}_100. The large and strong peak around 1040 cm^{-1} becomes weaker and composed by two bands at 950 cm^{-1} and 1010 cm^{-1} as consequence of the reaction with alkali. Calcium silicate hydrate (C-S-H) generally have a typical infrared absorption band around 960–970 cm^{-1} (Allali et al., 2016; Lecomte et al., 2006; Zhang et al., 2016), while here the peak at lower wavenumbers (around 950 cm^{-1}) can be attributed to a less polymerized structure. Furthermore in sPS_{800}_100 a rounded and displaced peak around 1433 cm^{-1} evidencs the presence of $Ca(OH)_2$, formed by the reaction of CaO with the alkaline solution.

3.3.3 Textural and microstructural properties

Figure 3.7a-e shows the microstructures of alkali activated sPS and sPS_{800} cements and the related EDS analyses performed on the different hydration products.

SEM and EDS analyses on sPS_FA_50/50 are performed with the aim to define the role of sPS during the synthesis. The matrix presented in Figure 3.7a shows the characteristic fly ashes structure and composition (primarily composed by N-A-S-H gel as resumed in the EDS graph), in which unreacted spherical particles and holes with zeolites clusters can be still distinguished. sPS particles are embedded in the gel mainly as aggregates, highlighting the low reactivity of the sludge, even if partially dissolved rims can be observed. sPS did not take part to the reaction, but contributes to increase the mechanical strength of the binder acting as filler, as denoted by mechanical tests results.

The contribution of lime (CaO) had relevant effects in the synthesis of sPS_{800}_100 as reported in Figure 3.7b. The matrix shows a quite homogeneous microstructure, in which unreacted and few rounded grains can be still recognized. Spherical voids of 30-50 micron in size are due to air bubbles trapped in the gel during the synthesis, while fractures are imputable to sample preparation. At higher magnification (10 Kx) gel structure formed by acicular fibres bounded in divergent clusters, that give rise to a quite porous microstructure can be observed. The acicular particles, less than 1 μm in size (image at magnification of 30 Kx), are distinctive of the early crystallization stages of calcium silicate hydrated compounds (C-S-H) (Hranice, 2002; Taylor, 1986), as confirmed by the large amount of calcium revealed by EDS analysis. A similar

microstructure and composition was found in literature using sandstone sediments (Dong et al., 2014; Li et al., 2014). The increase of sPS_{800}_100 mechanical strength values compared to sPS_100 is therefore due to the hydration and hardening mechanisms of calcium oxide combined with the alkaline solution that affects positively the strength of the hardening paste.

The micrographs of sPS_{800}_FA_50/50 (Figure 3.7c) evidence an articulated and rough microstructure. Conversely to sPS_FA_50/50 (Figure 3.7a), the interaction between FA and sPS_{800} takes place producing a sodium, calcium-alumino-silicate hydrate (N,C-A-S-H) gel (see related EDS analysis). The hydration products of CaO prevaile on the morphological features distinctive of a N-A-S-H gel, producing a disorganized gel formed by acicular fibres in which aggregates cannot be more recognised (10 Kx).

sPS_{800}_MK_50/50 is showed in Figure 3.7d. At low enlargement the analysis of the microstructure confirms the development of the alkali activated gel, which is however characterized by a inhomogeneous microstructure, as observable in the insertions corresponding to d1 and d2 areas in the figure. The d2 insert shows interconnected spherical particles of aluminosilicate gel, in which crystals, corresponding to zeolite A (detected by XRPD) can be observed. The corresponding EDS analysis evidences the absence of calcium, giving back a typical N-A-S-H gel composition. The cluster evidenced in d1 area displays a more compact structure formed by small acicular particles, already noted in sPS_{800}_100, highly rich in calcium. Calcium is found to be distributed not uniformly in the binder, this means that in the early stages of the reaction process, Sl-MK and sPS_{800} did not interact, giving rise to compositionally and structurally different gels. Studies on compatibility between different types of pre-synthetized gels obtained by mixing C-S-H or C-A-S-H with N-A-S-H gel (García-Lodeiro et al., 2010; Garcia-Lodeiro et al., 2011) led to observe the gradual degradation of N-A-S-H into C-A-S-H gel. The resulting product was an intermediate C-A-S-H gel characterized by the minimum CaO/SiO_2 and the maximum Al_2O_3/SiO_2 ratios. Furthermore the co-existence of C-A-S-H and N-(C)-A-S-H gels and the prevalence of one over the other depends on the calcium content and the alkalinity of the system (Yip et al., 2008; Yip et al., 2005). Effectively a third gel structure, with an intermediate composition, is noted (Figure 3.7d on the right and d3 EDS graph), in which acicular and flat structures can be distinguished. As already noted in other works (Chen et al., 2009; Ferone et al., 2015), the calcination of carbonate-containing wastes results to be a successful choice for the reuse of wastes themselves. Similarly, CaO resulting from heat treatment of sPS enhanced the reactivity of the sludge, which is however larger towards Sl-MK rather than FA.

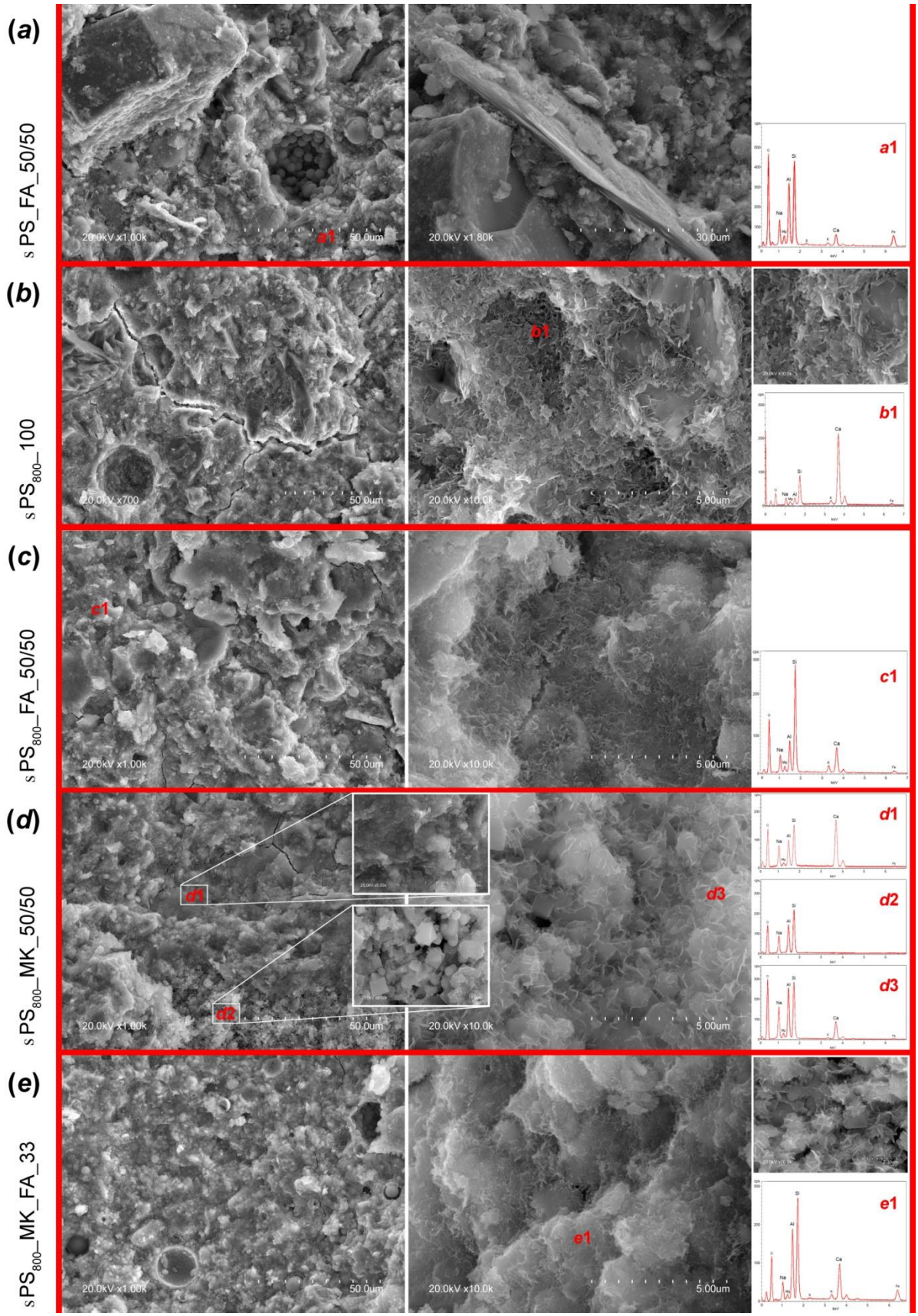

Figure 3.7. SEM micrographs and EDS analyses of alkali activated materials. (a) sPS_FA_50/50; (b) sPS_{800}_100; (c) sPS_{800}_ FA_50/50; (d) sPS_{800}_ MK_50/50; (e) sPS_{800}_ MK_FA_33. Scale bar and magnification are showed in each image.

sPS_{800}_MK_FA_33 (Figure 3.7e) shows the most compact and homogeneous microstructure (magnification of 1Kx) able to favour the strength development. At higher enlargement the laminar features of kaolinite, still recognizable, are replaced by a structurally non-uniform framework, in which needle-shaped elements already noted in the other samples are observable. Chemical analysis (relatives to e1 area) reveals a N,C-A-S-H composition. In the insertion (magnification 20Kx) flat structures (around 2 μm in size), may be ascribable to poorly defined portlandite ($CaOH_2$) (Hranice, 2002), as detected by X-ray diffraction.

3.3.4 Colorimetric analyses

In addition to the mechanical and microstructural characterizations, colorimetric analyses were carried out in order to evaluate the aesthetic features of selected samples derived from Pietra Serena sewage sludge by comparing to those of the Pietra Serena stone used as reference. L*,a*,b* space values are reported for each sample in Table 3.2.

The colour variation between the stone reference and alkali activated binders was evaluated by using the total colour difference, expressed as $\Delta E = sqrt((L^*_1-L^*_0)^2+(a^*_1-a^*_0)^2+(b^*_1-b^*_0)^2)$, where the colorimetric values concerning Pietra Serena stone were measured in a previous work (Clausi et al., 2016). Differences in colour hue angle, $h_{ab} = \tan^{-1}(b^*/a^*)$ were also calculated. Large differences in visual appearance are obtained for sPS_{800}_100 ($\Delta E = 18.5$ and $h_{ab} = 1.01$) and sPS_{800}_MK_50/50 ($\Delta E = 18$ and $h_{ab} = 0.88$), due both to the light color of Sl-MK and to the alteration of sPS_{800} powder color, produced by iron oxides, after heating. The presence of a dark starting material such as FA leads to an appreciable decrease of total colour differences, being $\Delta E = 8.8$ and 6.3, respectively, for sPS_FA_50/50 and sPS_{800}_FA_50/50, whereas very similar hue values to those of Pietra Serena stone are observed (–1.49 and –1.35). sPS_{800}_MK_FA_33 shows the smallest colour difference compared to the stone reference with a $\Delta E = 2.8$. The use of defined amount of Sl-MK and FA modifies positively the colour parameters. The application in the restoration field requires materials to be recognizable, although similar, to the original ones, and slight colour differences make the materials more suitable if used as replacement or to patch renders or fill-in gaps. In particular, sewage sludge obtained by the cutting of stone blocks could meet requirements of compatibility if used for the production of precasted decorative elements in substitution of the original stone.

3.3.5 Samples cured at room temperature

The maturation at temperatures that require the oven use, implies often the use of AAMs as precast elements. For this reason, the same mixtures that allowed to reach the best mechanical performances, were used to synthesize samples that were cured at room temperature, in order to evaluate a potential use in an outdoor setting. Taking into account the role of sPS and sPS_{800} in the synthesis, the mechanical performances were compared to those obtained with a curing at 85°C. Information about the labels, the starting materials proportions, the liquid/solid ratios and the mechanical test results of each sample are reported in Table 3.3.

3.3.5.1 Sample preparation and synthesis parameters

A sodium silicate solution supplied by Ingessil s.r.l. (Na_2O 14.37 wt%, SiO_2 29.54 wt%, H_2O 56.09 wt%) and modified by adding distilled water and dissolving sodium hydroxide (NaOH) in pellets, was used as alkaline activator. In the mixtures in which MK and FA were blended in the same proportion (1:1) with sPS or sPS_{800}, the sewage sludge were considered as aggregates, thus their contribution in the evaluation of the total SiO_2/ Al_2O_3 molar ratio was not taken into account. Common synthesis parameters, listed below, were selected in order to compare results obtained by different starting materials:

- for each formulation the same amount of sodium silicate solution (equal to 29 ml) was utilized. A waterglass characterized by a SiO_2/Na_2O ratio of 2.12 was used for mixtures with FA and sPS_{800}, while the adding of sodium in the mixtures with MK has led to a SiO_2/Na_2O = 1.01;
- for MK and FA based samples a SiO_2/ Al_2O_3 ratio of 2.77 and 5.81 respectively was selected while for both the Al_2O_3/Na_2O ratio equal 1.04 was defined;
- both for the sPS and FA based samples the same liquid/solid weight ratio of the specimens cured at 85°C for 20 hours was selected, while for the MK based samples the least liquid/solid weight ratio, capable to guarantee the workability of the slurry, was chosen.

The sodium silicate solutions were mixed to the different powders and, for the synthesis of the binders, the same procedure previously described (see paragraph 3.2.2*)* was used. A rapid hardening and a clear shrinkage, already after a few hours from the synthesis, was observed for the samples sPS_{800}_100_*RT* and sPS_{800}_FA_50_50_*RT*.

Specimens were cured in climatic room at 20°C in 65% R.H conditions for 7 days, after were demoulded and cured in the same conditions for other 14 days. At the end of the curing, specimens were frozen in acetone and ethanol before to be tested.

Table 3.3 Details of AAMs cured at 20°C in 65% R.H conditions for 28 days.

Sample	Starting materials weight proportion [a]	liquid/solid weight ratio	Compressive strength (MPa)	Flexural strength (MPa)
MK_100_*RT*	Sl-MK (1)	0.40	47(6)	5.7(3)
sPS_MK_50/50_*RT*	sPS/Sl-MK (1:1)	0.40	28(1)	4.4(1)
sPS_FA_50/50_*RT*	sPS/FA(1:1)	0.28	36(2)	4.6(8)
FA_100_*RT*	FA(1)	0.28	38(2)	4.9(7)
sPS_{800}_100_*RT*	sPS_{800} (1)	0.50	19 (1)	5.1(5)
sPS_{800}_MK_50/50_*RT*	sPS_{800}/Sl-MK (1:1)	0.40	37(2)	4.0(5)
sPS_{800}_FA_50_50_*RT*	sPS_{800}/FA (1:1)	0.28	38(4)	6.6(8)

Standard deviations are in parentheses.
[a] sPS: Pietra Serena sewage sludges; Sl-MK: Metakaolin; FA: Fly ashes; sPS_{800}: Pietra Serena sewage sludges annealed at 800°Cfor 2 hour.

3.3.5.2 Mechanical characterization

The hardened products obtained from the different experimental mixtures were characterized from the mechanical viewpoints. The mean values of flexural and compressive strength are reported in Table 3.3 and the comparison with the corresponding samples cured at 85°C for 20 hours plotted in Figure 3.8.

All samples showed an higher compressive strength if compared to the specimens synthesized with NaOH and cured at 85°C. The presence of soluble silica in the sodium silicate solution favours the polymerization process, producing a material with an increased mechanical strength as already reported in literature (Criado et al., 2005; Fernández-Jiménez et al., 1999).

Particularly enhanced were instead MK based samples, with compressive strength values of 28(1) MPa and 37(2) MPa for sPS_MK_50/50_*RT* and sPS_{800}_MK_50/50_*RT* respectively. An evident flexural strength improvement was also observed. Even if the resulting strengths were mainly offered by Sl-MK, sPS and sPS_{800} seem to contribute to mechanical strength improvement. Contrarily to those observed in sPS_MK_50/50, in sPS_MK_50/50_*RT* the mechanical strength values were not the half of MK_100_*RT*, that leads to suppose the suitability

of sPS to act as filler. An improvement of more than 10 MPa was revealed in sPS_{800}_MK_50/50_*RT* compared to sPS_{800}_MK_50/50, confirming the interaction between the heated sludges and the metakaolin.

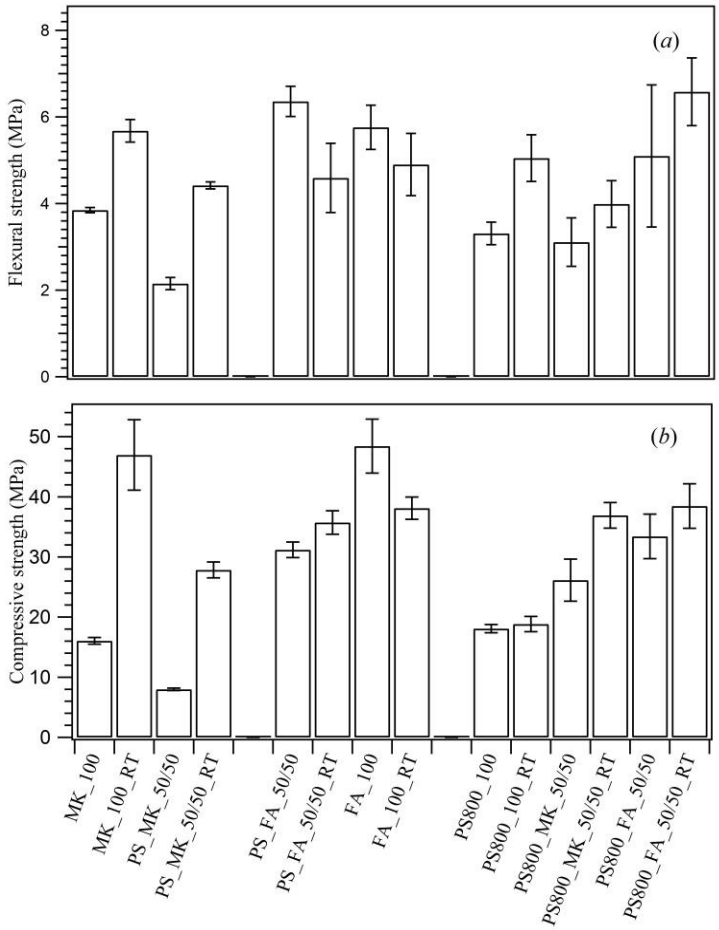

Figure 3.8. Comparison between the different alkali-activated specimens cured at 20°C in 65% R.H conditions for 28 days and the corresponding samples cured at 85°C. (a) Flexural strength and (b) compressive strength.

A slight increase of compressive strength and a decrease of flexural strength was observed for sPS_FA_50/50_*RT* and sPS_{800}_FA_50/50_*RT* if compared to the related 85°C cured samples. For the FA based samples the same behaviour described in the paragraph *3.3.1*can be proposed. The only difference, related to the improvement of the compressive strength, can be caused by the use of sodium silicate as activator solution that leads to a more efficient activation of Si and Al present in the starting materials. Is worth to evidence that the increase of mechanical strength values has not been so large for sPS_{800}_100_*RT* compared to sPS_{800}_100 (only an increase of about 2 MPa can be observed for the flexural strength). This result confirms that is the same amount of calcium oxide (CaO) to play the main role in the development of mechanical performances, while the greater contribution of silica in the alkaline activator not seems to produce considerable improvement on the contrary of the MK and FA based samples.

The room temperature curing combined with the use of the sodium silicate as activator solution could to be a suitable choice for the synthesis of alkali activated cements, especially because allows to reach considerable strength values avoiding the oven curing. Results confirm the possibility to obtain suitable materials for a wide range of applications, from decorative ones to binder phase in mortars, and to be applied directly in open environment.

References

Akbulut, H., Gürer, C., 2007. Use of aggregates produced from marble quarry waste in asphalt pavements. Building and Environment 42, 1921-1930.

Allali, F., Joussein, E., Kandri, N.I., Rossignol, S., 2016. The influence of calcium content on the performance of metakaolin-based geomaterials applied in mortars restoration. Materials and Design 103, 1-9.

Banchelli, A., Fratini, F., Germani, M., Malesani, P.G., Manganelli Del Fa, C., 1997. The sandstones of Florentine historic buildings: individuation of the marker and determination of the supply quarries of the rocks used in some Florentine monuments. Science and technology for cultural heritage 6, 13-22.

Bernal, S.A., de Gutierrez, R.M., Provis, J.L., Rose, V., 2010. Effect of silicate modulus and metakaolin incorporation on the carbonation of alkali silicate-activated slags. Cement and Concrete Research 40, 898-907.

Bernal, S.A., Rodríguez, E.D., Kirchheim, A.P., Provis, J.L., 2016. Management and valorisation of wastes through use in producing alkali-activated cement materials. Journal of Chemical Technology and Biotechnology.

Cantisani, E., Garzonio, C.A., Ricci, M., Vettori, S., 2013. Relationships between the petrographical, physical and mechanical properties of some Italian sandstones. International Journal of Rock Mechanics and Mining Sciences 60, 321-332.

Chen, J.-H., Huang, J.-S., Chang, Y.-W., 2009. A preliminary study of reservoir sludge as a raw material of inorganic polymers. Construction and Building Materials 23, 3264-3269.

Clausi, M., Tarantino, S.C., Magnani, L.L., Riccardi, M.P., Tedeschi, C., Zema, M., 2016. Metakaolin as a precursor of materials for applications in Cultural Heritage: Geopolymer-based mortars with ornamental stone aggregates. Applied Clay Science 132–133, 589-599.

Criado, M., Palomo, A., Fernández-Jiménez, A., 2005. Alkali activation of fly ashes. Part 1: Effect of curing conditions on the carbonation of the reaction products. Fuel 84, 2048-2054.

Dong, J., Wang, L., Zhang, T., 2014. Study on the strength development, hydration process and carbonation process of NaOH-activated Pisha Sandstone. Construction and Building Materials 66, 154-162.

Duxson, P., Fernández-Jiménez, A., Provis, J.L., Lukey, G.C., Palomo, A., van Deventer, J.S.J., 2006. Geopolymer technology: the current state of the art. Journal of Materials Science 42, 2917-2933.

Duxson, P., Provis, J.L., 2008. Designing precursors for geopolymer cements. Journal of the American Ceramic Society 91, 3864-3869.

Duxson, P., Provis, J.L., Lukey, G.C., van Deventer, J.S.J., 2007. The role of inorganic polymer technology in the development of 'green concrete'. Cement and Concrete Research 37, 1590-1597.

Felekoglu, B., 2007. Utilisation of high volumes of limestone quarry wastes in concrete industry (self-compacting concrete case). Resources, Conservation and Recycling 51, 770-791.

Fernández-Jiménez, A., de la Torre, A.G., Palomo, A., López-Olmo, G., Alonso, M.M., Aranda, M.A.G., 2006. Quantitative determination of phases in the alkaline activation of fly ash. Part II: Degree of reaction. Fuel 85, 1960-1969.

Fernández-Jiménez, A., Monzó, M., Vicent, M., Barba, A., Palomo, A., 2008. Alkaline activation of metakaolin-fly ash mixtures: Obtain of Zeoceramics and Zeocements. Microporous and Mesoporous Materials 108, 41-49.

Fernández-Jiménez, A., Palomo, A., 2005. Mid-infrared spectroscopic studies of alkali-activated fly ash structure. Microporous and Mesoporous Materials 86, 207-214.

Fernández-Jiménez, A., Palomo, J.G., Puertas, F., 1999. Alkali-activated slag mortars: Mechanical strength behaviour. Cement and Concrete Research 29, 1313-1321.

Ferone, C., Colangelo, F., Cioffi, R., Montagnaro, F., Santoro, L., 2013. Use of reservoir clay sediments as raw materials for geopolymer binders. Advances in Applied Ceramics 112, 184-189.

Ferone, C., Liguori, B., Capasso, I., Colangelo, F., Cioffi, R., Cappelletto, E., Di Maggio, R., 2015. Thermally treated clay sediments as geopolymer source material. Applied Clay Science 107, 195-204.

Fratini, F., Pecchioni, E., Cantisani, E., Rescic, S., Vettori, S., 2014. Pietra Serena: the stone of the Renaissance. Geological Society, London, Special Publications 407, 173-186.

García-Lodeiro, I., Fernández-Jiménez, A., Palomo, A., MacPhee, D.E., 2010. Effect of calcium additions on N-A-S-H cementitious gels. Journal of the American Ceramic Society 93, 1934-1940.

Garcia-Lodeiro, I., Palomo, A., Fernández-Jiménez, A., Macphee, D.E., 2011. Compatibility studies between N-A-S-H and C-A-S-H gels. Study in the ternary diagram Na2O–CaO–Al2O3–SiO2–H2O. Cement and Concrete Research 41, 923-931.

García, E., Alfonso, P., Labrador, M., Galí, S., 2003. Dedolomitization in different alkaline media: Application to Portland cement paste. Cement and Concrete Research 33, 1443-1448.

Gasparini, E., Tarantino, S.C., Conti, M., Biesuz, R., Ghigna, P., Auricchio, F., Riccardi, M.P., Zema, M., 2015. Geopolymers from low-T activated kaolin: Implications for the use of alunite-bearing raw materials. Applied Clay Science 114, 530-539.

Gasparini, E., Tarantino, S.C., Ghigna, P., Riccardi, M.P., Cedillo-González, E.I., Siligardi, C., Zema, M., 2013. Thermal dehydroxylation of kaolinite under isothermal conditions. Applied Clay Science 80-81, 417-425.

Horpibulsuk, S., Suksiripattanapong, C., Samingthong, W., Rachan, R., Arulrajah, A., 2015. Durability against Wetting–Drying Cycles of Water Treatment Sludge–Fly Ash Geopolymer and Water Treatment Sludge–Cement and Silty Clay–Cement Systems. Journal of Materials in Civil Engineering 28, 04015078.

Hranice, C., 2002. The effect of water ratio on microstructre and composition of the hydration products of Portland cement pastes. Ceramics− Silikáty 46, 152-158.

Hughes, T.L., Methven, C.M., Jones, T.G.J., Pelham, S.E., Fletcher, P., Hall, C., 1995. Determining cement composition by Fourier transform infrared spectroscopy. Advanced Cement Based Materials 2, 91-104.

Katz, A., 1998. Microscopic Study of Alkali-Activated Fly Ash. Cement and Concrete Research 28, 197-208.

Lecomte, I., Henrist, C., Liégeois, M., Maseri, F., Rulmont, A., Cloots, R., 2006. (Micro)-structural comparison between geopolymers, alkali-activated slag cement and Portland cement. Journal of the European Ceramic Society 26, 3789-3797.

Lee, W., Van Deventer, J., 2003. Use of infrared spectroscopy to study geopolymerization of heterogeneous amorphous aluminosilicates. Langmuir 19, 8726-8734.

Li, C., Zhang, T., Wang, L., 2014. Mechanical properties and microstructure of alkali activated Pisha sandstone geopolymer composites. Construction and Building Materials 68, 233-239.

Malesani, P., Pecchioni, E., Cantisani, E., Fratini, F., 2003. Geolithology and provenance of materials of some historical buildings and monuments in the centre of Florence (Italy). Episodes 26, 250-255.

Pacheco-Torgal, F., Castro-Gomes, J., Jalali, S., 2008. Alkali-activated binders: A review. Part 1. Historical background, terminology, reaction mechanisms and hydration products. Construction and Building Materials 22, 1305-1314.

Palomo, A., Blanco-Varela, M.T., Granizo, M.L., Puertas, F., Vazquez, T., Grutzeck, M.W., 1999a. Chemical stability of cementitious materials based on metakaolin. Cement and Concrete Research 29, 997-1004.

Palomo, A., Grutzeck, M.W., Blanco, M.T., 1999b. Alkali-activated fly ashes: A cement for the future. Cement and Concrete Research 29, 1323-1329.

Payá, J., Monzó, J., Borrachero, M.V., Tashima, M.M., 2014. Reuse of aluminosilicate industrial waste materials in the production of alkali-activated concrete binders, Handbook of Alkali-Activated Cements, Mortars and Concretes, pp. 487-518.

Provis, J.L., Bernal, S.A., 2014. Geopolymers and Related Alkali-Activated Materials. Annual Review of Materials Research 44, 299-327.

Provis, J.L., Lukey, G.C., Van Deventer, J.S.J., 2005. Do geopolymers actually contain nanocrystalline zeolites? a reexamination of existing results. Chemistry of Materials 17, 3075-3085.

Puertas, F., Martínez-Ramírez, S., Alonso, S., Vázquez, T., 2000. Alkali-activated fly ash/slag cements: Strength behaviour and hydration products. Cement and Concrete Research 30, 1625-1632.

Puertas, F., Palacios, M., Vázquez, T., 2006. Carbonation process of alkali-activated slag mortars. Journal of Materials Science 41, 3071-3082.

Rakhimova, N.R., Rakhimov, R.Z., 2015. Alkali-activated cements and mortars based on blast furnace slag and red clay brick waste. Materials & Design 85, 324-331.

Rashad, A.M., 2014. A comprehensive overview about the influence of different admixtures and additives on the properties of alkali-activated fly ash. Materials & Design 53, 1005-1025.

Richardson, I.G., 2004. Tobermorite/jennite- and tobermorite/calcium hydroxide-based models for the structure of C-S-H: applicability to hardened pastes of tricalcium silicate, β-dicalcium silicate, Portland cement, and blends of Portland cement with blast-furnace slag, metakaolin, or silica fume. Cement and Concrete Research 34, 1733-1777.

Ruiz-Santaquiteria, C., Fernández-Jiménez, A., Skibsted, J., Palomo, A., 2013. Clay reactivity: Production of alkali activated cements. Applied Clay Science 73, 11-16.

Siddique, R., Klaus, J., 2009. Influence of metakaolin on the properties of mortar and concrete: A review. Applied Clay Science 43, 392-400.

Taylor, H.F.W., 1986. Proposed Structure for Calcium Silicate Hydrate Gel. Journal of the American Ceramic Society 69, 464-467.

Taylor, H.F.W., 1997. Cement Chemistry. Thomas Telford.

Yang, K.-H., Lo, C.-W., Huang, J.-S., 2013. Production and properties of foamed reservoir sludge inorganic polymers. Cement and Concrete Composites 38, 50-56.

Yip, C.K., Lukey, G.C., Provis, J.L., van Deventer, J.S.J., 2008. Effect of calcium silicate sources on geopolymerisation. Cement and Concrete Research 38, 554-564.

Yip, C.K., Lukey, G.C., van Deventer, J.S.J., 2005. The coexistence of geopolymeric gel and calcium silicate hydrate at the early stage of alkaline activation. Cement and Concrete Research 35, 1688-1697.

Zhang, N., Li, H., Zhao, Y., Liu, X., 2016. Hydration characteristics and environmental friendly performance of a cementitious material composed of calcium silicate slag. Journal of hazardous materials 306, 67-76.

Zhang, T., Gao, P., Gao, P., Wei, J., Yu, Q., 2013. Effectiveness of novel and traditional methods to incorporate industrial wastes in cementitious materials—An overview. Resources, Conservation and Recycling 74, 134-143.

ASTM C 618: Standard Specification for Coal Fly Ash and Raw or Calcined Natural Pozzolan for Use in Concrete.

CONCLUSIONS

This PhD Thesis summarizes the results of three years of work focused on exploring the potentiality of AAMs for the synthesis of mortars and composites suitable for the conservation and restoration of materials belonging to the built Heritage. The structural, microstructural and physical-mechanical properties of AAMs have been studied in order to investigate their compatibility with existing materials. In particular, the interaction with some ornamental stones, widespread in the Italian architecture, has been the central idea of the whole work.

Geopolymers are promising materials with potential use in many application fields, in particular as high performance, environmental-friendly materials for structural applications and possible replacement for ordinary Portland cement. For this kind of applications, many studies focus on fly-ashes and other waste materials as precursors of geopolymers and alkali activated materials, with the purpose of reducing costs and CO_2 footprint. However, Cultural Heritage is a field in which metakaolin-based geopolymers may actually find application, thanks to their high durability and versatile range of physical properties that may possibly be tailored to guarantee functional and aesthetic compatibilities with the remnants of original materials.

In the first part of the work, geopolymers have been obtained after consolidation of a fluid slurry without the use of plasticizers and additives and resulted to be largely composed by amorphous binding material and showed high strength and low porosity. The presence of aggregates from ornamental stones, namely Pietra Serena and Pietra di Angera, resulted in a reduction of strength, which however falls in the masonry mortars class M20. This may open the way to use them as sacrificial material for restoration of stone objects, as compatibility depends on the support features, hence mechanical compatibility should be adjusted to each particular case also in function of the destination of use. In these mortars, microfines seem to contribute to further reduce carbonate formation, which is however low. An increase of compaction and reduction of porosity of the matrix with respect to the plain binder has also been observed, pore size distribution of the mortars are similar to those of the used ornamental stones, thus suggesting the possibility to tune breathability of the mortars by adjusting their formulation. Functional compatibility means not to damage the old masonry and in second place to be able to protect it against external actions. Water is one of the most effective destruction agents for old masonry: water transport, dissolution and transport of salts, but also biological colonization are issues to take into consideration and further studies are in hand to better evaluate them. The use of rock fines with metakaolin-based binders allows to obtain materials that mimic the stone, thus

reaching good aesthetic compatibility. In particular, mortars of the same color of the rock but slightly paler have been obtained. In restoration practice, this would allow to obtain materials that are recognizable, albeit similar, to the original substrate. In the quest of designing new, high-performance materials that meet the requirements of sustainability and compatibility with the artifacts, this study has shown good potentialities of metakaolin-based geopolymers for uses in Cultural Heritage.

The interactions between metakaolin-based geopolymers and widespread materials used in Cultural Heritage have been therefore studied. SEM investigations allowed to evaluate the adhesive processes involved at the contact zones at short length scale. Adhesion at the interfaces appeared to be good for all natural stones and artificial building materials considered here. A calcium carbonate layer was observed only in the historic mortar, although in all samples, the binder contains calcium at the interface, deriving from the stones or artificial material that modified the starting geopolymer composition. Calcium does not give rise to new crystalline phases, but in the binder in contact to the historic mortar, concrete and Pietra di Angera, rounded precipitation particles were observed. Difference in crystallinity influences calcite precipitation: in the mortar, the reaction layer is more developed for the presence of microcrystalline calcite grains, which are more soluble than those of the carbonatic stones used in this work. Furthermore, the different solubility in highly alkaline solutions of dolomite and calcite may influence the behavior of the Pietra di Angera and Pietra di Noto at interface. The binding matrix of stone materials used in the experimentation was noted to influence the adhesion properties. An alumino-silicate matrix as in Pietra Serena and in bricks seems to have greater physical affinity with geopolymer binder. Carbonate matrix instead produces a Ca-rich zone that may likely affect positively the final mechanical and physical properties. AAMs are currently not used for conservation purposes, however, the results obtained in this study are promising. In restoration practices, the versatility of AAMs would allow to obtain binders with different characteristics, thus increasing the compatibility with the substrate to repair.

The research was also focused at addressing the issue of materials recycle by evaluating the use of sewage sludge derived by the cultivation of Pietra Serena as precursor material in the synthesis of alkaline cements or geopolymers. The results show that samples produced exclusively by using the untreated sludge (sPS) do not achieve suitable strength properties. On the other hand, sPS mixed with fly ash (sPS/FA 1:3 or 1:1 proportions) may be used to develop materials with strength values and colours appropriate to be used as Pietra Serena stone substitute. In such materials, the sludge acts as fine filler, enhancing packing density and leading

to compressive strength slightly lower than FA_100. Nonetheless, these mixtures exhibit the advantage of an increased flexural strength with respect to their corrispectives without FA, an important feature to take into account in the evaluation of structural applications. The main reaction product is a N-A-S-H type gel, which is responsible of the good behaviour of the whole system. Mixtures with Pietra Serena sewage sludge content above 50% exhibit lower mechanical strength and thus are not recommendable for structural application purposes. Both the mechanical behaviour and the aesthetic features of AAMs obtained from the binary mixtures of sPS and metakaolin (Sl-MK) did not show the expected results, despite initially metakaolin was thought to be the most suitable material to be blended. The strength values obtained denote the sPS inefficiency as a filler and the low reactivity of its components capable of reacting with the metakaolin. However, AAMs from mixtures of sPs and Sl-MK produced by using sodium silicate (waterglass) as activator and cured at room temperature display a noticeably higher strength. The decarbonation process of the sewage sludge also provides a useful tool for the valorisation of this type of waste. The sPS_{800} behaviour is more similar to a pozzolanic cement, in which the calcium oxide produced is hydrated and reacts with the silica present in the material to generate a C-S-H gel and $Ca(OH)_2$. These products contribute to enhance the mechanical performances of the final material achieving a strength of 18 MPa after only one day. Likely, these strengths will increase with time and the carbonation process of the material. However, although the reactions were carried out by using NaOH solution, it should not be considered as a geopolymerization process in the strictest sense of the word. Particularly interesting were the binary mixtures sPS_{800}/FA and sPS_{800}/Sl-MK (proportion 1:1) and the ternary mixture sPS_{800}/FA/Sl-MK (proportions 1:1:1). In these mixtures, an interaction between the different precursors occurs, giving rise to a mixture of N,C-A-S-H / C-A-S-H gels, similar to those produced in so-called mixed alkali cements or hybrid cements. These materials after one day of curing show a heterogeneous microstructure in which one type of gel prevails on the other, depending on whether in its surroundings, a particle of flay ash, or of metakaolin or of CaO (sPS_{800}) is present. However, on the basis of the results published by other researchers on this type of cementitious systems (Palomo et al., 2014 and references therein), authors suppose that the microstructures would gradually turn into a single gel type C-A-S-H that contributes to increase the mechanical strengths. In any case, this work shows a double usability for the Pietra Serena sewage sludge. The sludge can be incorporated as filler in fly ash matrix by alkaline activation, or used in binary or ternary matrices with metakaolin and fly ash after decarbonation, which gives rise to calcium oxide and thus leads to the formation of N,C-A-S-H/C-A-S-H type

gels. The results obtained by curing samples at room temperature also confirm the suitability of a potential use in outdoor setting.

References

Palomo, A., Krivenko, P., Garcia-Lodeiro, I., Kavalerova, E., Maltseva, O., Fernández-Jiménez, A., 2014. A review on alkaline activation: New analytical perspectives. Materiales de Construcción 64, e022.

Hoy es un dia maravilloso, vamos a disfrutarlo.